DUPA α-Amanitin Conjugates for Targeted Prostate Cancer Therapy - Optimization and Evaluation of *In Vivo* Potency

Dissertation Zur Erlangung des akademischen Grades

Doctor rerum naturalium (Dr. rer. nat.)

Barbara Korsak

Organic and Bioorganic Chemistry OC III

Department of Chemistry

Bielefeld University

Thesis fully developed at Heidelberg Pharma Research GmbH

2020

Referee I Prof. Dr. Andreas Pahl

Chief Scientific Officer

Heidelberg Pharma Research GmbH

Institute of Experimental and Clinical Pharmacology and Toxicology,
University of Erlangen-Nürnberg

Referee II Prof. Dr. Norbert Sewald

Organic and Bioorganic Chemistry OC III

Department of Chemistry, Bielefeld University

Printed on age-resistant paper according to ISO ° 970

Statement

The following work was conducted between October 2015 and September 2018 in the Department of Biochemistry and Cell Biology at Heidelberg Pharma Research GmbH as a part of Magicbullet Initial Training Network founded by the Horizon 2020 Program. The project was developed in collaboration with Francesca Gallo M.Sc. from the Department of Chemistry of Heidelberg Pharma Research GmbH, who synthesized all chemical compounds and provided them in the amount sufficient for *in vitro* and *in vivo* studies. The author of this thesis designed, performed and interpreted the results of all biological assays presented within this work, namely: cytotoxicity, plasma stability and competitive inhibition *in vitro* assays as well as *in vivo* studies such as maximal tolerated dose determination, pharmacokinetic, biodistribution and efficacy assays.

Parts of this work were published in the patent: WO/2019/057964. The manuscript is currently in preparation and will be submitted to one of the journals publishing biopharmaceutical or bioconjugation specializing research.

Acknowledgements

First, I would like to thank to my supervisors Dr. Torsten Hechler and Prof. Dr. Andreas Pahl for choosing me four years ago as a PhD student and allowing me to undertake this interesting multidisciplinary project which shaped me as a scientist and as a person.

I would like to thank to Dr. Torsten Hechler for a great scientific guidance, allowing me to make mistakes, learn with them and your wise and supportive way of handling my small crises. Thank you for teaching me how to overcome problems and showing me that there is always a solution. Here I express my gratitude for countless hours of our scientific discussions and your career advices. I deeply appreciate your careful revision of this work and support with the manuscript preparation.

Prof. Dr. Andreas Pahl I would like to thank you for your scientific guidance, encouragement and teaching me how to see the "big picture" and look at the scientific projects in a translational way. I would like to especially thank you for the critical revision of this work and your support with the manuscript preparation.

I would like to thank to Dr. Christoph Müller for supervising chemistry aspects of the project and your availability to discuss chemistry-related questions.

Next, I would like to express my gratitude to Prof. Dr. Norbert Sewald for accepting the role of co-supervisor and for the outstanding organization of the Magicbullet project.

I would like to thank to all Group Leaders from Biochemistry Department of Heidelberg Pharma Research for triggering interesting scientific discussions and for sharing with me your knowledge. I especially thank to Anikó Palfi M. Sc. for your help with the molecular biology experiments and sharing your expertise in protein purification. I would like to thank you for your deep understanding and always being available to help me not only in a professional but also in the private situations, whenever I needed it. Thank you very much! I would like to thank to Dr. Christian Breunig for critical revision of the introduction to this thesis and being available to share with me your cell biology and molecular biology knowledge. Especial thanks to Dr. Stephanie Voß for critical revision of this work, helping me to get more in shape with scientific writing and interesting science- and life-related conversations in your office.

Next, I thank to Dr. Michael Kulke, Irina Dranova M. Sc. for your help with the design, execution and interpretation of the results of *in vivo* studies. Especial thanks to Dr. Michael Kulke for sharing your pharmacology expertise and always being open to discuss the results.

I especially thank to Dr. Christian Lutz for providing input into the biodistribution studies. Thank you for always being available to take a look at the data and sharing your endless knowledge in the field of bioanalytics and pharmacokinetics. I also thank to Dr. Thomas Philippi and Dr. Artjom Wischnjow for their help with the execution of the experiments.

I would like to thank to Francesca Gallo M. Sc. Without your work this project would never be possible! Thank you for being always available to discuss the rationale and science behind the design of the compounds. Thank you for your reliability and being patient, even when I asked you for providing additional batch of the conjugates almost in a “kilogram-scale”. Thank you for three years of collaboration. I could not imagine having a more reliable collaborator and friend than you!

I want to thank all my colleagues from the Magicbullet network. Already mentioned above Francesca and additionally to Andrea, Lucia and Sabine for establishing our funny quintet. Thanks to remaining colleagues: Eduard, Adina, Clemence, Lizeth, Ivan, Ana, Aby and JK for sharing this experience.

In the end I would like to thank to my closest family.

Dziękuję Ci Tato i Asiu za Wasze wsparcie, cierpliwość i za doping żeby skończyć to, co zostało zaczęte!

Obrigada Filipe! Sem o teu suporte e a tua paciência não era possível!

Thank you! Dankeschön! Dziękuję! Obrigada! Grazie!

List of abbreviations:

2-PMPA - 2-Phosphonomethyl pentanedioic acid

ADC - antibody drug conjugate

ADT - androgen deprivation therapy

AR- androgen receptor

ATAC - α-amanitin targeted antibody conjugate

BCMA - B cell maturation antigen

BRCA1 / BRCA 2 - breast cancer gene 1 / breast cancer gene 2

CAR T - chimeric antigen receptor T cell

CD19 - cluster of differentiation 19, B lymphocyte antigen CD 19

c-Myc - avian myelocytomatosis virus oncogene cellular homolog

CRPC - castrate resistant prostate cancer

CTLA-4 - cytotoxic T lymphocyte-associated antigen 4

CYP 17 - cytochrome 17

DNA - deoxyribonucleic acid

DOTA - tetra-aza-cyclododecane-tetraacetic acid

DRE - digital rectal examination

DUPA - 2-[3-1-ureido]pentanedioic acid

EC_{50}- concentration of a compound causing 50 % of response

ECD - extracellular domain

EpCAM- epithelial cell adhesion molecule

FOLH1 - folate hydrolase 1

GCP II - glutamate carboxypeptidase II

HOXB13 - homebox protein B13

IC_{50} - concentration causing 50 % inhibition of the cell growth

IL-2 - interleukin 2

ki67 - marker of cellular proliferation

LHRH - luteinizing hormone releasing hormone

mc - maleimidocaproyl linker

MMAE - monomethyl auristatin E

MMAF -monomethyl auristatin F

MoA - mode of action

MSR-1 - macrophage scavenger receptor 1

NAAG - N-acetyl-L-aspartyl-L-glutamate

NMDA - N-methyl-D-aspartate

NSAA - non-steroidal anti androgen therapy

OATP 1B3 - organic anion transporter isotype 1B3

p53 - tumor protein p53

PAP - prostatic acid phosphatase

PARP - poly ADP ribose polymerase

PCa- prostate cancer

PD-1 - programmed cell death protein 1

PD-L1 - programmed death-ligand 1

PHI - prostate health index

PI3K/AKT/mTOR - Phosphatidylinositol-3-Kinase/Protein Kinase B/ Mammalian Target of Rapamycin signaling pathway

POLR2A- gene encoding RNA Pol II

PSA - prostate specific antigen

PSMA - prostate specific membrane antigen

RNA - ribonucleic acid

RNA Pol II - ribonucleic acid polymerase II

ROS - reactive oxygen species

RP - radical prostatectomy

SMDC - small molecule drug conjugate

TNM - tumor, lymph node, metastasis classification of malignant tumors

TP53 - gene encoding p53

TubB - tubulysin B

TubH - tubulysin B hydrazide

Val-Ala-PAB - valine alanine para-amino benzoic acid linker

Abstract

Prostate cancer remains the 4th most common cancer worldwide and the 2nd most common cancer in men. The Prostate Specific Membrane Antigen (PSMA) attracted a great attention as a target for the development of personalized therapeutics. Out of two PSMA targeted antibody-drug conjugates (ADCs) in clinical development none up to the moment reached the market approval due to limited efficacy or dose limiting toxicities. One of the main limitations in the use of ADCs in solid tumor therapy seems to be restrained tumor penetration due to the high molecular size of this class of therapeutics. In this work a library of small molecule drug conjugates (SMDCs) as an alternative for large molecular ADCs was developed and tested *in vitro* and *in vivo*. As a targeting moiety providing PSMA specificity the well-known PSMA ligand 2- [3-(1, 3-dicarboxy propyl) ureido]pentanedioic acid (DUPA) was used. The targeting moiety was followed by supporting spacer providing DUPA positioning in the PSMA active site and enabling its conjugation to a cytotoxic payload α-amanitin which is the inhibitor of RNA Polymerase II. The inhibition of RNA Polymerase II represents a completely new mode of action distinct to other toxins currently used for ADCs and SMDCs development. The most potent DUPA-α-amanitin conjugates were identified: HDP 30.2284 (bearing Val-Ala-PAB linker), HDP 30.2301 (bearing C_6 non-cleavable linker) and HDP 30.2618 (bearing disulfide mono-hindered linker). Despite of an excellent *in vitro* profile, the lead SMDCs have shown only limited *in vivo* efficacy due to their very short half-life and limited tumor accumulation. In order to improve pharmacokinetic properties, the DUPA targeting moiety and the toxin were conjugated to an Fc portion of human IgG. DUPA-Fc-α-amanitin conjugate showed slightly lower *in vitro* activity compared to the SMDCs. *In vivo* a significantly prolonged half-life and complete tumor remission in PSMA positive LNCaP xenograft model was observed. These results indicate that for highly hydrophilic toxin such as α-amanitin the gradual tumor delivery and accumulation over time is essential for sustainable anti-tumor activity. Describe herein novel DUPA-Fc-α-amanitin conjugate enriches the current landscape of ADCs based on the scaffold with a molecular weight being approximately 60 % smaller than full format IgG. Additionally, DUPA-Fc-α-amanitin retains prolonged half-life which is characteristic for antibodies. Moreover, proposed herein Fc-small molecule-toxin platform creates the opportunity to optimize small-molecule-toxin conjugates with sub-optimal pharmacokinetic profile.

CONTENTS

Contents xv

1. General introduction 1

1.1 Prostate cancer 1

1.1.1 Molecular basis and diagnosis 1

1.1.2 Conventional and novel prostate cancer therapies 2

1.2 Prostate specific membrane antigen 5

1.2.1 PSMA in prostate cancer diagnosis and therapy 8

1.2.2 Anti-PSMA antibody-drug conjugates 9

1.3 Alpha-Amanitin 15

1.3.1 α-Amanitin origin, toxicity profile and molecular mode of action 15

1.3.2 α-Amanitin as a payload for development of antibody drug conjugates 18

1.4 DUPA based Small Molecular PSMA Inhibitors for Prostate Cancer Therapy 21

1.4.1 Discovery of urea-based PSMA inhibitors 21

1.4.2 Structural studies of urea-based inhibitors and PSMA interaction 22

1.4.3 DUPA based small molecule toxin conjugates 25

2. Objectives of the study 29

3. Materials and Methods 31

3.1 Materials 31

3.1.1 Laboratory equipment 31

3.1.2 Laboratory supplies and reagents 32

3.1.3 Buffers 33

3.1.4 Cell culture media 34

3.1.5 Antibodies 35

3.1.6 Cell lines 35

3.1.7 DUPA-α-amanitin conjugates 36

3.1.8 Animals 37
3.1.9 Software 37
3.2 Methods 38
3.2.1 Cell culture 38
3.2.2 Determination of PSMA expression by flow cytometry 39
3.2.3 *In vitro* cytotoxicity assays 39
3.2.4 Plasma stability studies 40
3.2.5 *In vitro* competitive binding assay 41
3.2.6 Western blot 41
3.2.7 Establishment of LNCaP and C4_2 xenograft model 42
3.2.8 Determination of maximum tolerated dose 42
3.2.9 *In vivo* efficacy studies 43
3.2.10 *In vivo* pharmacokinetic and biodistribution study 43
3.2.11 Mechanistic *in vivo* study of α-amanitin kidney accumulation after pre- and co-injection with PMPA 43
3.2.12 Preparation of serum and organ extracts for determination of α-amanitin concentration 44
3.2.13 Establishment of standard curve for detection of α-amanitin containing compounds by Enzyme-Linked Immunosorbent Assay (ELISA) assay 44
3.2.14 Competitive anti α-amanitin ELISA for determining the concentration of α-amanitin containing compounds in mouse serum and organ extracts 45
3.2.15 Establishment of standard curve for determination of serum concentration of DUPA-Fc-α-amanitin conjugate 45
3.2.16 Sandwich ELISA for determination of DUPA-Fc-α-amanitin serum concentration 46
3.2.17 Calculation of conjugates concentration in tissues 46
3.2.18 Statistical analysis 47
4. Results 49

4.1 DUPA -αlpha- amanitin conjugates bearing Val-Ala-PAB cleavable and C_6 non-cleavable linker 49

4.1.1 Establishment of a model for *in vitro* screening of DUPA-α-amanitin conjugates 49

4.1.2 DUPA-α-amanitin compounds –importance of supporting spacer.....50

4.1.3 Optimization of plasma stability 55

4.1.4 Single dose toxicity study of lead conjugates HDP 30.2284 and HDP 30.2301 62

4.1.5 Pharmacokinetic study of conjugates HDP 30.2284 and HDP 30.2301 65

4.1.6 Efficacy study of conjugates HDP 30.2284 and HDP 30.2301 66

4.1.7 Biodistribution study of lead conjugates HDP 30.2284 and HDP 30.2301.....71

4.2 DUPA-αlpha-amanitin conjugates bearing disulfide linker - enabling intracellular release of toxin and concomitant improving of *in vivo* tolerability.....76

4.2.1 Optimization of *in vitro* activity of DUPA-α-amanitin conjugates bearing disulfide linker 76

4.2.2 Single dose tolerability study of lead conjugate bearing disulfide monohindered linker HDP 30.2618 (1:0) 90

4.2.3 Pharmacokinetic study of lead conjugate bearing monohindered disulfide linker HDP 30.2618 (1:0) 91

4.2.4 Efficacy study of lead conjugate bearing disulfide monohindered linker HDP 30.2618 (1:0) 92

4.3 Optimization of the pharmacokinetic properties of DUPA -αlpha-amanitin conjugates - limiting kidney accumulation and prolongation of circulatory half-life.....95

4.3.1 Adapting strategy aiming to limit kidney accumulation - DUPA-α-amanitin conjugate bearing $(His\text{-}Glu)_2$ motif.....96

4.3.1.1 *In vitro* activity of small molecular weight DUPA-α-amanitin conjugate bearing $(His\text{-}Glu)_2$ linker HDP 30.2594..... 97

4.3.1.2 Head to head comparison of blood pharmacokinetics and kidney accumulation of HDP 30.2284 and an analogue bearing $(His\text{-}Glu)_2$ motif HDP 30.2594..... 98

4.3.2 Viable and ultimate strategy providing prolongation of half-life - DUPA-α-amanitin conjugate presenting human IgG1 Fc portion in the structure (DUPA-Fc-α-amanitin conjugate) 100

4.3.2.1 *In vitro* cytotoxicity and plasma stability of DUPA-Fc-α-amanitin conjugate 101

4.3.2.2 Determination of maximum tolerated dose for DUPA-Fc-α-amanitin conjugate 107

4.3.2.3 Determination of pharmacokinetic profile of DUPA-Fc-α-amanitin conjugate 108

4.3.2.4 Biodistribution study of DUPA-Fc-α-amanitin conjugate 109

4.3.2.5 *In vivo* efficacy study of DUPA-Fc-α-amanitin conjugate 111

5. Discussion and outlook 115

5.1 Impact of linker and conjugation strategy on *in vitro* activity and plasma stability of DUPA-αlpha-amanitin conjugates 115

5.1.1 Conjugates bearing Val-Ala-PAB cleavable linker and C_6 non-cleavable linkers 115

5.1.2 Compounds bearing disulfide linker 118

5.1.3 *In vitro* activity of conjugates aiming into the limitation of kidney accumulation - HDP 30.2594 and prolongation of pharmacokinetic profile - DUPA-Fc-α-amanitin 120

5.1.4 Summary of *in vitro* results 121

5.2 Impact of the linker strategy on *in vivo* tolerability of DUPA-alpha-amanitin conjugates 123

5.3 Biodistribution of DUPA-αlpha-amanitin conjugates 126

5.4 Impact of linker strategy and pharmacokinetic profile on *in vivo* efficacy 132

5.5 Conclusions and further strategies for DUPA-αlpha-amanitin conjugates optimization 137

6. Summary 141

7. Appendices and supplementary figures 145

8. References 153

LIST OF FIGURES

Figure 1.1 Crystal structure of PSMA with indicated both catalytic activities. 6

Figure 1.2 Schematic presentation of enzymatic cleavage cycle of NAAG by PSMA active site as resolved by crystallographic study. 7

Figure 1.3 Schematic presentation of main ADC components, internalization process and toxin release. 9

Figure 1.4 Structures of anti-PSMA antibody drug conjugates which underwent or are currently undergoing the clinical evaluation. 13

Figure 1.5 Chemical structures of amatoxins. 16

Figure 1.6 Structure of α-amanitin with positions suitable for the linker attachment. 18

Figure 1.7 Chemical structure of NAAG (N-Acetylaspartylglutamic acid), 2-PMPA (2-(Phosphonomethyl)-pentandioic acid) and DUPA (2-[3(1,3-dicarboxypropyl) ureido] pentanedioic acid. 22

Figure 1.8 PSMA cross section demonstrating the different interactions of three urea-based inhibitors with the PSMA entrance tunnel and PSMA active site. 23

Figure 1.9 Influence of supporting spacer structure on the activity of Glu-ureido based - DOTA conjugates for cancer imaging and therapy 24

Figure 1.10 Optimization of supporting spacer in DUPA - Tubulysin conjugates. 26

Figure 3.1 Schematic presentation of western blot transfer apparatus (Bio-Rad) and stacking of transfer components 41

Figure 4.1 Flow cytometry analysis of PSMA receptor expression in LNCaP (PSMA +++), 22RV1 (PSMA+) and PC3 (PSMA -) cell lines. 50

Figure 4.2 Chemical structures of HDP 30.1585 and HDP 30.1592. 51

Figure 4.3 Cytotoxic potential of HDP 30.1585 and HDP 30.1592 on LNCaP (PSMA +++), 22RV1 (PSMA +) and PC3 (PSMA -) cell lines. (IC_{50} is presented as median cell survival ± SEM, n=3). 52

Figure 4.4 Chemical structures of HDP 30.2284 and HDP 30.2301. 53

Figure 4.5 Cytotoxic potential of compounds HDP 30.2284 (Val-Ala-PAB) (upper panel), HDP 30.2301 (C_6 non-cleavable linker) (lower panel) and α-amanitin on LNCaP (PSMA +++), 22RV1 (PSMA +) and PC3 (PSMA -) cell lines. (IC_{50} is presented as median cell survival ± SEM, n=3). 54

Figure 4.6 Chemical structures of conjugates synthesized using acetamide chemistry: HDP 30.2515 (Val-Ala-PAB linker) and HDP 30.2523 (C_6 non-cleavable linker). 56

Figure 4.7 Cytotoxic potential of analogues synthesized using maleimide chemistry (in red) HDP 30.2284 and HDP 30.2301 and acetamide chemistry (in blue) HDP 30.2515 and HDP 30.2523. 57
Figure 4.8 Cytotoxic potential of maleimide and acetamide analogues bearing Val-Ala-PAB cleavable linker. 58
Figure 4.9 Cytotoxic potential of maleimide and acetamide DUPA-α-amanitin analogues bearing C_6 stable linker. 60
Figure 4.10 Tolerability of HDP 30.2284 measured as relative body weight change after single dose administration (Cb 17 Scid male mice, relative body weight ± SEM, n=3). 62
Figure 4.11 Tolerability of HDP 30.2301 measured as relative body weight change after single dose administration (Cb 17 Scid male mice, relative body weight ± SEM, n=3). 64
Figure 4.12 Pharmacokinetic profile and half-life of HDP 30.2284 and HDP 30.2301 in Cb 17 Scid male mice (median concentration ± SEM, n=3). 65
Figure 4.13 In vivo evaluation of antitumor activity of HDP 30.2284in Cb17 Scid mice xenografted with LNCaP tumors. 67
Figure 4.14 In vivo evaluation of antitumor activity of HDP 30.2301 in Cb 17 Scid mice xenografted with LNCaP tumors. 69
Figure 4.15 In vivo evaluation of antitumor activity of HDP 30.2284 and HDP 30.2301 in Cb17 Scid mice xenografted with C4_2 tumors at the optimized dosing regimen. 70
Figure 4.16 Biodistribution study of HDP 30.2284. 71
Figure 4.17 Concentrations of HDP 30.2301 in tumor, kidney and liver in Cb17 Scid male mice xenografted with LNCaP tumors. 73
Figure 4.18 Determination of kidney concentrations of conjugates HDP 30.2284 and HDP 30.2301 after pre and co-injection with 2-PMPA. 74
Figure 4.19 Schematic presentation of disulfide linker cleavage and toxin release by intracellular glutathione (GSH). 76
Figure 4.20 Chemical structure of DUPA-α-amanitin conjugates bearing disulfide linker featuring different levels of disulfide bond hindrance. 77
Figure 4.21 Dose-response cytotoxicity curves of conjugates bearing disulfide linker in three prostate cancer cell lines LNCaP (PSMA +++), 22RV1 (PSMA +) and PC3 (PSMA -). 78
Figure 4.22 Plasma stability results of HDP 30.2246 (0:0) in LNCaP cells (PSMA +++). MP -mouse plasma, HP- human plasma.80**Figure 4.23** Plasma stability results of HDP 30.2589 (0:1) in LNCaP cells (PSMA +++). MP -mouse plasma, HP- human plasma. 82
Figure 4.24 Plasma stability results of HDP 30.2609 (2:0) on LNCaP cells (PSMA +++). MP-mouse plasma, HP-human plasma. 84

Figure 4.25 Plasma stability results of HDP 30.2618 (1:0) on LNCaP cells (PSMA +++). MP -mouse plasma, HP- human plasma. 86
Figure 4.26 Plasma stability results of HDP 30.2619 (1:1) in LNCaP cells (PSMA +++). MP -mouse plasma, HP- human plasma. 88
Figure 4.27 Tolerability of compound HDP 30.2618 (1:0) after single dose administration. 91
Figure 4.28 Pharmacokinetic profile and half-life of HDP 30.2618 (1:0). 92
Figure 4.29 Efficacy and tolerability of the therapy with HDP 30.2618. 93
Figure 4.30 Schematic presentation of IgG uptake and recycling via FcRn receptor. 96
Figure 4.31 Chemical structure of compound HDP 30.2594. 97
Figure 4.32 Cytotoxic potential of compound HDP 30.2594 on LNCaP (PSAM +++), 22RV1 (PSMA+) and PC3 (PSMA -) prostate cancer cell lines. 97
Figure 4.33 Head to head comparison of blood pharmacokinetics and kidney biodistribution of HDP 30.2284 (administered dose 0.184 mg/kg) and HDP 30.2594 (administered dose 0.149 mg/kg) after single dose i.v. injection. 99
Figure 4.34 Schematic presentation of the DUPA-Fc-α-amanitin conjugate structure. 101
Figure 4.35 Cytotoxic potential of the DUPA-Fc-α-amanitin conjugate on three prostate cancer cell lines expressing different levels of PSMA: LNCaP (PSMA +++), 22RV1 (PSMA +) and PC3 (PSMA -). 102
Figure 4.36 Plasma stability of DUPA-Fc-α- amanitin conjugate**.** 103
Figure 4.37 Determination of cytotoxic potential of DUPA-Fc-α-amanitin conjugate after stressing in three different matrices in LNCaP (PSMA +++) cells. 105
Figure 4.38 In vivo tolerability of DUPA-Fc-α-amanitin conjugate (Cb 17 Scid mice, n=3). 108
Figure 4.39 Serum concentration and half-life of DUPA-α-amanitin conjugate (shown is median concentration ± SEM, Cb17 Scid male mice, n=3). 109
Figure 4.40 Biodistribution study of DUPA-Fc-α-amanitin and released toxin after single dose administration of 1 mg/kg in the tumor, liver and kidney extracts. 110
Figure 4.41 Antitumor activity of DUPA-Fc-α-amanitin conjugate in LNCaP xenografts (PSMA +++). 112

Figure 5.1 1) Maleimide chemistry and alternative **2)** acetamide chemistry as the strategy to avoid retro Michael reaction and improve plasma stability of conjugates. 117

LIST OF MOST IMPORTANT TABLES

Table 4.1 Dose of HDP 30.2284 used in MTD study with indicated equivalents of α-amanitin. 62

Table 4.2 Doses of HDP 30.2301 used in MTD study with indicated equivalents of α-amanitin..... 65

Table 4.3 Tabulated summary of IC_{50} values of DUPA-α-amanitin conjugates bearing disulfide linker in three prostate cancer cell line LNCaP (PSMA +++), 22RV1 (PSMA +) and LNCaP (PSMA -). 79

Table 4.4 IC_{50} summary -plasma stability results of HDP 30.2246 (0:0) in LNCaP cells (PSMA +++).81

Table 4.5 IC_{50} summary -plasma stability results of HDP 30.2589 (0:1) in LNCaP cell line (PSMA +++). 82

Table 4.6 IC_{50} summary - plasma stability results of HDP 30.2609 (2:0) on LNCaP cells (PSMA +++). 85

Table 4.7 IC_{50} summary - plasma stability results of HDP 30.2618 (1:0) on LNCaP cells (PSMA +++). 86

Table 4.8 IC_{50} summary - plasma stability results of HDP 30.2619 (1:1) on LNCaP cells (PSMA +++). 89

Table 4.9 Dose of HDP 30.2618 used in MTD study with indicated equivalents of α-amanitin. 91

Table 4.10 Summary of the in vitro stability results cytotoxic potential of DUPA-Fc-α-amanitin conjugate upon stressing in human plasma mouse plasma and PBS in LNCaP cell line (PSMA +++). 106

Table 4.11 Dose of DUPA-Fc-α-amanitin used in MTD study with indicated equivalents of α-amanitin 108

Table 5.1 Selected from the literature examples demonstrating similar or lower in vitro activity of SMDCs compared to unconjugated toxin..... 122

Table 5.2 Maximal tolerated doses of conjugates in Cb 17 Scid mice with indicated corresponding equivalents of α-amanitin dose (n = 3)..... 124

1. GENERAL INTRODUCTION

1.1 PROSTATE CANCER

1.1.1 Molecular basis and diagnosis

The prostate is a male hormone responsive organ located between urethra and bladder. It can be affected by the three common pathologies: 1) prostatitis 2) benign prostatic hyperplasia and 3) malignant cancer. Prostate cancer (PCa) is diagnosed in about a million of men each year and is the 4th most deadly cancer amongst all neoplastic diseases with ca. 300 000 related deaths each year [1, 2].

Although, the etiology of PCa is not totally understood, some of the epigenetic and genetic factors are clearly correlated with the occurrence of this disease. The age was identified as the most common risk factor for PCa development. The frequency of the disease in man above 50 years old was determined to be only 0.1 %. Between the age of 50 and 65 this risk starts to grow steadily and achieves maximum at the age above 65. It was estimated that 85 % of prostate cancer cases were diagnosed in man at this age. Besides age the other identified epigenetic factors related to PCa incidence were diet, especially the consumption of red meat and dairy products and lifestyle risk factors such as smoking and alcohol consumption [3]. Moreover, the studies have shown important differences in PCa incidence between various geographical regions [4]. It is not clearly defined whether the differences observed in the various geographical regions are due to the epigenetic factors or are rather gene related. It is also suggested that differences in the incidence of diagnosis might be related to socio-economic factors [5-7].

Besides epigenetic factors also numerous genes involved in the pathogenesis of PCa were identified. Due to genetic complexity of neoplastic diseases it is impossible to describe herein all genetic alterations related with the PCa incidence. Amongst most commonly described are: deleterious germline mutation of *BRCA2* typical for hereditary type of disease which increases the relative risk of prostate cancer before the age of 60 by 5–23 folds [8, 9], mutation in the DNA sequence encoding homebox protein B13 (*HOXB13)* which normally plays an important role in the urogenital development and acts as a tumor suppressor gene, or *c-myc* amplification which positively correlates with the Gleason score [10]. The genetic mutations, beyond involvement in the molecular mechanisms promoting the PCa

progression, might be additionally involved in the resistance to the therapy. One of such examples is a truncating mutation of the ligand binding domain of Androgen Receptor (AR) responsible for the lack of response to a very important therapeutic option for PCa patients, the anti-androgen therapy. Besides of resistance to the therapy, this particular mutation in AR was shown to be clearly related with PCa progression [11].

Current advancements in the determination of molecular basis of PCa create new opportunities for the exploitation of novel methods for early detection, diagnosis and development of new personalized therapeutic options based on the molecular profile of the disease.

1.1.2 Conventional and novel prostate cancer therapies

The choice of the most suitable therapy for PCa management strongly depends on the stage of the disease at the moment of diagnosis. Patients diagnosed at early stages with asymptomatic, local and non-disseminated small tumor undergo active surveillance which is based on the regular determination of PSA levels and digital rectal examinations (DRE). Curative treatment options are recommended in the cases of metastatic risk or locally advanced tumors and include radical prostatectomy followed by post-operative radiotherapy [11]. Commonly prostatectomy besides of radiation therapy is followed by androgen deprivation therapy (ADT), which is known as medical or chemical castration. There are two main groups of drugs used in ADT. The mode of action of the first group is based on the luteinizing hormone-releasing hormone (LHRH) agonists. The second group are LHRH antagonists which compared to LHRH agonists lead to more effective and faster decrease of androgens produced by testicles. Although initially all patients tend to respond to the hormonal ADT, the duration of the response is limited and followed by the progression to castrate resistant prostate cancer (CRPC). One of the reasons of ADT resistance is the expression of a truncated version of androgen receptor (AR) which is constitutively active and capable of regulation of the genes involved in the progression of the disease. It was shown that the expression levels of aberrant AR version were nearly 20 times higher in CRPC compared to hormone sensitive prostate cancer [12]. The newer class of androgen deprivation therapeutics consists of cytochrome 17 (CYP 17) inhibitors which are aiming into the inhibition of androgens biosynthesis and biological functions are commonly combined with corticosteroids (dexamethasone or prednisolone) which relieve the signs of pain, edema and inflammation [13].

As the disease progresses to metastatic CRPC, patients are treated with systemic chemotherapy with docetaxel, carbazitaxel or mitoxantrone [14-16]. Bone metastases often appearing at this stage of the disease are commonly treated with ^{223}Radium-bone targeted alpha-emitter which is a form of palliative care often combined with oral administration of bisphosphonates to delay the occurrence of first skeletal events such as spinal cord compressions and fractures.

Unfortunately, the majority of commonly used PCa therapies fail to show the expected efficacy, significantly prolong the patient's survival and improve their quality of life. None of the aforementioned therapeutic options is considered to be curative and virtually the majority of patients will progress to CRPC and further to metastatic PCa. Ideally, therapeutic options including drugs with new modes of action (MoA) should be offered at the earlier stages of the disease, when the chances for improvement and response rates are higher. There is still a huge room for an improvement in the PCa care.

Some of the examples of therapeutics with the new modes of action already approved or currently undergoing the clinical evaluation are given below.

The latest FDA approval of non-steroidal anti-androgen (NSAA) Apalutamide drawn a special attention to the new class of oral androgen receptor antagonists. Apalutamide is a silent antagonist of AR and demonstrated higher anti-androgenic activity and several-fold reduced central nervous system distribution in comparison with second generation anti-androgens e.g. Enzalutamide. A Placebo controlled study has shown that Apalutamide improved metastasis free survival by 24 months compared to placebo and significantly improved the time to symptomatic progression in CRPC [17, 18].

The phosphatidylinositol-3-kinase (PI3K)/AKT and mammalian target of rapamycin (mTOR) signaling pathway (PI3K/AKT/mTOR pathway) was shown to be essential for the regulation of cell cycle. Involvement of this signaling pathway in the progression of PCa was demonstrated in numerous studies [19, 20]. The inhibition of PI3K/AKT/mTOR signaling pathway showed to be positively correlated with androgen receptor expression and partially restored the sensibility for anti-androgen therapy. Particularly the AKT inhibitor AZD5363 (AstraZeneca) and the Phosphatidylinositol-4,5-bisphosphate 3-kinase (PI3K) beta/delta inhibitor AZD8186 (AstraZeneca) demonstrated significant antitumor activity in pre-clinical models in combination with androgen deprivation therapy [21]. AZD8186 is undergoing clinical evaluation in the therapy of solid tumors including PCa (ClinicalTrials.gov Identifier: NCT01226316).

Poly ADP ribose polymerase (PARP) is a family of proteins which plays a key role in the coordination of single strain DNA breaks, by recruitment of DNA repairing enzymes. The fact that >20 % PCas demonstrate a somatic DNA repair gene defect makes a logical rationale for the use of PARP inhibitors in PCa therapy [22]. Olaparib- a PARP inhibitor clinically approved for the therapy of hereditary breast and ovarian cancer with BRCA1/BRCA2 mutation was tested in a Phase II clinical study in metastatic PCa patients which were unresponsive to the standard of care. In this group of patients the response rate was evaluated for 33 % [23, 24].

The first of the clinically approved immunotherapies for the treatment of prostate cancer was Stipulcel-T- a dendritic cell-based vaccine. The patient's dendritic cells are isolated using leukapheresis and subsequently fed with an antigen found in 95 % of PCa cases -prostatic acid phosphatase (PAP)[25]. Dendritic cells recognizing PAP are amplified and infused back into the patient to induce the immune response against PAP expressing PCa cells. Stipulcel-T has demonstrated a long-lasting clinical benefit over placebo with very little side effects. Unfortunately, Stipulcel-T clinical use is limited due to the laborious and costly infusion preparation [26].

Recently especially high attention is given to immune checkpoint inhibitors which were shown to be efficacious in the treatment of malignancies such as advanced melanoma, advanced non-small cell lung carcinoma or Hodgkin lymphoma [27]. Cytotoxic T-Lymphocyte-Associated protein 4 (CTLA-4, CD152) is a key negative regulator of T cell activation. An anti CTLA-4 antibody ipilimumab demonstrated complete response in limited number of cases of mCRPC patients. The recently released placebo controlled study in a larger cohort demonstrated improvement in progression free survival, but no effect of ipilimumab on the overall survival in advanced PCa patients [28]. A number of clinical studies aiming into understanding whether the use of anti CTLA-4 antibody in combination with the standard of care in PCa patients can improve the response rate is currently ongoing [29].

The second immune checkpoint inhibitor - an antibody directed against programmed death-ligand 1 (PD-1, CD279)–pembrolizumab activates the immune response [29]. The clinical evaluation of pembrolizumab in combination with radiotherapy in PCa is currently ongoing [18].

Prostate Specific Membrane Antigen (PSMA) is a validated target for PCa therapy. PSMA targeting is a main topic of this thesis, and in the next chapter special attention will be given to the structure of this protein and PSMA targeted delivery of toxins in the prostate cancer therapy. Here only one example of a new PSMA targeted chimeric antigen receptor-engineered T (CAR T) undergoing clinical evaluation is discussed.

CAR T cell therapy relies on the isolation of patient T cells and their transduction most commonly with a lentiviral vector encoding chimeric receptor which recognizes an antigen presented on the cancer cells. Modified T cells more efficiently recognize neoplastic cells and induce specific anti-tumor response after infusion into the patient. Although in a phase I clinical trial patients treated with PSMA targeted CAR T cells demonstrated 20 % of responses, the efficacy of the treatment was limited due to the depletion of interleukin 2 (IL-2) which is necessary for CAR T cell expansion and survival [30]. Currently the optimization of CAR T PSMA targeted therapy in clinical setting is ongoing. Although CAR T therapy is promising option for PSMA positive PCa therapy, it brings certain challenges related to the manufacturing costs and requirement of preparation of infusion for each patient individually [31]. Thus, more viable option giving an access to the off-the-shelf product seem to be PSMA targeted antibody drug conjugate or alternatively a small molecule drug conjugate.

1.2 PROSTATE SPECIFIC MEMBRANE ANTIGEN

Prostate-specific membrane antigen (PSMA) is physiologically expressed in prostate [32], proximal tubules of the kidney [33], brain, small intestine, lacrimal and salivary glands [34]. PSMA is encoded by the folate hydrolase 1 (*FOLH1)* gene, and is a 750 amino acid, membrane associated type II glycoprotein with a predicted molecular weight of 84 kDa. The intracellular PSMA domain consists of 19 amino acids at the amino terminal region of the protein, which is followed by a single 22 amino-acid transmembrane domain and a large 709 amino acid extracellular domain (ECD). There are 9 potential glycosylation sites in the extracellular domain of PSMA and carbohydrates constitute for approximately 20-25 % of additional PSMA molecular weight (apparent molecular weight of PSMA is approximately 110 kDa). Glycosylation of ECD was shown to be necessary for proper PSMA folding and full enzymatic activity of the receptor [35]. The extracellular part of PSMA is further divided into the three domains: 1) protease domain (residues 57-116 and 352-590, in green *Figure 1.1*), 2) apical domain (residues 117-351 in dark blue *Figure 1.1*), which constitutes an insert between two protease domains, and 3) C-terminal domain (591-750 in yellow *Figure 1.1*). All three domains are involved in the substrate recognition. PSMA forms a dimer with the interface between two units located at C-terminal domain (in yellow *Figure 1.1*) [35, 36].

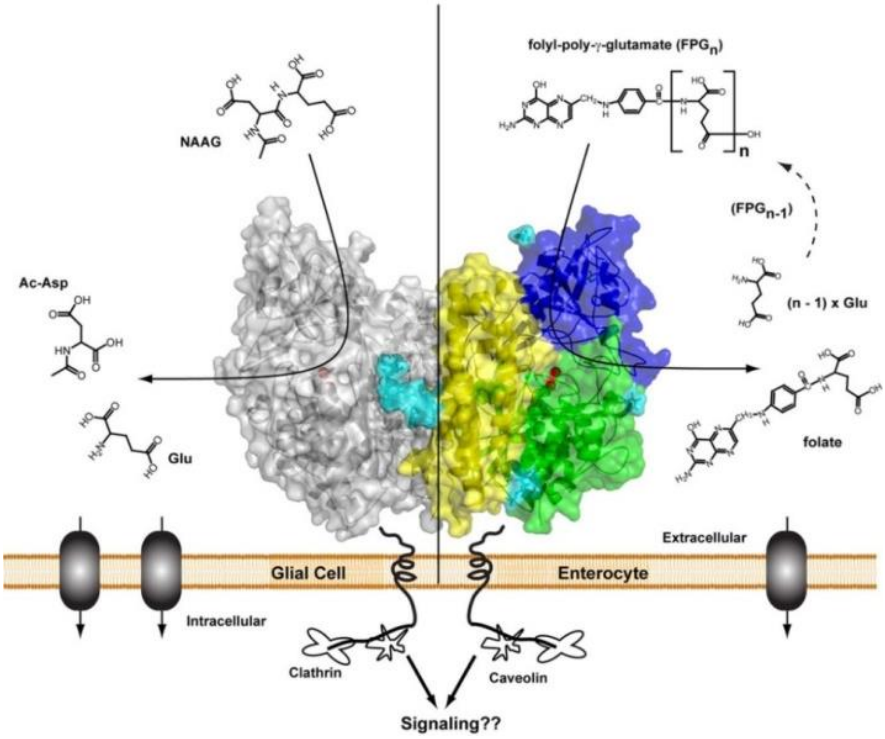

Figure 1.1 Crystal structure of PSMA with indicated both catalytic activities.

> **Left panel:** N-acetyl-L-aspartyl-L-glutamate (NAAG) hydrolytic activity of PSMA characteristic for the central nervous system. **Right panel:** folate hydrolase 1 (FOLH1) activity presented mainly in the gastrointestinal tract. Both activities are based on the catalytic hydrolysis of γ-glutamates from the indicated substrates. The figure was taken from [35].

PSMA presents two major enzymatic activities: 1) folate hydrolase 1 (FOLH1) in the gastrointestinal tract and 2) glutamate carboxypeptidase II (GCP II) in the central nervous system. Both are based on the catalytic hydrolysis of γ-glutamates from substrates such as poly-γ-glutamated folic acid or N-acetyl-L-aspartyl-L-glutamate (NAAG) (*Figure 1.1*). Physiologically PSMA expression is restricted to the small intestine brush border where the folate hydrolase plays an important role in enabling the intestinal transport of dietary folic acid through the hydrolysis of polyglutamated dietary folate - vitamin B_9 (Right panel of *Figure 1.1*). Additionally, PSMA is found in the central nervous system where it catalyzes the hydrolysis of the *N*-acetyl-L-aspartyl-L-glutamate (NAAG) to *N*-acetyl-L-aspartate and L-glutamate (Left panel of *Figure 1.1* and *Figure 1.2*) with the latter being the most common neurotransmitter in the central nervous system [35].

The active site of the PSMA is localized in the cavity which might be reached *via* 20 Å entrance tunnel-like structure [37]. The cycle of NAAG hydrolysis on the molecular level

involving the active site of PSMA and a water molecule is presented in *Figure 1.2*. The arginine patch (Arg-463, Arg-534 and Arg-536) is involved in the correct positioning of the substrate for catalysis by interacting with negatively charged C-terminal glutamate residue. The Arg-210 situated on the opposite site of the cavity supported by Asn-519 is also involved in recognition and positioning of the substrate (*Figure 1.2*). Glu-424 is an active site of the PSMA and one of its carboxylate oxygens is bound to the hydrogen in the water molecule. Two zinc atoms at the active site are bridged by the β-carboxylate of Asp-387 and coordinated by the side chains of His-377, Glu-425, Asp-453 and His-553 (*Figure 1.2*). Glu-424 is involved in the deprotonation of water molecule bound to two zinc atoms. In this state the water molecule is activated and ready for nucleophilic attack of NAAG or another substrate peptide bond leading to cleavage and product dissociation (*Figure 1.2*) [36].

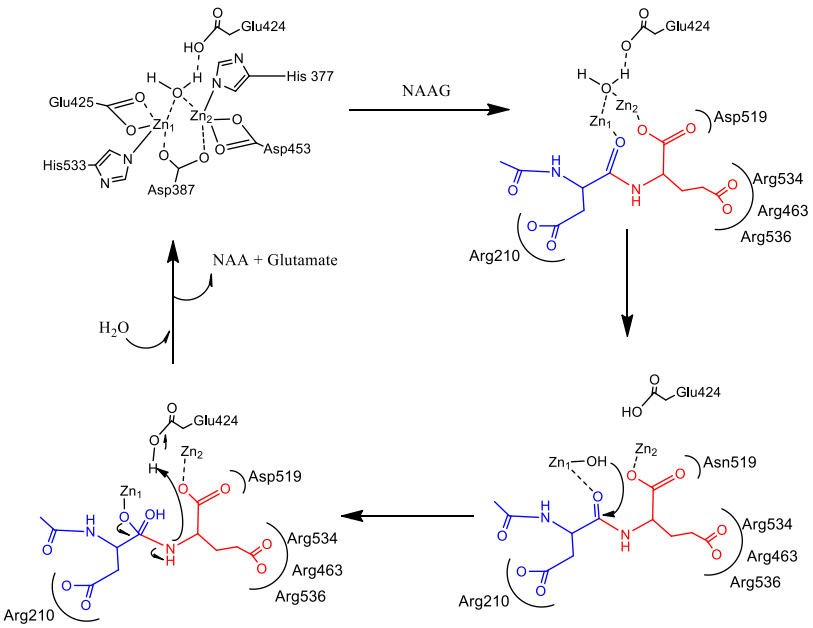

Figure 1.2 Schematic presentation of enzymatic cleavage cycle of NAAG by PSMA active site as resolved by crystallographic study.

Description in the text above. The figure was re-drawn from [36].

Importantly, the structural studies of natural substrates interaction with PSMA allowed for the design of ligands which can be used as inhibitors of PSMA enzymatic activity in neurological diseases or PCa therapy and diagnosis. The discovery of these molecular entities and their therapeutic applications will be discussed in detail in section 1.4.

1.2.1 PSMA in prostate cancer diagnosis and therapy

PSMA is overexpressed in 90 % of prostate carcinomas. The high PSMA expression correlates with PCa aggressiveness, is increased in metastatic disease and implies the resistance to androgen therapy. The reason of PSMA expression in PCa is currently not completely understood but it is suggested that increased demand for folates necessary for DNA synthesis of quickly proliferating prostate cancer cells may play an important role [38]. Although PSMA is present in normal prostatic epithelium, the expression in PCa is reported to be ca. 1000 times higher compared to physiological tissue [39, 40]. PSMA is abundantly expressed not only in metastatic PCa but also in castrate-resistant prostate cancer (CRPC). All aforementioned properties make PSMA an excellent target for therapy. Three main groups of PSMA targeted diagnostics/therapeutics are: 1) radio-imaging-agents, 2) radio-therapeutics and 3) PSMA targeted antibody drug conjugates (ADCs) or small molecule drug conjugates (SMDCs).

Initially anti-PSMA monoclonal antibodies were employed in prostate cancer radio-imaging. The first anti-PSMA agent for immune-scintigraphy - ProstaScint® (Cytogene Corporation) is a murine monoclonal antibody (7E11/CYT 356, capromab) labeled with Indium-111 (^{111}In) [41]. ProstaScint® recognizes the intracellular domain of PSMA and detects only necrotic or apoptotic cancer cells what limits the sensitivity of radioimaging using this compound. To improve this property a second generation anti-PSMA antibody - J591 which recognizes the extracellular domain of PSMA was developed (Weill Cornel Medical College). J591 was conjugated to tetraazacyclododecane-tetraacetic acid (DOTA) - a chemical chelator- and subsequently labeled with ^{111}In. The imaging of PCa using this agent demonstrated an improved sensitivity compared to ProstaScint®[41]. Although antibodies represent a great potential for tumor targeting, their long half-life led to a poor contrast at early imaging time points and poor tumor penetration particularly for bone metastases commonly found in advanced stages of the PCa. Anti-PSMA antibodies are currently displaced by small molecular PSMA targeted urea based binders which provide preferential pharmacokinetic profile, biodistribution and imaging contrast [37]. Although antibody format represents certain limitations it remains the preferential format applied in the development of PSMA targeted toxin delivery discussed in detail in the next section.

1.2.2 Anti-PSMA antibody-drug conjugates

The key goal of targeted cancer therapy is to develop agents that can effectively eradicate the tumor and concomitantly spare the normal tissue. Antibody drug conjugates (ADCs) combine the high tumor selectivity of the antibodies and the high anti-tumor potency of small molecular cytotoxic agents (payloads). The third important component of ADC is a linker providing covalent binding between toxin and antibody recognizing targeted antigen. Upon binding the ADC-receptor complexes are internalized *via* receptor mediated endocytosis (*Figure 1.3*). PSMA undergoes mainly clathrin mediated internalization which is the desired pathway for ADC uptake [42].

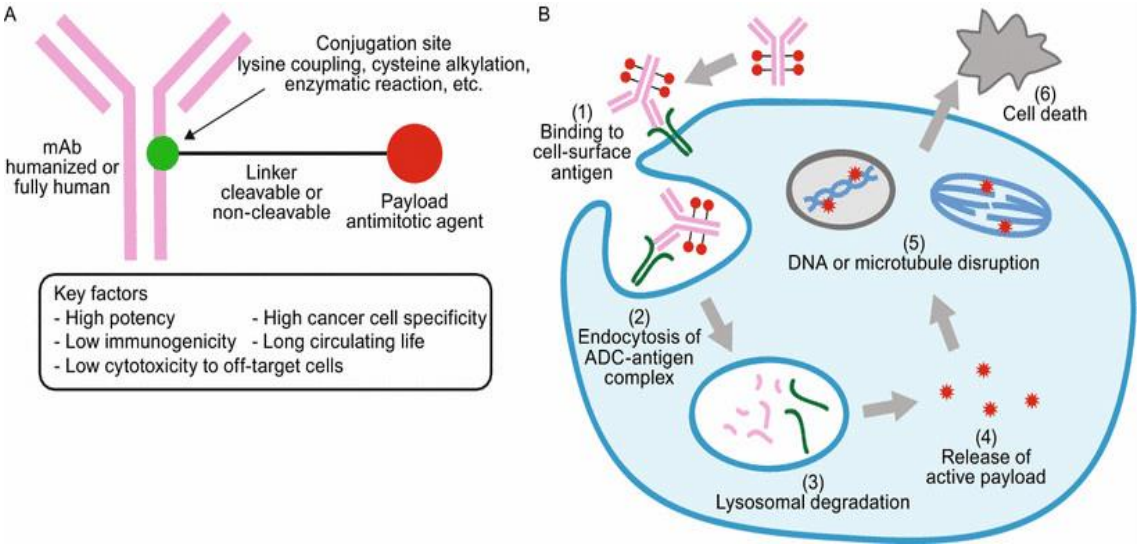

Figure 1.3 Schematic presentation of main ADC components, internalization process and toxin release.
A. The structure of the ADC indicating its three main components: antibody, linker and toxin;
B. Internalization and intracellular mechanism of action for microtubule inhibitors-based ADCs. Figure was taken from [43].

It was also demonstrated that PSMA interacts with Filamin A, which directs PSMA into the endosomal recycling compartment [42]. Despite of clathrin mediated internalization PSMA udergoes caveolin mediated PSMA endocytosis which appears mainly in the PSMA expressing cells of microvascular endothelium [44]. Additionally, it was demonstrated that PSMA is three times more efficiently internalized upon antibody binding compared to internalization of receptor in the absence of antibody ligand. The aforementioned PSMA properties and almost exclusive PSMA overexpression in PCa make a strong rationale for the development of anti-PSMA targeted ADCs [42].

The most commonly used payloads in the development of PSMA targeting ADCs are: 1) microtubule targeting agents, particularly the maytansinoid derivative DM-1 and monomethyl auristatin MMAE, 2) DNA crosslinking pyrrolobenzodiazepine monomers and dimers, 3) DNA alkylators such as duocarmycins and 4) the RNA polymerase II inhibitor: α-amanitin. These toxins cannot be administered in their native form in cancer therapy due to very narrow therapeutic widow.

The linker strategy has shown to play a crucial role in the ADCs activity. In general, there are two main types of linker strategies applied in the ADC technology:

1) Non-cleavable linkers which allow for the release of the toxin only after the lysosomal degradation of the ADC scaffold:
    a. thioether linker
    b. maleimidocaproyl (mc) linker
2) Cleavable linkers which prevent pre-mature release of toxin in extracellular environment yet designed to enable efficient payload release at the target site upon receptor mediated endocytosis:
    a. enzymatically cleavable linkers – mainly cathepsin B recognized motifs (Valine-Alanine), (Valine-Citrulline), followed by p-aminobenzoic acid for self-immolation and release of the toxin in the native form
    b. disulfide linkers cleaved by intracellular reductases, mainly glutathione
    c. acid labile linkers such as hydrazone cleaved in acidic pH of lysosomes

The linkers most commonly employed in the development of anti-PSMA ADCs are cleavable ones particularly the disulfide and cathepsin B motifs [45-47].

Initially PSMA was used as a target for the development immunotoxins based on a toxins of natural origin such a ricin [48]. Although, different strategies were applied in the development of PSMA targeted therapeutics in order to give a sufficient background for introduction of presented herein research work only ADCs based on small molecular toxins will be discussed below.

The first anti-PSMA targeted antibody-toxin conjugate was based on a deimmunized version of the J591 antibody, which was reacted with N-succinimidyl 4-(2-pyridyldithio)pentanoate (SPP) and subsequently coupled to DM1 resulting in disulfide linkage between toxin and antibody yielding MLN2704 (Millenium Pharmaceuticals) (*Figure 1.4* A). In MLN2704 the disulfide linker is hindered by a methyl group on the carbon directly neighboring with the antibody side. Introduction of steric hindrance is a commonly used strategy allowing

to increase the disulfide bond stability and prevent premature release of the toxin before reaching the target on the cell surface [45]. Moreover, it was demonstrated that the introduction of a steric hindrance around disulfide bond had a major impact on plasma stability and conjugate efficacy *in vivo* [49]. MLN2704 was tested *in vitro* in three clones of 22RV1 prostate cancer cell line expressing different levels of PSMA. The activity of MLN2704 varied accordingly to the levels PSMA expression and was ranging between 0.2-20 nM. In *in vivo* experiments the anti-tumor activity of MLN2704 in PSMA positive CWR22 model was dose dependent. Complete tumor regression was observed only at the highest tested dose - 60 mg/kg, but anti-tumor effect was not sustained after therapy cessation as the tumors started to re-grow 6 weeks upon last administration. MLN2704 was shown to deplete the bone metastases by 80 % in 22RV1 metastatic model [45]. Altogether collective preclinical data showed anti-tumor activity without apparent toxicities what supported further clinical studies of this compound. Unfortunately, after phase II study development of MLN2704 was discontinued due to disulfide linker instability and rapid deconjugation. Especially the last feature of MLN2704 led to significant neurotoxicity and a narrow therapeutic window related to the free payload [50].

The second PSMA targeted ADC which entered clinical development combines MMAE and full human anti-PSMA IgG conjugated *via* Val-Cit-PAB linker (Progenics Pharmaceuticals) (*Figure 1.4* B). The anti-PSMA antibody was produced by immunization of XenoMouse and recognizes an antigen on the interface of the PSMA receptor dimer (*Figure 1.1*). MMAE was conjugated to the interchain cysteines of the antibody using maleimide coupling. In *in vitro* assays the conjugate demonstrated high cytotoxic potential with IC_{50} values in the picomolar range of concentration. Preclinical efficacy was shown in disseminated C4-2 xenografts with the dose 6 mg/kg leading to complete tumor regression in 40 % of animals which lasted up to 500 days. Moreover, the activity of this conjugate was demonstrated in docetaxel acquired resistance model [46]. Phase I clinical study of PSMA-MMAE ADC was carried out in metastatic cancer patients and demonstrated good tolerability and reductions in PSA and circulating tumor cells levels [51, 52] but in the following phase II study this ADC demonstrated limited antitumor activity [53]. Lately analogous to the clinically evaluated conjugate was tested in various preclinical xenograft models. The results obtained in this non-clinical studies suggest that the PSMA expression was probably not a good predictor of the clinical response [54]. It suggests that besides of targeted antigen density other important factors are involved in the treatment outcomes.

Due to the limited clinical efficacy and unacceptable toxicities of the aforementioned conjugates new toxins such as pyrrolobenzodiazepine dimers (PBDs) or α-amanitin are employed in the preclinical and clinical development of PSMA-targeting ADCs.

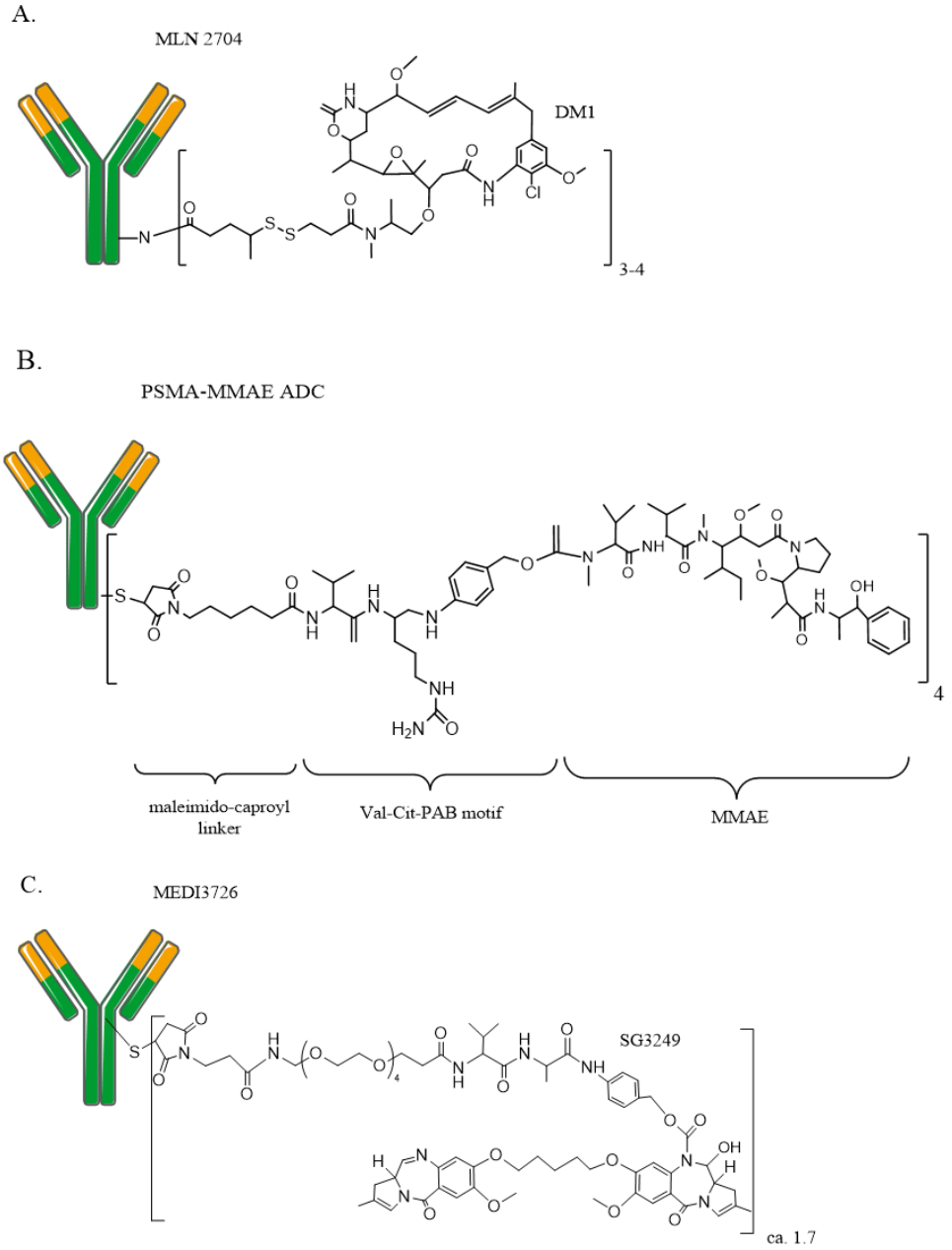

Figure 1.4 Structures of anti-PSMA antibody drug conjugates which underwent or are currently undergoing the clinical evaluation.

A. MLN2704 (Millenium Pharmaceuticals) - DM1 was conjugated *via* disulfide linker to random lysines in the structure of the anti-PSMA antibody; **B.** PSMA-MMAE ADC (Progenics Pharmaceuticals) - anti PSMA antibody interchain cysteines were conjugated to the MMAE *via* Valine-Citruline-PAB self immolative linker; **C.** MEDI 3726 (Medimmune)is an anti-PSMA antibody conjugated to pyrrolobenzodiazepine dimer *via* cathepsin B cleavable linker to the interchain cysteines of the antibody**.**

The conjugate which is currently undergoing clinical evaluation is MEDI3726, an anti-PSMA antibody conjugated to the pyrrolobenzodiazepine dimer payload tesirine (SG3249), a DNA

cross-linking agent (*Figure 1.4* C). Tesirine was designed to combine potent anti-tumor activity with desirable physicochemical properties such as favorable water solubility and improved conjugation characteristics. MEDI3726 is an ADC consisting of an engineered anti-PSMA J591antibody variant containing three point mutations: C214S in the light chain and C226V and C229V in the heavy chain hinge allowing for site-specific conjugation of the toxin using maleimide strategy at position C220 [47]. The conjugate was tested *in vitro* in a panel of PSMA-positive prostate cancer cell lines demonstrating excellent selectivity and cytotoxicity in the sub-nanomolar range of concentration. *In vivo* MEDI3726 showed excellent antitumor activity in the LNCaP and the castration resistant CWR22Rv1 prostate cancer models. Importantly, the conjugate was efficacious in human prostate cancer patient-derived xenografts (PDX). MEDI3726 is currently undergoing evaluation in Phase I/Ib clinical study in subjects with metastatic castration resistant prostate cancer (ClinicalTrials.gov Identifier: NCT02991911)[54].

An attractive direction in the development of ADCs is the employment of toxins with new modes of action, distinct from commonly used microtubule inhibitors, DNA alkylators or cross-linking agents. Such a new mode of action is provided by α-amanitin which is the most selective known inhibitor of eukaryotic RNA Pol II. The Targeted Antibody α-Amanitin Conjugate (ATAC) technology platform developed by Heidelberg Pharma Research GmbH was implemented in the preclinical development of an anti-PSMA targeted ADC. Initially the humanized anti PSMA antibody 3f11 was conjugated to the: 1) random lysines in the structure of antibody using non-cleavable linker, 2) random lysines in the structure of antibody using Val-Ala-PAB cleavable linker, 3) interchain cysteines in the structure of 3f11 using non-cleavable linker [55]. Drug antibody-ratio (DAR) of these three conjugates was varying from 2.7 - 4.7. All compounds were tested in parallel in the CWR22Rv1 PSMA positive prostate cancer xenograft and were administered as a single dose corresponding to 150 μg/kg of unconjugated α-amanitin equivalents. Limited *in vivo* efficacy was observed for the conjugate synthesized using maleimide chemistry bearing the stable linker. The two conjugates with the cleavable linkers demonstrated similar anti-tumor activity with the tumor regression observed until day 20 after single dose administration [55]. Recently the results for anti PSMA α-amanitin based thiomab based ADC was published [56]. Toxin was conjugated *via* Val-Ala-PAB linker to the antibody bearing mutation C256D allowing to obatin defined DAR=2. A complete tumor remission was observed with 4 mg/kg

at single dose adminsitration and at 2 mg/kg and 4 mg/kg applying multiple dosing regimen [56].

1.3 ALPHA-AMANITIN

1.3.1 α-Amanitin origin, toxicity profile and molecular mode of action

Amatoxins is a related group of toxins produced by basidiomycetes mushrooms, predominantly Amanita type. Structurally amatoxins are bicyclic, ribosomally expressed octapeptides which undergo post-translational modification by cyclization and hydroxylation of the side chains [57]. Chemically amatoxins are divided into two groups: 1) neutral amatoxins including: α-amanitin, γ-amanitin, amaninamide, amanullin and proamanullin and 2) acidic amatoxins which include: β-amanitin, ε-amanitin, amanin and amannullic acid (*Figure 1.5*) [58]. Amatoxins differ in their structure regarding the number of hydroxymethyl or methyl group in position R_1, hydroxyl groups in positions R_2, R_4 and R_5 and presence of amide or carboxyl group in a position R_3 (*Figure 1.5*). Due to the bicyclic structure amatoxins are heat stable and the toxin is not inactivated during mushroom preparation for consumption. Moreover, amatoxins are completely insensitive for extreme pH changes and are not susceptible to any known digesting enzymes. Additionally, a high water solubility makes them highly bio-available and toxic upon ingestion [58].

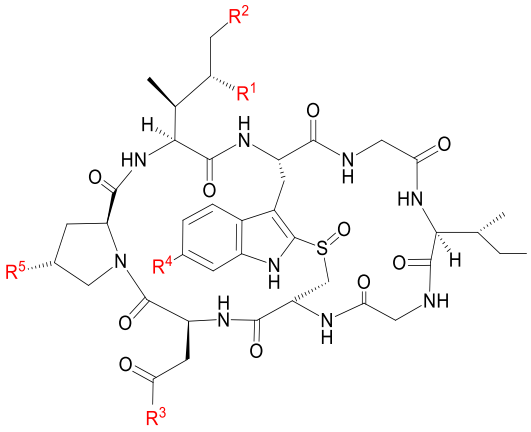

Derivative	R^1	R^2	R^3	R^4	R^5
α-amanitin	CH_2OH	OH	NH_2	OH	OH
β-amanitin	CH_2OH	OH	OH	OH	OH
γ-amanitin	CH_3	OH	NH_2	OH	OH
ε-amanitin	CH_3	OH	OH	OH	OH
Amanin	CH_2OH	OH	OH	H	OH
Amanin amide	CH_2OH	OH	NH_2	H	OH
Amanullin	CH_3	H	NH_2	OH	OH
Amanullic acid	CH_3	H	OH	OH	OH
Proamanullin	CH_3	H	NH_2	OH	H

Figure 1.5 Chemical structures of amatoxins.

Figure was re-drawn from [58].

First clinical symptoms of intoxication appear ca. 24 h after mushroom ingestion and include gastrointestinal disorders, hematuria followed by a latent period when liver and renal function deteriorate leading to seizures, coma and death. Supportive therapy consists of gastric decontamination and liver transplantation in case of severe liver damage [59]. Elimination of amatoxins from the blood stream appears very rapidly. Kidney filtration is the main elimination mechanism and only minor amounts are eliminated with bile *via* intestine.

In humans upon ingestion amatoxins were undetectable in plasma ≥ 48 h after consumption [60]. The best characterized toxicity profiles amongst all amatoxins are those of α-amanitin and β-amanitin. The organs of toxicity for both are liver and kidney [58, 61]. The liver is expected to be exposed to high concentrations of amanitin due to the first pass mechanism and direct transport of toxin from gastrointestinal tract to the liver *via* hepatic portal vein. Organic anion transporter 1B3 (OATP 1B3) expressed in sinusoidal membrane of liver was identified as the main mediator of liver uptake [62].

Due to small molecular size the excretion of α-amanitin is mainly *via* renal filtration thus the kidney toxicity is also expected. In a mouse model the concentration of α-amanitin found in the kidney was 6-90 times higher than in the liver [63]. The damage was reported 72 h after single dose administration of α-amanitin. Moreover, a histopathological changes such as loss of the brush border, necrosis of epithelial cells in the proximal and distal tubules of the nephrons are described [64]. Lately it was postulated that α-amanitin may generate the reactive oxygen species (ROS) in the kidney [65]. Biochemical analysis revealed a shift in the reductional/oxidational balance towards the oxidative status suggesting a relationship between α-amanitin related renal toxicities and ROS generation. Although, amatoxins are considered to trigger mainly hepatotoxicity the kidney is also reported as the organ of toxicity [65].

After internalization of α-amanitin into the cells it interacts with the eukaryotic RNA polymerase II (RNA Pol II). Inhibition of RNA Pol II by α-amanitin dramatically decreases the transcription rate from several thousand nucleotides per minute to only a couple of base pairs per minute [66]. Structurally RNA Pol II consists of 12 subunits which create a huge 550 kDa complex. The crystal structure of the RNA Pol II complex was resolved for 10 out of 12 subunits and was lacking the two smallest subunits (Rbp4 and Rbp7) which are dispensable for RNA Pol II transcriptional activity [67]. The two largest subunits of the complex Rbp1 and Rbp2 are crucial for RNA Pol II activity and together create a structural fold called "bridge helix" which is an active site of the complex that enables the interaction between unpaired DNA and newly synthesized RNA strain [66]. It was shown that the “bridge helix” is essential for the unconstrained DNA translocation during transcription. Resolution of RNA Pol II co-crystal with α-amanitin showed the formation of several hydrogen bonds between the “bridge helix” region of Rbp 1 and α-amanitin, which constrains the position of Rbp1 and Rbp2 and prevents the DNA translocation. The strongest interaction between

the “bridge helix” of RNA Pol II and α-amanitin was demonstrated for the hydroxyl group of hydroxyproline in the α-amanitin structure (-OH at the position R_5 in *Figure 1.5*). This particular hydroxyl group is involved in the hydrogen-binding to the bridge helix residue A822 in RNA Pol II structure, which plays a key role in the inhibition [66]. As the consequence of RNA Pol II inhibition, a progressive decrease in the cellular mRNA production and a deficient protein synthesis is observed, ultimately leading to apoptotic cell death. This mode of action distinct from other known toxins makes α-amanitin an attractive payload for the development of SMDCs and ADCs. Lately the route of full α-amanitin synthesis was published [68]. Currently the α-amanitin development at Heidelberg Pharma Research GmbH is focused on the optimization of scalable processes for the production of fully synthetic and conjugable α-amanitin derivatives providing better plasma stability and antitumor activity [69].

1.3.2 α-Amanitin as a payload for development of antibody drug conjugates

Structure activity relationship studies of the α-amanitin-RNA Pol II complex allowed to determine which groups within the toxin structure are not essential for α-amanitin interaction with RNA Pol II and might be used for the attachment of a linker for the further conjugation to targeting moieties. For conjugation of α-amanitin to targeting ligands the following three positions were identified: the carboxyl group of side chain of aspartic acid (Asn 7) of α-amanitin (*Figure 1.6* R_1), the δ-hydroxyl group of dihydroxy-isoleucine side chain (Ile 1) (*Figure 1.6* R_2) and the 6´-hydroxyl group of hydroxy-tryptophan side chain (Trp 2) (*Figure 1.6* R_3) [70].

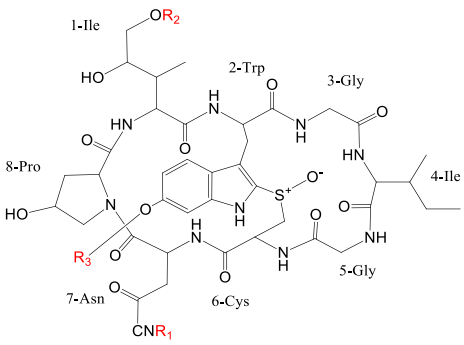

Figure 1.6 Structure of α-amanitin with positions suitable for the linker attachment.

Positions suitable for linker attachment are marked in red. The figure was adapted from [70].

α-amanitin is attractive as a payload for targeted therapeutics due to its unique mode of action distinct from other toxins employed in ADCs development: microtubule inhibitors (tubulysins, auristatins), topoisomerase inhibitors (camptothecin), DNA cross-linkers (pyrolobenzodiazepines), DNA strand breakers (calicheamycines), DNA alkylators (ducarmycins) which act mainly on rapidly dividing cells. It was demonstrated that α-amanitin ADCs were active in growth phase arrested LNCaP cells [55]. On the base of these results it can be postulated that also dormant and slowly dividing tumor stem cells may respond to a therapy with α-amanitin ADCs. An additional advantage arising from the use of α-amanitin as a payload is that the copy number of the molecular target for α-amanitin, the RNA polymerase II in mammalian cells, is in the range of a ten to hundred thousand which is much lower compared to the number of intracellular target such as microtubule [70]. Considering the 1:1 stoichiometry of α-amanitin-RNA Pol II binding even a low number of internalized α-amanitin molecules would allow to completely inhibit the activity of RNA Pol II [71].

Lately there was discovered a relationship between the deletion of *TP53* gene encoding p53 protein and sensitivity to α-amanitin therapy. Deletion of one of the gene copies is a common alteration found in human tumors. Liu *et al.* demonstrated that *TP53* is often co-deleted with the gene encoding human RNA Pol II - *POLR2A* resulting in a lower number of RNA Pol II copies in cancer cells [72]. Both genes are located in the neighboring regions on chromosome *p17* which deletion is commonly detected in variety of cancers but up to the moment specific *POLR2A*-*TP53* co-deletion was demonstrated in colorectal and prostate cancer [72, 73]. The *TP53* co-deletion with *POLR2A* indicates that there might be a significant population of cancer patients more sensitive to the therapy with targeted α-amanitin conjugates. Additionally, it creates the possibility of *p17* deletion employment as a biomarker allowing to predict response to the therapy with ATACs.

One of the most detailed characterizations of α-amanitin targeted antibody conjugates was presented for an ATAC targeting EpCAM antigen [74]. EpCAM is overexpressed in the majority of adenocarcinomas including colon, breast, pancreatic and ovarian cancer. The conjugate consists of chimeric chi-HEA125 antibody conjugated *via* lysine residues to the glutarate linker positioned at the δ-hydroxyl group of dihydroxy-isoleucine side chain of α-amanitin (*Figure 1.6* position R_2). The conjugate demonstrated specific toxicity towards EpCAM expressing cells which correlated with the levels of EpCAM receptor expression. Importantly, in contrast to other toxins α-amanitin does not penetrate the cell membrane

due to high hydrophilicity and thus the cytotoxic potential of the naked toxin is very low - IC_{50} in the micromolar range of concentration (see section 4.1.2). Once it is conjugated to the targeting moiety, such as antibody the cytotoxic potential is dramatically improved - in the case of the EpCAM-α-amanitin conjugate for ca. 4 orders of magnitude. In *in vivo* experiments the durable anti-tumor activity was demonstrated in EpCAM positive BxPc3 xenograft model. Moreover, histological analysis has shown that the proliferation rate of tumors treated with conjugate was lower than of those treated with naked antibody as demonstrated by Ki67 staining [74].

Currently, antibody targeted α-amanitin conjugates recognizing solid tumor targets such as PSMA [55, 56] and hematological targets such as CD19 [75] or B cell maturation antigen (BCMA) [47] are in pre-clinical development.

Although currently the full IgG format seems to be the optimal for targeted toxin delivery it features certain limitations. A large molecular size and a high affinity of the antibody to the target may limit the ability of penetration especially into solid tumors. Moreover, the immunogenicity of ADCs or unspecific toxicities due to the long circulatory half-life and payload deconjugation might be an issue. The alternative smaller formats such as antibody fragments, peptides or chemically synthesized ligands recognizing tumor specific antigens allowing to overcome aforementioned limitations are under development [76-79].

The reports about small molecule α-amanitin targeted conjugates are scarce. Thus, it is difficult to judge whether α-amanitin SMDCs can be better than α-amanitin based ADCs. Recently the paper published by Bodero *et al.* reports a comparable *in vitro* toxicity of unconjugated α-amanitin and *iso*-DGR-α-amanitin and RGD-α-amanitin conjugates for targeted delivery to cells overexpressing integrins most probably due to problems with internalization of the target [80]. The second example of α-amanitin SMDCs proposes the conjugation of α-amanitin to pH low insert peptide (pHLIP), which is a water-soluble membrane peptide that interacts weakly with a cell membrane at neutral pH [81]. Once the pH changes to slightly acidic (pH <7.0), e.g. in the acidic tumor microenvironment, pHLIP inserts into the lipid bilayer of the cell membrane and forms a stable transmembrane alpha-helix delivering the payload. It was demonstrated that pHLIP could transport α-amanitin through the membrane and demonstrated 4-5 times higher anti-proliferative potential in at pH 6 (internalizing conditions) compared to pH 7.4 (non-internalizing conditions) [81].

The conjugation of α-amanitin to small molecules targeting cancer antigens creates an attractive alternative approach for the targeted α-amanitin delivery especially for solid

tumors. It is still not explored whether α-amanitin based SMDCs might provide similar or better anti-tumor activity compared to α-amanitin ADCs.

1.4 DUPA BASED SMALL MOLECULAR PSMA INHIBITORS FOR PROSTATE CANCER THERAPY

1.4.1 Discovery of urea-based PSMA inhibitors

Limited utility of anti-PSMA antibodies for PCa and metastasis radio-imaging application triggered the development of small molecular PSMA ligands which design was based on the structure of natural PSMA substrates.

The initial idea for the therapeutic use of small molecular weight PSMA ligands acting as PSMA inhibitors was the treatment of the excessive glutamate activation present in numerous neurodegenerative diseases [82]. The natural PSMA ligand NAAG (*Figure 1.7*) is an agonist of glutamate receptor mGlu3 and agonist/antagonist of N-methyl-D-aspartate (NMDA) receptor abundantly expressed in central nervous system. The alterations in PSMA expression and glutamate signaling were described in a panel of neurological disorders thus, it was postulated that PSMA inhibitors may play an important role in the neuroprotection [82]. The PSMA inhibitors were selected from the chemical library of small molecules with functional groups known to inhibit the metallopeptidases. Amongst all screened compounds the group of hydroxyphosphinyl derivatives have demonstrated most optimal binding affinity to PSMA. The hits were further optimized by rational design based on the observation that the glutamate moiety of natural PSMA ligand-NAAG was important for the recognition by the enzyme whereas the aspartate region played a less important role (*Figure 1.7*). From the group of optimized ligands 2-PMPA (Ki = 0.275 nM) demonstrated the highest affinity to PSMA and proved to provide significant protection against brain injury in mice stroke preclinical models (*Figure 1.7*) [83, 84]. 2-PMPA discovery prompted the further development of numerous small molecular PSMA inhibitors [85].

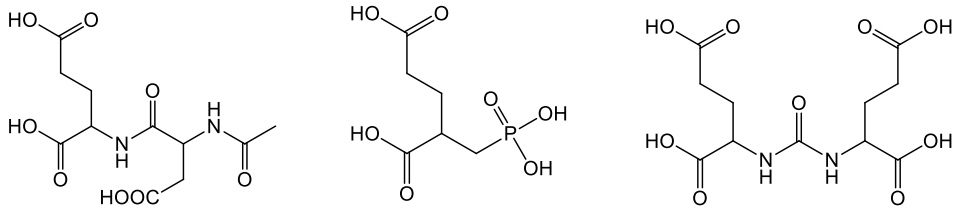

N-Acetylaspartylglutamic acid (NAAG) | 2-(phosphonomethyl) pentanedioic acid (2-PMPA) | 2- [3-(1, 3-dicarboxy propyl) ureido] pentanedioic acid (DUPA)

Figure 1.7 Chemical structure of NAAG (N-Acetylaspartylglutamic acid), 2-PMPA (2-(Phosphonomethyl)-pentanedioic acid) and DUPA (2-[3(1,3-dicarboxypropyl) ureido] pentanedioic acid.

The structures show the homology and the rational design of PSMA inhibitors based on the natural PSMA ligand structure - NAAG.

The resolution of the PSMA crystal structure and advancements in the field of computational modeling allowed for *in silico* docking study of the library of known PSMA inhibitors which confirmed that urea based ligands bind at the catalytic site efficiently and show high affinities [86, 87]. Amongst over 100 *in silico* tested PSMA urea based inhibitors known to recognize PSMA, particularly the 2- [3-(1, 3-dicarboxy propyl) ureido] pentanedioic acid (DUPA) fitted well into the active site of PSMA and demostrated a high affinity (K_i = 8 nM) (*Figure 1.7*). Aditionally, one of the 3-carboxypropyl groups in the DUPA structure can be modified for the conjugation of radionuclide chelator groups or toxic cargos for development of radioimaging agents and targeted therapeutics. Currently, the DUPA motif is the most commonly applied small molecule in targeted PCa radio-imaging and therapy [37, 88].

1.4.2 Structural studies of urea-based inhibitors and PSMA interaction

Structural studies of the PSMA and urea-based ligands complexes provided important insights allowing for the rational design of optimized small molecules for PSMA targeted therapy. Resolution of co-crystal with known urea-based inhibitors demonstrated that the active site of the PSMA receptor: two Zn^{2+} atoms and the so called S´ glutamate recognition pocket, both important for substrate recognition, are buried in the second part of the PSMA protease domain (*Figure 1.1*) and might be reached only *via* an irregularly shaped 20 Å long tunnel [37, 77] (*Figure 1.8*). This entrance tunnel constitutes of three structural arrangements: 1) S1 accessory pocket (*Figure 1.8* A), 2) arginine patch (*Figure 1.8* B) and 3) arene binding site (*Figure 1.8* C). The tunnel structure was demonstrated to be relatively

spacious and can effectively bind the diverse motifs, which allows for some level of freedom in the design of a supporting spacer structurally fitting into the contours of tunnel leading to the PSMA active site. The supporting spacer allowing to reach the active site of PSMA upon conjugation of such big and bulky structures as toxins or radioligands chelators is essential for the development of conjugates with desired biological properties [37].

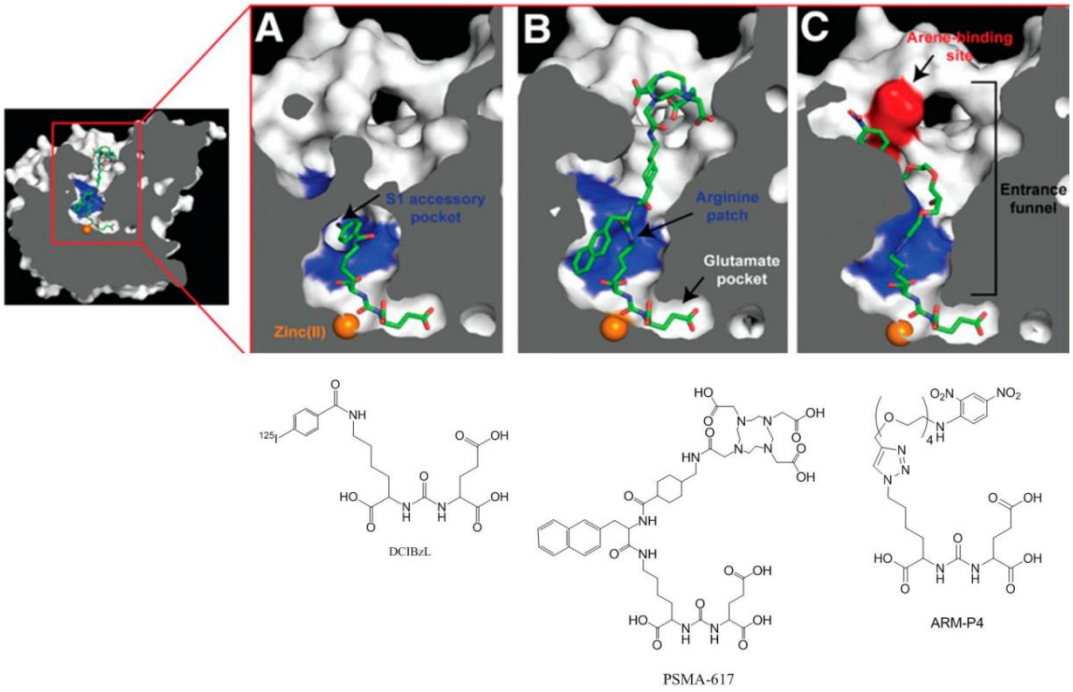

Figure 1.8 PSMA cross section demonstrating the different interactions of three urea-based inhibitors with the PSMA entrance tunnel and PSMA active site.

For all three molecules the interaction of S1' glutamate recognition pocket and dinuclear zinc active site is necessary for inhibitor recognition. Zinc ions are shown as orange spheres, and PSMA ligands are shown as stick representations. **A.** A cross-section of PSMA entrance tunnel interaction with 2-{3-[1-carboxy-5-(4-iodo-benzoylamino)-pentyl]-ureido}-pentanedioic acid (DCIBzL), the image shows the interaction of S1'glutamate recognition pocket in the irregularly shaped entrance tunnel; **B.** PSMA-617 within entrance tunnel showing the interaction of the linker with the arginine patch; **C.** Interaction of inhibitor ARM-P4 with the PSMA tunnel and arene binding (marked in red). The figure was taken and adapted from [37].

The structure of the supporting spacer despite of providing the delivery of urea-based ligands to the active site influences parameters such as affinity, receptor mediated internalization, tumor biodistribution and even pharmacokinetic properties [89, 90]. The detailed influence of the structural modification of the supporting spacer modification on the activity of urea-based ligands were performed during the optimization of compound DKFZ-PSMA-617 selected from a small library of compounds as an optimal ligand

for PCa PET imaging and radiotherapy. The general structure of the tested conjugates with brief description of properties is presented in *Figure 1.9* A. Beside an excellent *in vitro* properties DKFZ-PSMA-617 demonstrated optimal *in vivo* features such as tumor to background ratio and low kidney uptake in imaging experiments in mice. This agent is suitable for labeling with nuclides for radio-diagnosis: ^{68}Gd and radiotherapy: ^{177}Lu and ^{225}Ac and is currently evaluated in the clinical setting in advanced prostate cancer [37].

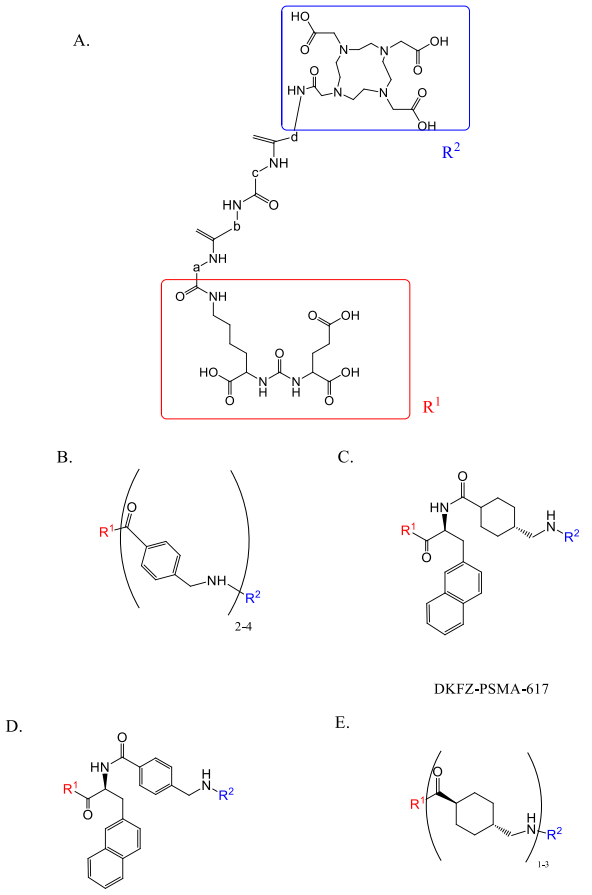

Figure 1.9 Influence of supporting spacer structure on the activity of Glu-ureido based - DOTA conjugates for cancer imaging and therapy.

A. General structure of the PSMA targeted Glu-ureido based - DOTA library of conjugates for cancer imaging and therapy. Library was used for the determination of structure activity relationship as determined by Benešová *et al.* **B-E.** Exemplary structures of the spacers having different influence on the properties of urea-based imaging agents. **B.** An example of linker with different arrangements of aromatic rings - demonstrated high PSMA inhibitory properties; **C.** example from the group of the linker with naphthyl-alanine and cyclohexane arrangements - DKFZ-PSMA-617 - demonstrated high tumor targeting properties and limited kidney accumulation, chosen for clinical development; **D.** example of linkers with 2-napthyl alanine and benzene in the structure - demonstrated lower internalization rate compared to DKFZ-PSMA-617; **E.** examples of linkers with increasing number of cyclohexane moieties - demonstrated poor accumulation in tumor. The figure was adapted and re-drawn from [90].

The detailed optimization study presented by of Benešová *et al.* clearly demonstrated that the linker structure strongly influences *in vitro* and *in vivo* properties of urea based agents. The structure of the supporting spacer should be carefully considered while designing the PSMA targeted small molecular diagnostics or therapeutics.

1.4.3 DUPA based small molecule toxin conjugates

Initially the urea-based ligands have emerged mainly as targeting ligands for prostate cancer radiodiagnosis and radiotherapy but recently also as carriers for targeted toxin delivery. The main rationales for the design of DUPA based small molecular-toxin conjugates with an expected short half-life are to: 1) provide better tumor penetration compared to high molecular weight ADCs, 2) avoid undesired toxicities by very rapid renal clearance and 3) improve the therapeutic window compared to unconjugated toxin. The ability of DUPA to deliver cargos to the endo-lysosomal compartment of PSMA positive cells was demonstrated by confocal imaging of fluorescent DUPA-rhodamine B conjugate [77]. Moreover, it was demonstrated that DUPA is a suitable targeting moiety for the delivery of versatile toxic warheads such as taxanes, vinca alkaloids, and topoisomerase inhibitors. The incorporation of the optimized supporting spacer was shown to be the prerequisite for efficient PSMA recognition, binding and yielding the cytotoxic effect. Initially the supporting spacer consisting of the following sequence: aminooctanoic acid - phenylalanine - phenylalanine (Aoc-Phe-Phe) has shown to have no influence on the DUPA´s binding affinity and allowed for the efficient delivery of various toxins [77, 91].

The full optimization of the supporting spacer was presented for a DUPA-tubulysin B hydrazide conjugate. The initially proposed conjugate DUPA-Tub H I (*Figure 1.10 A*) was characterized by poor water solubility which as a part of optimization was improved by the implementation of a supporting spacer with more hydrophilic groups which at the same time would not impact the interaction with the PSMA tunnel like structure. To this end conjugate DUPA-Tub H III was designed (*Figure 1.10 B*). *In vitro* DUPA-Tub H III conjugate demonstrated toxicity in the nanomolar range comparable with the cytotoxicity of unconjugated TubH in PSMA receptor positive LNCaP cell line. In LNCaP xenografts the conjugate showed remarkably lower toxicity compared to the naked tubulysin B and the ability to inhibit the growth of tumors during the period of conjugate administration. In order to further optimize the efficacy and tolerability of DUPA-TubH a panel of compounds bearing modifications in

supporting spacer was tested [87]. Amongst all, EC 1169 (*Figure 1.10 C*) demonstrated no drug related toxicities, complete response in all animals and the longest duration of the tumor response in LNCaP xenografts [76]. In 2014 EC 1169 entered the phase I clinical study in metastatic castrate resistant prostate cancer patients (ClinicalTrials.gov Identifier: NCT02202447) [91].

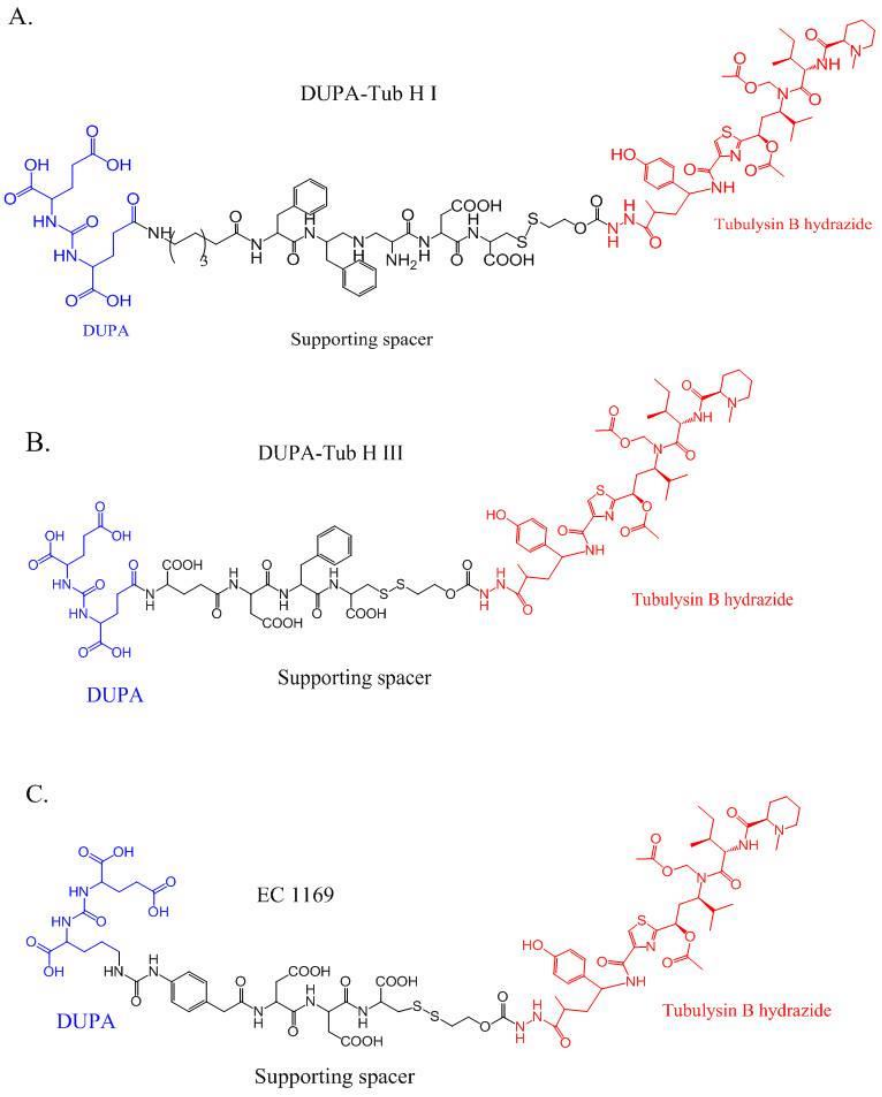

Figure 1.10 Optimization of supporting spacer in DUPA - Tubulysin conjugates.

Conjugates bearing different supporting spacers were sythetized in order to evaluate the solubility and specificty of final conjugate. **A.** Initially designed conjugate - featured not sufficient water solubility; **B.** Conjugate with spacer featuring hydrophilic groups- conjugate demonstrated better water solubility and satisfactory anti-tumor activity; **C.** EC 1169 conjugate - provided good water solubility and demonstrated the most durable anti - tumor response in LNCaP xenografts, chosen for clinical development.

Other than for the tubulysin conjugate preclinical *in vivo* data are reported for DUPA targeted delivery of the following toxins: paclitaxel (PTX) [92], docetaxel (DTX) [93] and topoisomerase inhibitor indenoisoquinoline [94]. Similarly, as for tubulysin conjugates the requirement for implementation of supporting spacer was demonstrated for the paclitaxel-DUPA conjugate. This conjugate bearing only a very short disulfide spacer showed significantly lower cytotoxic potential *in vitro* compared to unconjugated paclitaxel. The *in vivo* tolerability and efficacy were comparable with unconjugated toxin [92]. The same supporting spacer as presented in *Figure **1.10** A* was implemented in the development of DUPA-indotecan conjugate. The *in vitro* evaluation showed slightly higher IC_{50} for conjugate compared to unconjugated toxin (11.4 nM *vs.* 2.0 nM, respectively). In *in vivo* experiment in a 22RV1 xenograft model DUPA-indotecan conjugate demonstrated a complete tumor regression during the period of administration and lower toxicity compared to the naked indotecan [94]. The importance of the spacer length was also stressed for docetaxel-DUPA conjugates [93].

All presented examples confirm that the spacer structure has a tremendous impact on the activity of DUPA-toxin conjugates. Given examples corroborate the structure activity relationship results obtained for urea-based radio-diagnostic compounds presented in section 1.4.2. It was demonstrated that DUPA ligand is suitable for the conjugation with a panel of toxins but α-amanitin was not included in this panel. The excellent targeting properties of DUPA, the completely new mode of action of α-amanitin and growing interest in the development of SMDCs as alternative for ADCs prompted the development of novel DUPA-α-amanitin conjugates.

2. OBJECTIVES OF THE STUDY

The goals of work presented within this PhD project were:

1. Determining the structure activity relationship between biological activity and different linker strategies used for the synthesis of DUPA-α-amanitin conjugates.

2. Assessment whether targeting of α-amanitin to PSMA positive prostate cancer using the small molecular targeting moiety - DUPA can lead to sustainable tumor growth inhibition in *in vivo* prostate cancer xenograft models.

3. Determining main factors influencing the *in vivo* activity of this class of conjugates - pharmacokinetic parameters determination and biodistribution studies.

4. Optimization of conjugates structure in order to provide improved pharmacokinetic parameters and better *in vivo* efficacy.

3. MATERIALS AND METHODS

3.1 MATERIALS

3.1.1 Laboratory equipment

Table 3.1

Equipment	Supplier
Incubator	Thermo Fischer Scientific
Analytical balance	Kern AEJ
Technical balance	Sartorius
Double Neubauer Chamber	Optik Labor
Microplate reader FLUOSTAR Optima	BMG Labtec
Hydrospeed ELISA Washer	Tecan
Orbital plate shaker	neoLab
Water bath	Memmert
Tabletop centrifuge FRESCO 17	Thermo Fischer Scientific
Centrifuge Multifuge X3R	Thermo Fischer Scientific
Plenary ball mill, Precellys 24 Tissue Homogenizer	Bertin Instruments
Flow cytometer FACSCalibur	Beckton Dickinson
Optical microscope CK2	Olympus
Heat block	VWR
Vortex	neoLab
Rotational vacuum concentrators RVC 2-25 Cdplus	MartinChrist
Western Blot electrophoresis chamber	Bio Rad
Western Blot transfer chamber	Bio Rad

3.1.2 Laboratory supplies and reagents

Table 3.2

Supply / Reagent	Supplier
Cell culture flasks T25, T75, T175	Greiner Bio-One
Cell culture plate Cell Carrier-96 Black, Optically clear bottom	Perkin Elmer
Penicillin 10 000 U/mL Streptomycin 10 mg/mL	Sigma
L-glutamine	Sigma
FCS	Biowest
Charcoal stripped FCS	Gibco
PBS	PAN Biotech
Accutase	Sigma
Trypsin/EDTA	Sigma
Trypan blue solution	Sigma
Human plasma	BioTrend
Mouse plasma	BioTrend
Pre-casted 10 % polyacrylamide gels	Bio-Rad
Page Ruler protein marker	ThermoFischer Scientific
PVDF membrane	ThermoFischer Scientific
Skimmed milk	Roth
Filter paper	Whatman
Western blot films	G&E Healthcare
Cell Titer Glo reagent	Promega
2-PMPA	Tocris
Grinding beads	MP Biomedicals
Poly-D-Lysine	Sigma
FastPrep®Tube	MP Biomedicals
Ethanol	Roth
Milk powder	Roth
BSA	Roth
Tween 20	Sigma

Table 3.2 *Continued from the previous site*

Supply / Reagent	Supplier
Tris -HCl	Roth
Paraformaldehyde 16 % ethanol free ultrapure	Polysciences
30 % H_2O_2	Fluka
DMSO	Sigma
TMB-working solution	1.1 mL TMB-stock solution (1 mg/mL in DMSO) in 9.9 mL 0.1 M sodium-acetate-buffer pH 6.0 + 2.2 µL 30 % H_2O_2
Matrigel® Matrix Phenol Red-Free	Corning
α-amanitin	Heidelberg Pharma Research GmbH
HEPES buffer, 1M in H_2O	Sigma
Smart Block ™	Candor Bioscience GmbH
Sample Buffer	Candor Bioscience GmbH
Tris -HCl	Roth
Paraformaldehyde 16 % ethanol free ultrapure	Polysciences
Sample Buffer	Candor Bioscience GmbH

3.1.3 Buffers

Table 3.3

Buffer	Composition
PBS	137 mM NaCl, 2.7 mM KCl, 10 mM Na_2HPO_4, 2 mM KH_2PO_4
TMB dilution buffer	0.1 M $C_2H_3NaO_2$ in H_2O, pH=6.0,
ELISA wash buffer	PBS + 0.05 % Tween 20
ELISA blocking buffer	3 % BSA in PBS
ELISA sample buffer	1 % BSA in PBS + 20% ethanol
FACS fixation solution	0.5 % paraformaldehyde in PBS
FACS staining medium	PBS, 25 mM HEPES, 3% FCS, 0.02% Na-azide
1x Tris, glycine, SDS gel running buffer	25 mM Tris, 192 mM glycine, 0.1% SDS

Table 3.3 *Continued from the previous site*

Buffer	Composition
TBST buffer	50 mM Tris, 150 mM NaCl, 0,1 %, Tween 20
Western blot blocking buffer	5 % skimmed milk in TBST buffer
Western blot transfer buffer	25 mM Tris, 192 mM glycine, pH = 8.0 + 20 % methanol
4 x Laemlii reducing sample buffer	250 mM Tris-HCl pH = 6.8, SDS 8 %, Glycerol 40 %, 2-Mercaptoethanol 8 %, Bromophenol Blue 0.02 %

3.1.4 Cell culture media

Table 3.4

Medium[1]	Supplier
RPMI	PAN Biotech
DMEM	PAN Biotech
RPMI without Phenol red	PAN Biotech

[1]Appendix1 indicates detailed composition of each cell culture media.

3.1.5 Antibodies

Table 3.5

Antibody	Supplier
α-amanitin- biotin conjugate	Heidelberg Pharma Research GmbH
Streptavidin HRP conjugate	Sigma
Anti-amanitin polyclonal antibody	Heidelberg Pharma Research GmbH
Anti-human PSMA antibody h3/F11-D265C Var16	Heidelberg Pharma Research GmbH
Goat anti-Human IgG (H+L) Cross-Adsorbed Secondary Antibody, Alexa Fluor 488	Thermo Fischer Scientific
Rabbit anti-Human-IgG-HRP	Abcam ab98576

3.1.6 Cell lines

Table 3.6

Cell lines	Source	Cell culture medium
LNCaP	ATCC	RPMI supplemented with 10 % FCS; Pen/Strep; L-Gln
22RV1	DSMZ	RPMI/DMEM 1/1 supplemented with 20 % FCS, Pen/Strep; L-Gln
PC3	DSMZ	RPMI supplemented with 10 % FCS; Pen/Strep; L-Gln
C4_2	ATCC	RPMI supplemented with 10 % FCS; Pen/Strep; L-Gln;
HEK293 WT	CLS	1:1 DMEM/F12 supplemented with10 % FCS; Pen/Strep; L-Gln
HEK293 OATP1B3	Heidelberg Pharma Research GmbH	1:1 DMEM/F12 supplemented with 10 % charcoal stripped FCS; without antibiotics; Poly-D-Lysine coated culture dishes

3.1.7 DUPA-α-amanitin conjugates

The conjugates HDP 30.1585 and HDP 30.1592 based on the urea motif were synthesized and kindly provided by Dr. Christoph Müller from the Department of Chemistry of Heidelberg Pharma Research GmbH. All remaining eleven DUPA-based compounds were synthesized and kindly provided by Francesca Gallo from the Department of Chemistry Heidelberg Pharma Research GmbH. Supporting spacer is defined in section 4.1.2.

Table 3.7

Compound code /Name	Molecular weight (Da)	Linker structural characteristics
HDP 30.1585	1363.48	No supporting spacer, acetamide Val-Ala-PAB cleavable
HDP 30.1592	1553.68	No supporting spacer, acetamide C_6 non-cleavable
HDP 30.2284	2246.52	Supporting spacer, maleimide Val-Ala-PAB cleavable
HDP 30.2301	1957.18	Supporting spacer, maleimide C_6 non-cleavable
HDP 30.2515	2093.34	Supporting spacer, acetamide Val-Ala-PAB cleavable
HDP 30.2523	1917.16	Supporting spacer, acetamide C_6 non-cleavable
HDP 30.2246	1850.09	Supporting spacer, disulfide
HDP 30.2589	1864.12	Supporting spacer, disulfide (0:1) *mono-hindered
HDP 30.2609	1848.16	Supporting spacer, disulfide (2:0) *double-hindered
HDP 30.2618	1834.13	Supporting spacer, disulfide (1:0) *mono-hindered
HDP 30.2619	1848.16	Supporting spacer, disulfide (1:1) *double-hindered
HDP 30.2594	2625.85	Supporting spacer, $(His\text{-}Glu)_3$Val-Ala-PAB cleavable
DUPA-Fc-α-amanitin conjugate	61443.92	Supportingspacer-PEG_3-Fc-Dibenzocyclooctyne-(DBCO)-Val-Ala-PAB

*The hindered disulfide conjugates are denoted by the number of methyl group on the DUPA site and the amanitin site, e.g. the conjugate with one monomethyl group on the DUPA site and no hindrance on the α-amanitin site is abbreviated as (1:0).

All compounds were provided as lyophilizates. Stock solution of DUPA-Fc-α-amanitin conjugate was provided as a liquid in PBS.

3.1.8 Animals

Table 3.8

Mice strain	Genetic background	Reference	Supplier
CB17 Scid	CB-17/Icr, BALB/c congenic background with Ig hb-Cb allel from the C57BL/Ka strain	Bosma *et al.* 1980	Janvier

3.1.9 Software

Table 3.9

Software	Supplier
GraphPad Prism	GraphPad Software, La Jolla California USA

3.2 METHODS

3.2.1 Cell culture

Cell lines were authenticated using Multiplex Cell Authentication by Multiplexion (Heidelberg, Germany) as described recently [95]. The single nucleotide polymorphism (SNP) profiles matched known profiles or were unique. The purity of cell lines was validated using the Multiplex cell Contamination Test by Multiplexion (Heidelberg, Germany) as described previosly [96]. No Mycoplasma, Squirrel Monkey Retrovirus (SMRV) or interspecies contamination was detected. All cell lines were adherently growing and were cultured in their respective cell culture medium as indicated in section 3.1.6 at 37 ºC, 5 % CO_2 saturation and 100 % humidity atmosphere. Once the cells reached 80 % of confluence the media was removed. Cells were gently washed with PBS to remove FCS traces and detached from culture flasks by incubation with trypsin/EDTA. Following complete detachment trypsin was neutralized by the addition of fully supplemented cell culture media at the double volume of the volume of the trypsin. Cell conglomerates were separated by repeated pipetting. A fraction of cell suspension was left in the culture flask for further cultivation and filled to the volume for cell culture maintenance. Exact volumes of reagents for maintenance of cell culture at different sizes of flasks are indicated in *Table 3.10*. The ratio of dilution for passaging each cell line is indicated in *Table 3.11.*

Table 3.10 Conditions for mammalian adherent cells culturing and reduction.

Flask	Medium volume (mL)	PBS volume (mL)	Trypsin volume (mL)
T25	5	5	0.5
T75	15	15	1.5
T175	35	35	3.5

Table 3.11 Dilution ratio used for different cell lines passaging.

Cell line	Dilution ratio	Medium
LNCaP	1:10	RPMI
22RV1	1:5	RPMI/DMEM 1:1 + 20 % FCS
PC3	1:5	RPMI
HEK293 WT	1:10	RPMI
HEK293 OATP1B3	1:10	RPMI with charcoal stripped FBS

3.2.2 Determination of PSMA expression by flow cytometry

The expression of PSMA receptor in prostate cancer cell lines was determined by flow cytometry. LNCaP, 22RV1 or PC3 cells were fixed in fixation solution (0.5 % paraformaldehyde in PBS) for 10 min and washed with PBS. 5×10^5 cells per sample were stained for 45 min in 100 µl of FCS staining medium containing 10 µg/ml anti-human PSMA antibody h3/F11-D265C Var16 recognizing the extracellular domain of PSMA. Subsequently, the cells were washed 3x with 500 µl of PBS and stained for 45 min at room temperature with 100 µl 1: 500 dilution of Goat anti-Human IgG (H+L) Cross-Adsorbed Secondary Antibody conjugated to Alexa Fluor 488.The cells were washed 3x with 500 µl of PBS and re-suspended in 300 µl of PBS for the measurement. The mean fluorescence intensity was measured for 10,000 gated events. The data were analyzed using flow cytometry on a FACSCalibur device (BD Biosciences) and associated software (BD Biosciences).

3.2.3 *In vitro* cytotoxicity assays

For cytotoxicity 2×10^3 cells/well of each cell line were plated in 96-well black clear bottom plates in 90 µL of the respective cell culture media and incubated overnight to allow for the cells attachment. Approximately 16 h after cells plating the test substance was added to the cell culture medium. The starting concentration of the compounds was 1×10^{-5} M. Starting from 1×10^{-5} M a panel of serial 1:5 dilutions of the test compounds in the respective cell culture media was prepared. 10 µl of the compound dilutions were added to each well and incubated for additional 96 h. Exemplary layout and standard conjugate concentrations for cytotoxicity experiments are presented in *Table 3.12*.

Table 3.12 Standard layout of 96 well plate for CellTiterGlo® 2.0 cytotoxicity experiments.

	1	2	3	4	5	6	7	8	9	10	11	12
		Compound 1			Compound 2			Compound 3			Control	
A	Blank	1×10^{-5} M			1×10^{-5} M			1×10^{-5} M			100 %	
B		2×10^{-6} M			2×10^{-6} M			2×10^{-6} M				
C		4×10^{-7} M			4×10^{-7} M			4×10^{-7} M				
D		8×10^{-8} M			8×10^{-8} M			8×10^{-8} M				
E		1.6×10^{-8} M			1.6×10^{-8} M			1.6×10^{-8} M				
F		3.2×10^{-9} M			3.2×10^{-9} M			3.2×10^{-9} M				
G		6.4×10^{-10} M			6.4×10^{-10} M			6.4×10^{-10} M				
H		1.28×10^{-10} M			1.28×10^{-10} M			1.28×10^{-10} M				

Cell viability was determined with CellTiterGlo® 2.0 assay (Promega) according to manufacturer´s guidelines. Following 96 h incubation with serial dilutions of the compounds, 100 µl of CellTiterGlo® 2.0 reagent was added directly to 100 µl of the cell culture media. Plates were shaken for 2 min on an orbital plate shaker to allow for cell lysis and complete ATP release. Subsequently, cell lysates were incubated for another 8 min in darkness without shaking. Luminescence signal intensities were measured exactly 10 min after CellTiterGlo® 2.0 reagent addition in a microplate reader (FluostarOptimaBMGLabtec). Background was determined from wells with medium only with CellTiterGlo® 2.0 reagent and subtracted from each value. The 100 % control was set up as non-treated cells. Percent of cell viability was reported as $\frac{I_{sample} - I_{background}}{I_{control} - I_{background}} x\ 100\ \%$. Unless indicated otherwise dose response cytotoxicity curves presented the average cell viability and error bars represents the SEM of experiments performed in triplicate. Determination of sigmoidal dose response curves and calculation of IC_{50} values was performed using GraphPad Prism 7.0 software. Cytotoxicity experiments with each of tested compounds were repeated at least twice with the most representative results being presented in the results part.

3.2.4 Plasma stability studies

DMSO stock solutions of the compounds were prepared at a concentration of $1x10^{-2}$ M and diluted 1:10 in human plasma (HP), mouse plasma (MP) and PBS to a final concentration of $1x10^{-3}$ M. The dilutions were incubated at 37° C for a total of 96 h. 50 µl were taken under

sterile conditions at time-points: 0 min, 6 or 8 h, 24 h, 48 h, 72 h and 96 h. Samples were stored at -70° C until the day of analysis. The thawed samples were diluted in cell culture media for their use in a cytotoxicity assay. Cytotoxic potential of stressed compounds was determined as described in section 3.2.3.

3.2.5 *In vitro* competitive binding assay

Solutions containing the conjugate and 2-PMPA (Tocris) were prepared as 1:5 serial dilutions in culture medium. The compounds were added to the respective cells and incubated for 96 h. Starting concentration of the tested compounds was 1×10^{-5} M and 1×10^{-3} M (100 x molar excess over conjugate) for the competitor. In the case of bivalent binder (DUPA-Fc-α-amanitin), 2-PMPA was added in 200 x molar excess over the conjugate. Cell viability was determined by CellTiterGlo 2.0 assay as described in section 3.2.3.

3.2.6 Western blot

The samples were prepared in 3x non-reducing Laemmli sample buffer. 10 % polyacrylamide gel was placed in western blot chamber (Bio-Rad) in TGST buffer. 5 µl of protein marker and 10 ng of protein/lane were loaded and run for ca. 10 min. at 85 V to allow the samples to enter the stacking gel followed by 140 V ca. 45 min. for separation. The PVDF membrane was activated in 100 % methanol for 30 seconds and rinsed in transfer buffer. The blotting was performed in transfer buffer as indicated in *Figure 3.1* for 30 min. at 250 mA.

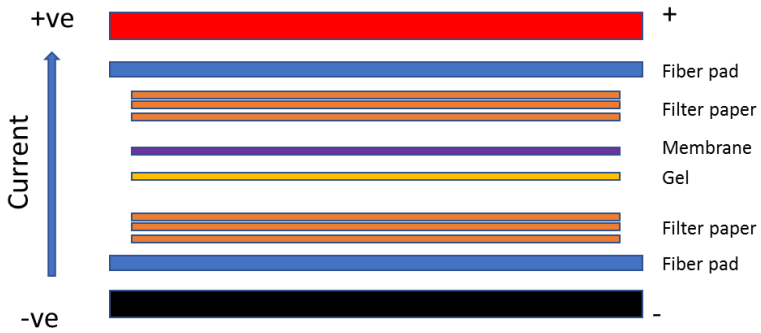

Figure 3.1 Schematic presentation of western blot transfer apparatus (Bio-Rad) and stacking of transfer components.

After the transfer the membrane was rinsed in TBST and incubated for 2 h in TBST containing 5 % milk powder for blocking of unspecific binding (western blot blocking buffer). Primary anti-α-amanitin antibody was diluted 1:10,000 in blocking buffer and incubated with the

membrane overnight at 4^{o} C. After overnight incubation the membrane was washed 3x5 min. in TBST buffer and subsequently incubated with secondary anti rabbit antibody conjugated to HRP for 2 h at room temperature. The membrane was washed in TBST buffer (3 x 5 min.) and chemiluminescent western-blot ECL reagent (Bio-Rad) was added on the top of the membrane. Finally, photosensitive film was exposed for different times (10 sec. - 1 min.) to obtain the optimal signal intensity.

3.2.7 Establishment of LNCaP and C4_2 xenograft model

All animal experiments were performed in accordance with the German Animal Welfare Act following an approval by the Baden-Württemberg animal oversight committee (Regierungspräsidium Karlsruhe, Germany).

All experiments were performed in CB 17 Scid mice strain male mice due to the androgen-dependent prostate cancer model which requires male hormones for growth. 6-8 weeks old mice were inoculated subcutaneously with 2.5 x 10^6 LNCaP or C4_2 tumor cells in 200 µl red phenol free RPMI/Matrigel (1:1) into their right flank. Once a mean tumor volume of ca. 100 mm^3 was reached, the animals were randomized. Animals were humanely euthanized when: 1) the net body weight loss was more than 20 % (compared to the body weight at the moment of randomization), 2) a tumor volume of more than 2000 mm^3 was reached, 3) in case of tumor ulceration or 4) when other clinical symptoms like lack of motility, hind leg paralysis, cachexia, poor general health condition or general signs of pain occurred.

3.2.8 Determination of maximum tolerated dose

The maximum tolerated dose (MTD) was determined in tumor free CB 17 Scid male mice. Tested compounds were administered as sterile solutions in PBS at pH 7.4 containing a maximal amount of 5 % DMSO. Survival and clinical signs were determined daily. Body weight was determined twice a week. Three animals per group were injected with a doubling ascending dose from a dose with no effect until clinical signs such as: 1) net body weight loss more than 20 %, 2) lack of recovery and/or one of the following symptoms like lack of motility, hind leg paralysis, cachexia, poor general health condition or general signs of pain, were observed. The next dose level was administered only after at least an 7-day long follow-up period. After administration of the dose the animals were monitored for ca. 2 weeks.

3.2.9 *In vivo* efficacy studies

In vivo efficacy experiments were carried out in LNCaP or C4_2 xenografts. Once the tumors reached a volume of ca. 100 mm^3, animals were randomized according to the tumor sizes in the study arms each containing 8-10 animals. The compounds were administered at doses and frequency determined on the base of toxicity and pharmacokinetic study. Tumors were measured in two dimensions using electronic external calipers and calculated using the formula $V = \frac{W^2 \text{ x } L}{2}$, (L= length and W= perpendicular width of the tumor, L>W). If an unusual growth was observed the tumor volume was measured in three dimensions: L, W and D and the volume calculated using use the following formula: $V = \frac{L \text{ x } W \text{ x } D \text{ x } \pi}{6000}$

3.2.10 *In vivo* pharmacokinetic and biodistribution study

Tumor bearing animals (n=3) were injected with a dose corresponding to 5 x MTD in case of HDP 30.2284 (0.184 mg/kg) to secure a detectable concentration of α-amanitin in organ and tumor extracts and serum. All other compounds were administered with doses corresponding to: ½ MTD: HDP 30.2301 at 1.23 mg/kg; HDP 30.2618 at 0.6 mg/kg; unconjugated α-amanitin at 0.075 mg/kg; and DUPA-Fc-α-amanitin conjugate at 1.0 mg/kg. In case of small molecular drug conjugates serum was isolated 5 min., 15 min., 30 min., 1 h, 2 h, 4 h, 6 h or 8 h, 24 h and 48 h upon administration and in case of DUPA-Fc-α-amanitin conjugate 15 min., 1 h, 2 h, 4 h, 6 h, 24 h, 3 days, 7 days and 14 days upon administration. Additionally, for HDP 30.2284, HDP 30.2301 and DUPA-Fc-α-amanitin kidneys and livers were isolated. All collected organs and sera were snap-frozen in liquid nitrogen and stored at -70° C until the day of sample preparation as described in section 3.2.12.

3.2.11 Mechanistic *in vivo* study of α-amanitin kidney accumulation after pre- and co-injection with PMPA

Determination of toxin concentration in the kidney of animals treated with HDP 30.2284 and HDP 30.2301 after pre-injection with 100x molar excess and co-injection with 50 x molar excess of PMPA over conjugates was performed. Conjugates were administered at doses corresponding with 75 µg/kg of α-amanitin: 0.184 mg/kg for HDP 30.2284 and 0.160 mg/kg for HDP 30.2301. 6 h after co-administration animals were sacrificed and organ extracts prepared as indicated in section 3.2.12.

3.2.12 Preparation of serum and organ extracts for determination of α-amanitin concentration

Snap frozen organs and sera isolated for pharmacokinetics and biodistribution studies were thawed. Ca. 100 mg of the organ was transferred to a FastPrep® tube. Triple volume of mixed gender human plasma with regard to the exact mass of the organ prepared for analysis was added to the tube. One gridding ball was added to each tube and the samples were homogenized using a planetary ball mill. The homogenate was centrifuged for 5 min. at 14,000 rpm (Thermo Fischer Scientific, Tabletop centrifuge FRESCO 17) and the supernatant was collected. 60 µl of the tissue supernatant or 60 µl of mouse serum collected in pharmacokinetic study was precipitated with 240 µl of 100 % ethanol and incubated for 20 min. at -20 ^{o}C to ensure complete protein precipitation. After centrifugation for 5 min. at 14,000 rpm (Thermo Fischer Scientific, Tabletop centrifuge FRESCO 17), the supernatants were collected and evaporated using a rotational vacuum concentrator (Martin Christ GmbH) for 3 h at 53^{o} C. Samples were tested in a competitive anti α-amanitin ELISA as described below in section 3.2.14.

3.2.13 Establishment of standard curve for detection of α-amanitin containing compounds by Enzyme-Linked Immunosorbent Assay (ELISA) assay

For determination of standard curve for the detection of α-amanitin containing compounds 1 mM stock solutions of HDP 30.2284, HDP 30.2301, HDP 30.2618 or α-amanitin were prepared in 100 % DMSO. The standards were prepared as serial 1:3 dilutions as indicated in the scheme below:

1) **8100 nM:** 6.48 µl of DMSO stock of 1 mM standard stock + 793.52 µl of human serum
2) **2700 nM**: 150 µl of 1 + 300 µl of human serum
3) **900 nM**: 150 µl of 2 + 300 µl of human serum
4) **300 nM**: 150 µl of 3 + 300 µl of human serum
5) **100 nM**: 150 µl of 4 + 300 µl of human serum
6) **33 nM**: 150 µl of 5 + 300 µl of human serum
7) **11 nM**: 150 µl of 6 + 300 µl of human serum
8) **3.7 nM**: 150 µl of 7 + 300 µl of human serum
9) **1.2 nM**: 150 µl of 8 + 300 µl of human serum
10) **0.4 nM:** 150 µl of 9 + 300 µl of human serum

60 µl of the standard solutions was precipitated with 240 µl of 100 % ethanol, incubated for 20 min. at -20° C to ensure complete protein precipitation and centrifuged for 5 min. at 14,000 rpm (Thermo Fischer Scientific, Tabletop centrifuge FRESCO 17). The supernatants were collected and evaporated using rotational vacuum concentrators (RVC 2-25 Cd plus, Martin Christ GmbH) for 3 h at 53° C and stored at -20° C until analysis. Samples were tested in competitive anti α-amanitin ELISA as described below in section 3.2.14.

3.2.14 Competitive anti α-amanitin ELISA for determining the concentration of α-amanitin containing compounds in mouse serum and organ extracts

For a competitive anti-α-amanitin ELISA, ELISA plates were coated overnight with 50 µl of anti-α-amanitin serum (polyclonal rabbit, produced by Heidelberg Pharma Research GmbH) c = 6.67 µg/ml diluted in PBS. The plates were blocked for 1 h at 37° C in ELISA blocking buffer and washed 3x with ELISA wash buffer using an automated Hydrospeed ELISA Washer (Tecan). Evaporated ethanol organ extracts, serum extracts or standards were reconstituted in ELISA sample buffer and mixed with 50 µl 1nM biotin-α-amanitin conjugate, reconstituted in ELISA sample buffer. 50 µl of the 1:1 mixture was applied to the ELISA plate in duplicate and incubated for 1 h at 37° C. The plate was washed 3x with 300 µl wash buffer using an automated Hydrospeed ELISA Washer (Tecan). 50 µl of streptavidin-HRP (1 µg/ml) was added in each well and incubated for 1 h at 37° C and 300 rpm. After washing, detection was performed by addition of 100 µl of 0.1 mg/mL TMB reagent reconstituted in 0.1 M sodium acetate buffer containing 0.001 % H_2O_2. Reaction was developed for 15 min. and quenched with 50 µl 1M H_2SO_4. Absorbance was determined at 450 nm and corrected with the background absorbance at 570 nm (FluostarOptima BMG Labtec). The concentration of α-amanitin containing compounds was calculated based on interpolating the sigmoidal standard curve using GraphPad Prism software.

3.2.15 Establishment of standard curve for determination of serum concentration of DUPA-Fc-α-amanitin conjugate

ELISA was performed as described above (3.2.14) with the following changes:

Standard dilutions of DUPA-α-amanitin conjugate were prepared in Sample Buffer (Candor Biosciences GmbH) as follows:

1) 400 pM: 40 µl of 10 nM DUPA-Fc-α-amanitin stock + 960 µl of Sample Buffer
2) 200 pM: 400 µl of 1 + 400 µl of Sample Buffer

3) 100 pM: 400 µl of 2 + 400 µl of Sample Buffer
4) 50 pM: 400 µl of 3 + 400 µl of Sample Buffer
5) 25 pM: 400 µl of 4 + 400 µl of Sample Buffer
6) 12.5 pM: 400 µl of 5 + 400 µl of Sample Buffer
7) 6.3 pM: 400 µl of 6 + 400 µl of Sample Buffer
8) 3.2 pM: 400 µl of 7 + 400 µl of Sample Buffer
9) 1.6 pM: 400 µl of 8 + 400 µl of Sample Buffer

Standards were analyzed together with samples as described in section 3.2.16.

3.2.16 Sandwich ELISA for determination of DUPA-Fc-α-amanitin serum concentration

ELISA was performed as described in section 3.2.14 with the following changes. Sera were thawed and diluted in Sample Buffer (Candor Biosciences GmbH) in two steps 1) 1:100 and 2) 1:10 to reach a final dilution of 1:1,000 (0.1 % of mouse serum). 50 µl of sample was applied on the blocked ELISA plate coated with α-amanitin capture serum in duplicate and incubated at 37° C for 1 h with shaking at 300 rpm (Orbital microplate shaker, neoLab). After washing step 50 µl 1:10,000 dilution of secondary antibody Rabbit anti-Human-IgG-HRP (Abcam ab98576) reconstituted in Sample Buffer (Candor Biosciences GmbH) was added per well and incubated at 37° C for 1 h with shaking at 300 rpm. After washing step detection was performed by addition of TMB reagent as described in the section 3.2.14.

3.2.17 Calculation of conjugates concentration in tissues

Concentration in murine plasma was directly extrapolated from sigmoidal standard curve in ELISA.

Calculation of concentration of each conjugate in the murine organs (per gram of wet tissue) was performed based on the following data:

- Concentration of compound in organ plasma extract extrapolated from sigmoidal standard curve in ELISA
- Exact volume of plasma used for organ extract preparation
- Molecular weight of the tested compound:
    - M_w HDP 30.2284 = 2,246.5 g/mol

- M_w HDP 30.2301 = 1,957.18 g/mol
- M_w HDP 30.2618 = 1,834.13 g/mol
- M_w DUPA-Fc-α-amanitin = 61,443.92 g/mol

- Exact mass of the analyzed organ

3.2.18 Statistical analysis

Statistical analysis was performed using GraphPad software 7.0.The Mann-Whitney test was used to compare the tumor volumes of different experimental arms *in vivo*. Level of significance was set at values **P* <0.05, ***P* < 0.01 and ****P* < 0.001, *****P* < 0.0001. For the comparison of kidney concentration of toxin paired *t*-test was used. Level of significance was set at values **P*<0.05, ***P* < 0.01 and ****P* <0.001. The concentration of α-amanitin containing compounds and DUPA-Fc-α-amanitin conjugate was calculated based on the interpolated standard curve using GraphPad Prism software 7.0. The half-life of small molecular conjugates was calculated using a one phase decay exponential non-linear curve fit. Half-life of DUPA-Fc-α-amanitin was calculated on the base of two-phase decay non-linear curve fit. Statistical differences in animals survival was calculated using Log-rank test.

4. RESULTS

4.1 DUPA -ALPHA- AMANITIN CONJUGATES BEARING VAL-ALA-PAB CLEAVABLE AND C_6 NON-CLEAVABLE LINKER

It is known that no general assumptions can be made regarding the optimal linker strategy for the development of ADCs and SMDCs. Comparative analysis of the literature data reporting development of targeted therapeutics suggest that the linker strategy must be tailored for each conjugate individually. Matching between technology allowing to obtain the optimal activity of a conjugate depends on numerous factors such as: type of cancer, type of target, intracellular processing of the target in case if target is internalized and toxin properties [97]. Linker strategy has been shown to have a great impact on the activity and toxicity of conjugates in the field of targeted therapeutics [98]. The linkers most commonly used in ADC and SMDCs development are 1) protease cleavable linkers, mainly the motifs recognized by intracellular proteases - mainly cathepsin B [47, 55, 99], 2) chemically labile disulfide linkers sensitive for a high glutathione concentration [49, 100] and 3) stable (non-cleavable) linkers [101]. The preclinical development of DUPA-α-amanitin conjugates was initiated with the characterization of a compound bearing a Val-Ala-PAB cathepsin B cleavable linker which is one of the most commonly applied linkers in the ADCs research. For the purpose of profiling studies and determination of structure activity relationship the analogous conjugates bearing a C_6 non-cleavable linker were produced and tested.

4.1.1 Establishment of a model for *in vitro* screening of DUPA-α-amanitin conjugates

For *in vitro* tests of DUPA-α-amanitin conjugates three cell lines expressing different levels of PSMA receptor were chosen: LNCaP, 22RV1 and PC3 [102]. LNCaP cell line is reported to express high levels of PSMA, 22RV1 expresses moderate levels of PSMA and PC3 cell line is reported to be PSMA negative. PSMA receptor expression analysis in all three prostate cancer cell lines was performed using flow cytometry. Cells were stained using a primary anti-PSMA antibody produced at Heidelberg Pharma Research GmbH recognizing the extracellular domain of the receptor and a secondary anti-human antibody labeled with Alexa 488 (*Figure 4.1*, right panel). As a control staining only with the secondary antibody was performed (*Figure 4.1*, left panel).

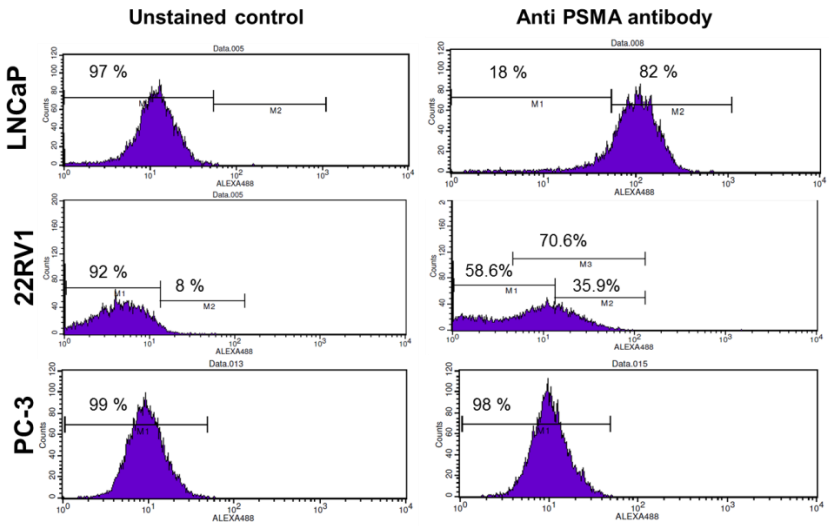

Figure 4.1 Flow cytometry analysis of PSMA receptor expression in LNCaP (PSMA +++), 22RV1 (PSMA+) and PC3 (PSMA -) cell lines.

In case of LNCaP cells stained with anti-PSMA antibody a clear shift of the cell population to the right side of the histogram and a clear increase in mean fluorescence intensity was observed. The 22RV1 cell line did not give an unequivocal result. On the histogram of 22RV1 cells stained with the PSMA antibody a shift to higher fluorescence intensity compared to the unstained cells was observed. This shift was not such evident as in case of LNCaP. Moreover, a sub-population of cells which were PSMA negative was evident confirming the heterogeneous PSMA expression in 22RV1 cell line. The PC3 cell line was completely PSMA negative since the non-stained cells histogram was overlapping with the PSMA antibody stained histogram. Obtained results of PSMA expression in tested cell lines are in accordance to the literature data [102].

4.1.2 DUPA-α-amanitin compounds –importance of supporting spacer

All DUPA-α-amanitin conjugates were screened for their cytotoxic potential in three prostate cancer cell lines: LNCaP, 22RV1 and PC3. After 96 h of incubation cell viability was assessed using CellTiterGlo® 2.0 reagent. Prolonged 96 h period was chosen due to the mode of action of α-amanitin-amanitin, which is inhibition of RNA Polymerase II and subsequent inhibition of protein synthesis. Since it is reported in the literature that half-life of some functional proteins may be as long as 45 h and a full-blown potential of α-amanitin ADCs using α-amanitin as a payload was observed after 96 h of incubation with the conjugate a 96 h incubation time was used in the following cytotoxicity studies [74, 103].

The two first screened compounds were HDP 30.1585 bearing a C_6 non-cleavable linker and HDP 30.1592 bearing a Val-Ala-PAB cleavable linker directly conjugated to the glutamic acid-urea targeting moiety (*Figure* 4.2). In both compounds the linker was attached to the 6-OH tryptophan of α-amanitin. Attachment of a linker at this position is known to have no impact on the α-amanitin activity [70]. Cytotoxic potential of both conjugates is shown in *Figure 4.3*.

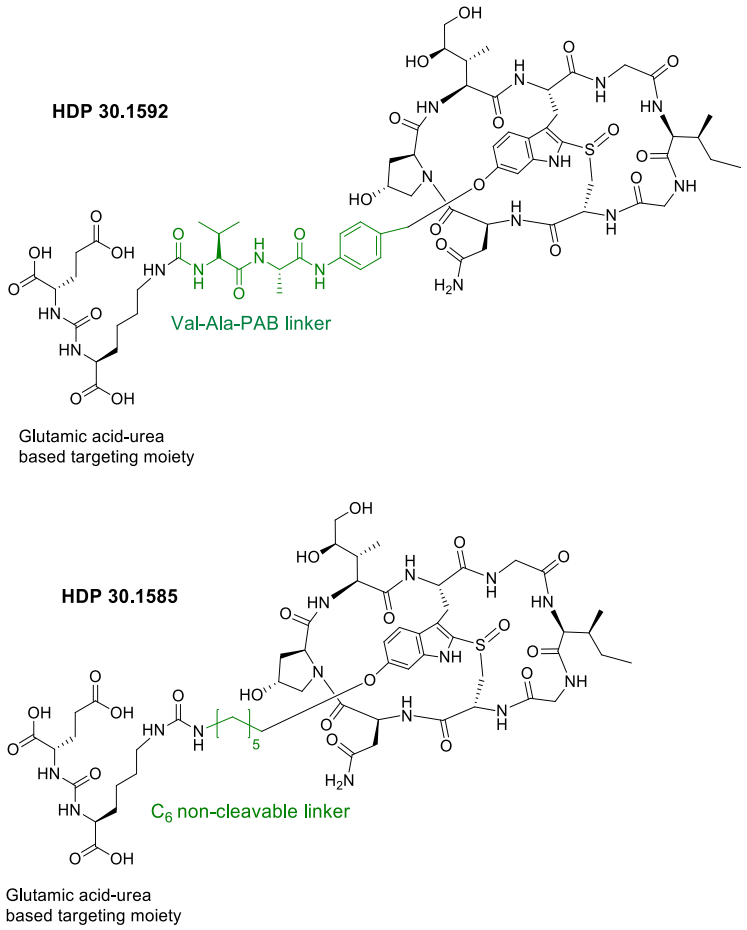

Figure 4.2 Chemical structures of HDP 30.1585 and HDP 30.1592.

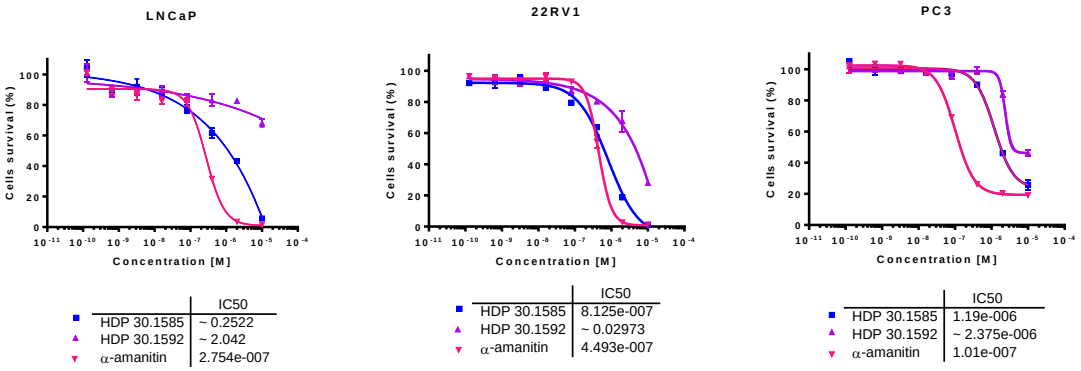

Figure 4.3 Cytotoxic potential of HDP 30.1585 and HDP 30.1592 on LNCaP (PSMA +++), 22RV1 (PSMA +) and PC3 (PSMA -) cell lines. (IC_{50} is presented as median cell survival ± SEM, n=3).

The results of cytotoxicity *in vitro* have demonstrated lower cytotoxic potential of both conjugates in PSMA positive cells compared to unconjugated α-amanitin (*Figure 4.3*). Unconjugated toxin showed an IC_{50} value in high concentration of 275.4 nM and 449.3 nM due to the high hydrophilicity and limited membrane permeability. HDP 30.1592 (Val-Ala-PAB cleavable linker) demonstrated the lack of cytotoxic potential on LNCaP cells. Only at highest concentrations approximately 80 % killing of moderately PSMA expressing 22RV1 cell line was observed. HDP 30.1585 (C_6 non-cleavable linker) performed slightly better with an IC_{50} value in the micromolar range which is higher compared to the IC_{50} value of unconjugated α-amanitin. The results obtained on PC3 - PSMA negative cell line which are similar to those obtained for PSMA positive cells suggest that both conjugates are not selective and that there is no benefit from attachment of α-amanitin to the DUPA targeting moiety using these particular linkers.

As already discussed in section 1.4.3 the presence of supporting spacer, fitting into tunnel-like shaped structure of PSMA is critical for efficient ligand binding at the active site and efficient toxin delivery by DUPA moiety. In this study the 8-aminooctanoic acid-phenylalanine-phenylalanine (8-Aoc-Phe-Phe), linker identical to reported in the literature PSMA targeted DUPA-TubH delivery was employed [77]. Further on this motif will be named "supporting spacer". HDP 30.2284 (Val-Ala-PAB cleavable linker) and HDP 30.2301 (C_6 stable linker) are analogues of HDP 30.1585 and HDP 30.1592, respectively (*Figure 4.4*). Both compounds were synthesized by coupling maleimide activated derivatives of α-amanitin to the cysteine in the structure of supporting spacer.

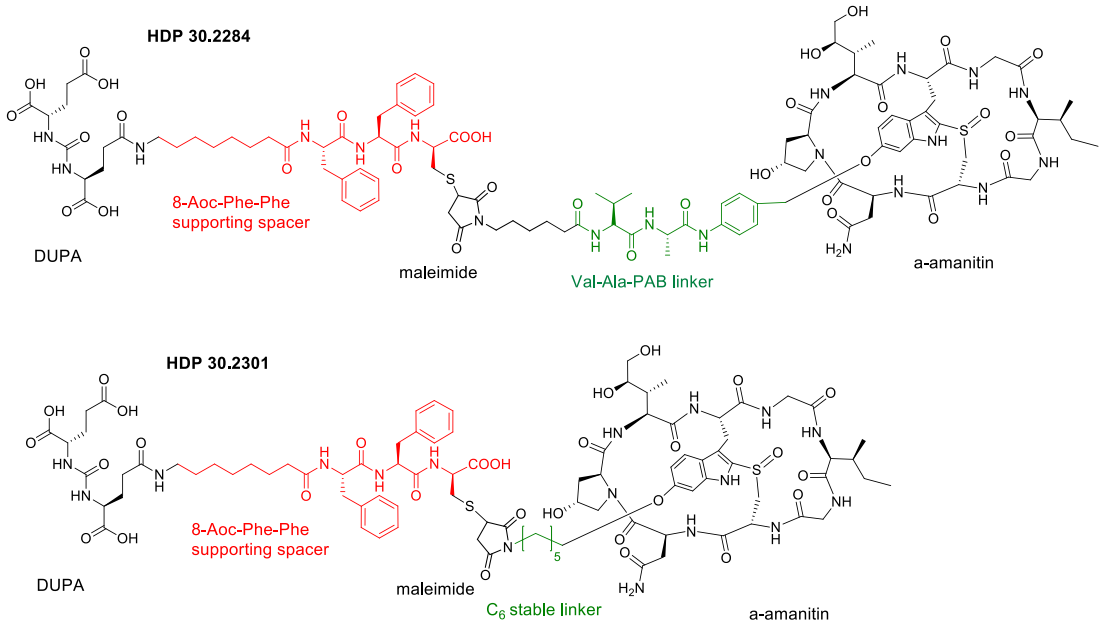

Figure 4.4 Chemical structures of HDP 30.2284 and HDP 30.2301.

The cytotoxic potential of both compounds bearing the optimized spacer is presented in *Figure 4.5*.

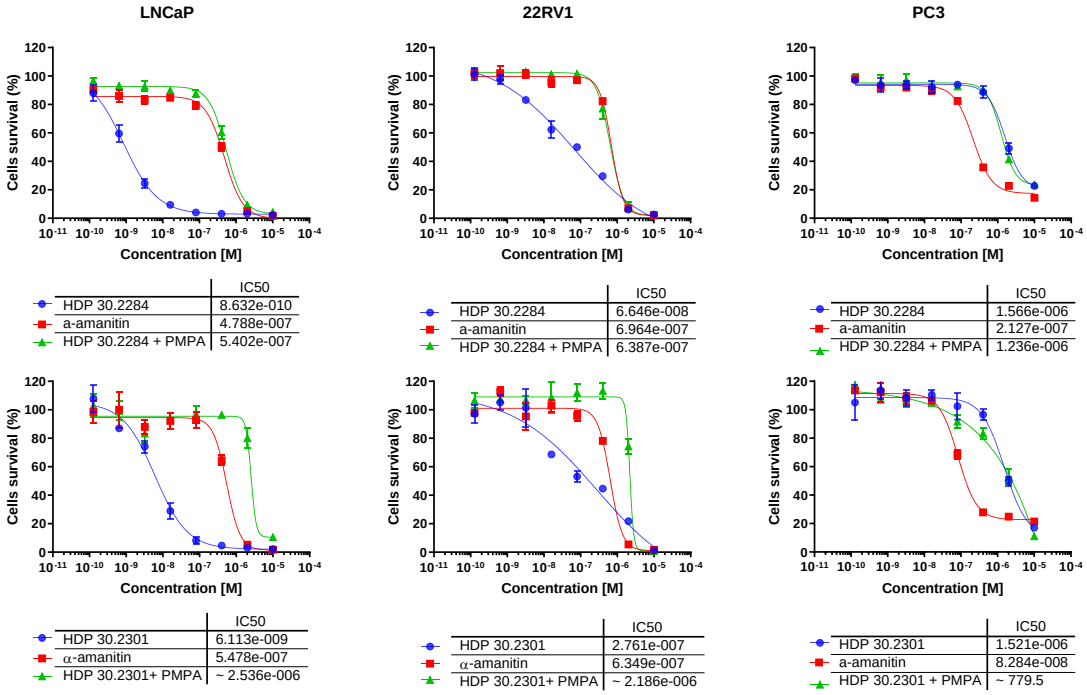

Figure 4.5 Cytotoxic potential of compounds HDP 30.2284 (Val-Ala-PAB) (upper panel), HDP 30.2301 (C_6 non-cleavable linker) (lower panel) and α-amanitin on LNCaP (PSMA +++), 22RV1 (PSMA +) and PC3 (PSMA -) cell lines. (IC_{50} is presented as median cell survival ± SEM, n=3).

The difference in the activity of both conjugates in receptor positive and negative cell lines was evident. HDP 30.2284 showed an IC_{50} value at the sub-nanomolar concentration (0.86 nM) and was ca. 1800x more toxic in the PSMA positive LNCaP cells than in PSMA negative PC3 cells. In LNCaP cells the cytotoxic potential of unconjugated α-amanitin was ca. 555x lower compared to HDP 30.2284 (*Figure 4.5*).

HDP 30.2301 has shown an IC_{50} value of ca. 6 nM which was approximately seven-fold higher compared to Val-Ala-PAB linker bearing analogue HDP 30.2284. HDP 30.2301 was approximately 250 times more potent on PSMA positive LNCaP cells than on PSMA negative PC3 cells and approximately 90 times more potent than unconjugated α-amanitin on LNCaP cells (*Figure 4.5*). Moreover, the cytotoxic potential of both optimized conjugates HDP 30.2284 and HDP 30.2301 was determined in the presence of the DUPA competitive inhibitor - 2-PMPA (PMPA). Cytotoxic activity of both conjugates was completely abolished in the presence of 100 molar excess of the inhibitor. The activity of both compounds was positively correlated with levels of PSMA receptor expression. As expected, moderate cytotoxicity was observed on 22RV1 cells with heterogeneous PSMA expression

and the IC_{50} in the range of concentration similar to this observed for naked toxin (IC_{50} at approximately 10^{-7} M) was observed for PC3 cells (*Figure 4.5*).

Comparing the cytotoxicity results obtained for HDP 30.1585 and HDP 30.1592 lacking supporting spacer with the cytotoxicity results for HDP 30.2284 and HDP 30.2301 bearing the supporting spacer the absolute necessity of the 8-Aoc-Phe-Phe motif for efficient PSMA active site binding and activity of conjugates was confirmed [77] (also discussed in Section 1.4.2). 8-Aoc-Phe-Phe supporting spacer was employed in the development of all described further DUPA-α-amanitin conjugates.

4.1.3 Optimization of plasma stability

Aiming for optimization of plasma stability compound HDP 30.2515 an analogue of described in previous section HDP 30.2284 and compound HDP 30.2523 an analogue of HDP 30.2301 were developed. The structure of both conjugates: HDP 30.2515 and HDP 30.2523 synthesized using acetamide chemistry are presented in *Figure 4.6*. Implementation of acetamide chemistry in the synthesis of DUPA-α-amanitin SMDCs was motivated by fact, that for ADCs using acetamide conjugation a better stability in plasma compared to maleimide synthesized analogues was observed [104]. Acetamide compounds were designed and assessed *in vitro* in order to verify whether this can be also observed for small molecule toxin conjugate.

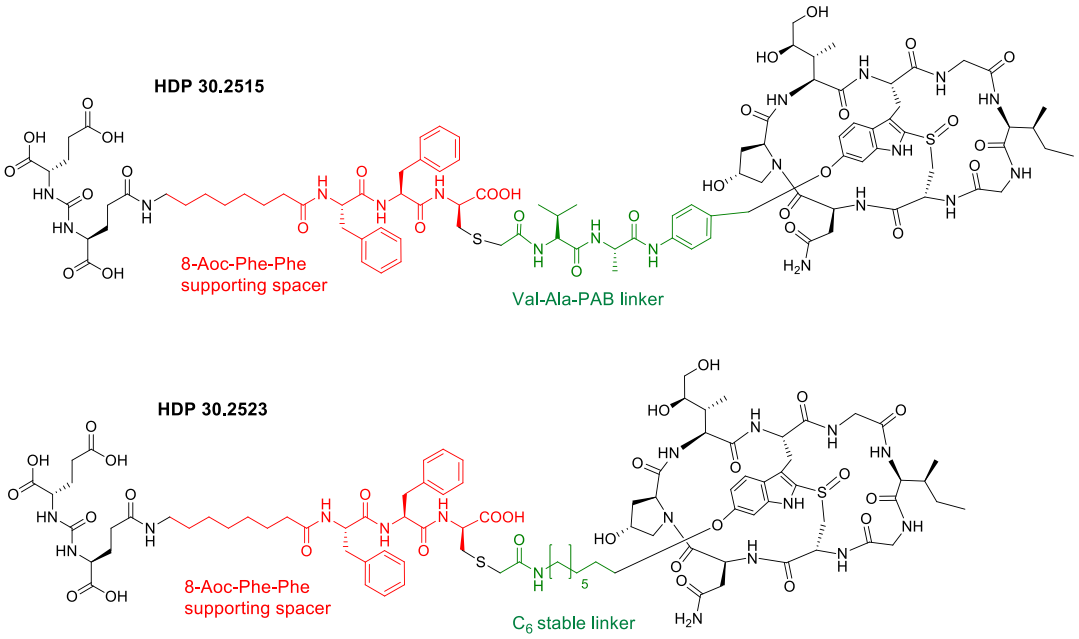

Figure 4.6 Chemical structures of conjugates synthesized using acetamide chemistry: HDP 30.2515 (Val-Ala-PAB linker) and HDP 30.2523 (C_6 non-cleavable linker).

Comparison of cytotoxic activity of the parental maleimide compounds and their acetamide analogues is presented in *Figure 4.7*.

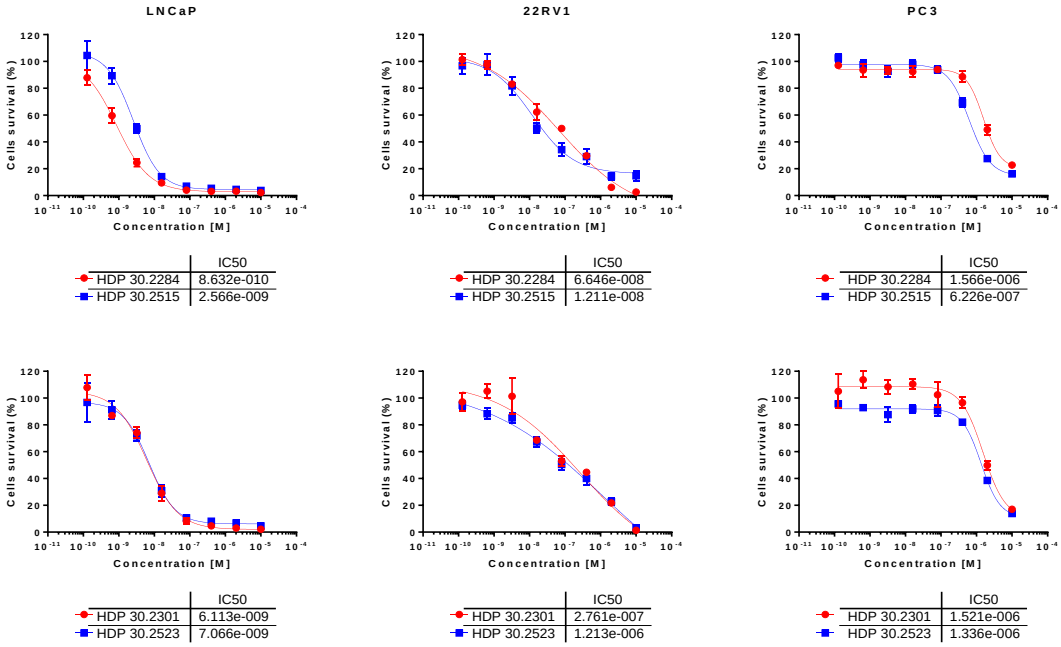

Figure 4.7 Cytotoxic potential of analogues synthesized using maleimide chemistry (in red) HDP 30.2284 and HDP 30.2301 and acetamide chemistry (in blue) HDP 30.2515 and HDP 30.2523.

Compounds with Val-Ala-PAB cleavable linker are presented in the upper panel and compounds with C_6 non-cleavable linker in the lower panel. Conjugates were tested in LNCaP (PSMA +++), 22RV1 (PSMA +) and PC3 (PSMA -) prostate cancer cell lines. (IC_{50} is presented as median cell survival ± SEM, n=3).

HDP 30.2515 showed a high cytotoxic potential on LNCaP and 22RV1 cell lines (IC_{50} = 2.57 nM and IC_{50} = 12.0 nM, respectively) and a complete lack of activity on PC3 PSMA negative cells, which is in the range of IC_{50} value observed for unconjugated toxin (section 4.1.2). Cytotoxicity of HDP 30.2515 was slightly lower compared to the maleimide bearing analogue HDP 30.2284 on LNCaP cells (2.57 nM *vs.* 0.86 nM, respectively). Similarly, as observed for the maleimide analogues, HDP 30.2515 bearing Val-Ala-PAB cleavable linker was more potent compared to HDP 30.2523 bearing C_6 non-cleavable linker. The difference in cytotoxic potential of analogues bearing a C_6 stable linker (HDP 30.2301 *vs.* HDP 30.2523) on both PSMA positive cell lines was negligible. Again, the PC3 cell line was not sensitive for the therapy with neither HDP 30.2301 nor HDP 30.2523. As expected, elimination of the maleimide ring from the structure did not have an impact on in *vitro* activity.

Further step aiming into characterization of the aforementioned pairs of conjugates was determination of their *in vitro* plasma stability.

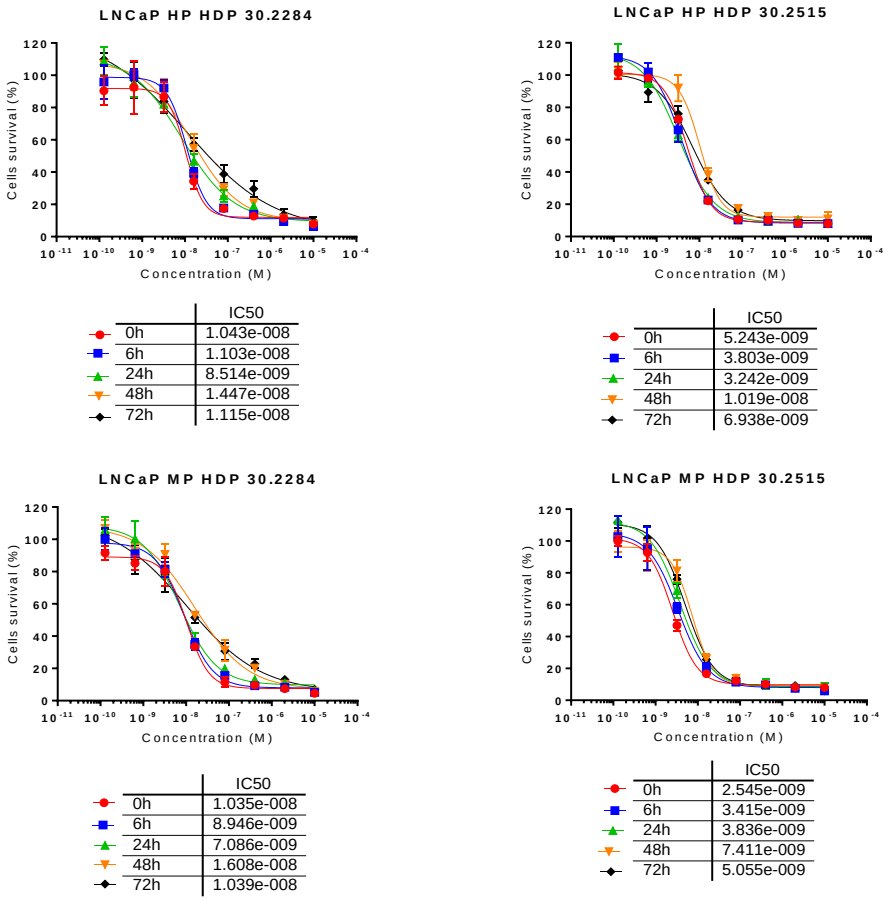

Figure 4.8 Cytotoxic potential of maleimide and acetamide analogues bearing Val-Ala-PAB cleavable linker.

Cytotoxicity of HDP 30.2284 (maleimide) and HDP 30.2515 (acetamide) in the time-course after incubation in human plasma (HP, upper panel) and mouse plasma (MP, lower panel) on LNCaP (PSMA +++) cell line. (IC_{50} is presented as median cell survival ± SEM, n=3).

The plasma stability of conjugates synthesized using maleimide and acetamide chemistry was directly compared in accordance to the procedure described in section 3.2.4. The results are presented in *Figure 4.8* and *Figure 4.9*.

Even a very short exposure of HDP 30.2284 for plasma results in ca. 12-fold increase in IC_{50} value (ca. 10 nM IC_{50} upon exposure to mouse or human plasma *vs.* 0.86 nM without exposure to plasma *Figure 4.8 vs. Figure 4.7*). Although, IC_{50} values obtained for the compound HDP 30.2284, even after prolonged time of stressing in plasma are similar to those obtained at time-point 0 h the shapes of cytotoxicity curves upon prolonged stressing, ≥ 24h for human plasma and ≥ 48h for mouse plasma are flattened. The cytotoxicity of HDP 30.2284 is impaired at effective concentrations ≥ 10nM. The acetamide

analogue of HDP 30.2284 – compound HDP 30.2515 independently to the duration of stressing in plasma demonstrated IC_{50} always in the one-digit nanomolar concentration, and in contrast to HDP 30.2284 profiles of sigmoidal response-curves were similar to the non-exposed for the plasma conjugate (Figure 4.7 and *Figure 4.8*). In conclusion IC_{50} was not affected even after prolonged stressing in both human and mouse plasma and the stability of acetamide analogue came out to be improved compared to maleimide counterpart.

Similar plasma stability experiment was performed for the compounds presenting a non-cleavable C_6 linker (HDP30.2301 – maleimide, chemical structure presented in *Figure 4.4* vs. HDP 30.2523 – acetamide, chemical structure presented in *Figure 4.6*).

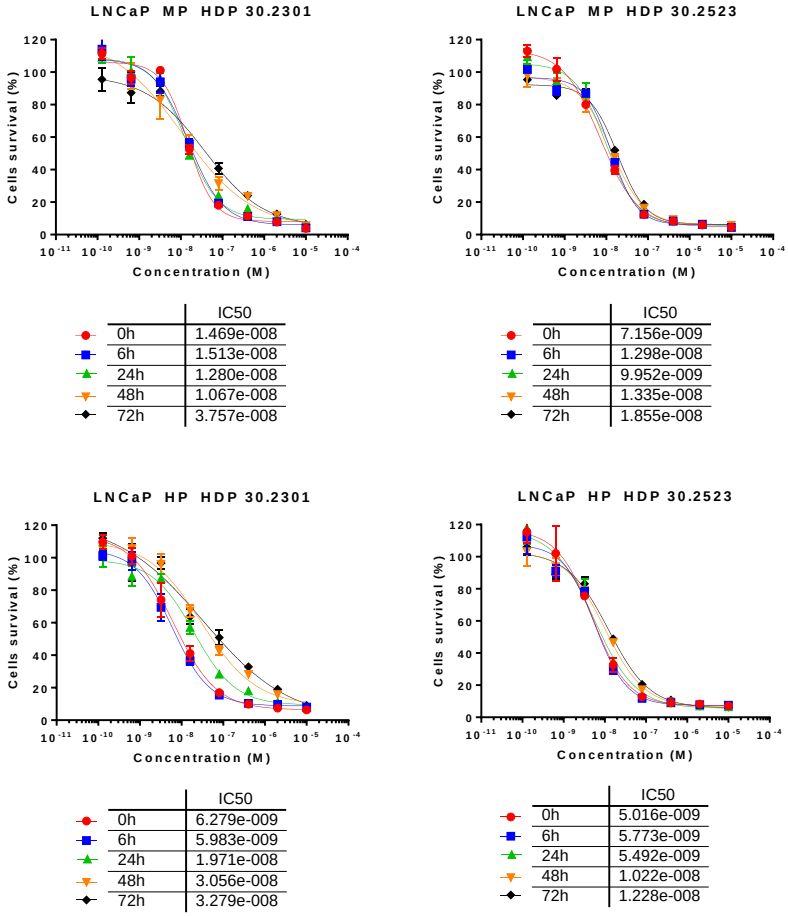

Figure 4.9 Cytotoxic potential of maleimide and acetamide DUPA-α-amanitin analogues bearing C_6 stable linker.

HDP 30.2301 (maleimide) and HDP 30.2523 (acetamide) in time-course after incubation in mouse plasma (MP, upper panel) and human plasma (HP, lower panel) in LNCaP (PSMA +++) cell line.

The cytotoxic potential of HDP 30.2301, synthesized using maleimide chemistry was decreasing with the longer time of stressing in plasma (*Figure 4.9*, left upper and lower panel). The loss of cytotoxic potential is not as prominent for plasma stressed acetamide synthesized analogue HDP 30.2523 (*Figure 4.9* right upper and lower panel). For HDP 30.2301 a decrease in the IC_{50} from 0 h to 72 h of incubation in plasma is approximately 20 % in mouse plasma and approximately 40 % in human plasma. In the case of the acetamide analogue - compound HDP 30.2532 a cytotoxic potential decreased approximately 10 % in mouse plasma and approximately 20 % in human plasma comparing the curves corresponding to 0 h and 72 h. Both compounds showed similar stability in mouse and human plasma. These results are in line with observations made for the pair

of compounds featuring cleavable linker. In conclusion also for compounds featuring C_6 non-cleavable linker the conjugate synthesized using acetamide strategy HDP 30.2532 showed improved plasma stability compared to maleimide analogue - HDP 30.2301.

It was demonstrated that avoidance of maleimide in the structure of the DUPA-α-amanitin conjugate improved the plasma stability. Considering the small molecular size of the conjugates < 3 kDa the short *in vivo* half-life in the range of minutes or hours is expected. Although, acetamide conjugates HDP 30.2515 and HDP 30.2523 demonstrated better plasma stability, maleimide synthesized HDP 30.2284 and HDP 30.2301 did not show significantly impaired cytotoxic potential up to 6 h after incubation in plasma (*Figure 4.8* and *Figure 4.9*). Based on this result and expected short half-life it can be assumed that plasma stability is not a relevant factor i*n vivo.* Moreover, it was demonstrated in the field of ADCs that extending linker half-life beyond the pharmacokinetic half-life is not likely to have an impact on a drug exposure and subsequent efficacy [104]. Based on the literature search and conjugates performance *in vitro*, HDP 30.2284 and HDP 30.2301 were selected for further characterization *in vivo*. Presented in this chapter comparative plasma stability results favoring the use of acetamide conjugation strategy are valuable and will be considered in the further development of molecules - especially with prolonged half-life (described further is section 4.3.2).

4.1.4 Single dose toxicity study of lead conjugates HDP 30.2284 and HDP 30.2301

For DUPA-α-amanitin lead small molecule drug conjugates acute toxicity in a dose-escalation study was tested in accordance to the procedure described in section 3.2.8. The dose of administered HDP 30.2284 and α-amanitin equivalents are presented in *Table 4.1*. The relative body weight change upon single dose administration is presented in *Figure 4.10*.

Table 4.1 Dose of HDP 30.2284 used in MTD study with indicated equivalents of α-amanitin.

Compound	Dose HDP 30.2284 [mg/kg]	Dose of α-amanitin [µg/kg]
HDP 30.2284	0.368	150
HDP 30.2284	0.184	75
HDP 30.2284	0.092	37.5
HDP 30.2284	0.046	18.75
HDP 30.2284	0.023	9.37

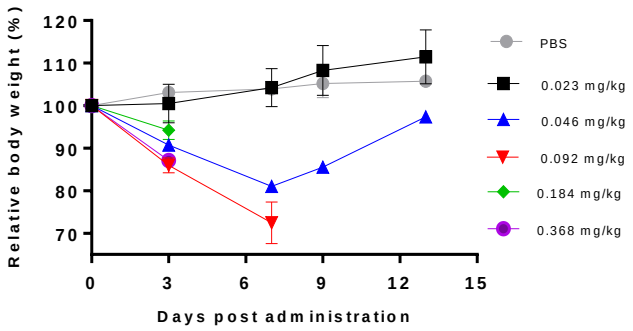

Figure 4.10 Tolerability of HDP 30.2284 measured as relative body weight change after single dose administration (Cb 17 Scid male mice, relative body weight ± SEM, n=3).

Determination of MTD was started with the dose of 0.368 mg/kg HDP 30.2284, which corresponds to the equivalent of unconjugated α-amanitin MTD - 150 µg/kg in tested Cb 17 Scid mouse strain (internal Heidelberg Pharma Research GmbH data). Further dosing levels were adjusted based on the outcome of the first administered dose, after at least one-week observation. The dose of 0.368 mg/kg of HDP 30.2284 caused severe toxicity which was expressed as a rapid body weight loss of approximately 15 % three days after

administration (*Figure 4.10*). At day four after administration all three animals from this group showed deterioration of all clinical parameters and at day five were found dead. This suggests that conjugation of DUPA to α-amanitin *via* Val-Ala-PAB linker increases the toxicity. Macroscopic evaluation of the organs upon autopsy showed congested kidneys and no changes in other vital organs (data not shown). Similar symptoms were observed for a double descending dose of 0.184 mg/kg (*Figure 4.10* and *Table 4.1*). The animals were found dead at day five upon administration. After administration of a 0.092 mg/kg dose the animals demonstrated similar symptoms e.g. a significant body weight loss at day three following administration. All animals were humanely euthanized at day eight due to an unacceptable body weight loss of ca. 30 % and general bad condition. The dose of 0.046 mg/kg redounded the marginally acceptable weight loss of approximately 20 % at day seven. The follow up of the animals showed weight re-gain and complete recovery at day 13 following administration. Only at the dose of 0.023 mg/kg, corresponding to a reduction by a factor of 16 in relation to the initially administered dose, HDP 30.2284 was completely tolerated and showed a profile similar to the vehicle injected group (*Figure 4.10*). Based on this result the MTD of HDP 30.2284 was set for 0.046 mg/kg after single administration, which is approximately 4 times lower compared to the unconjugated toxin regarding the equivalents of α-amanitin.

Since HDP 30.2284 showed lower tolerability compared to the unconjugated toxin a high safety margin was applied in the choice of first dose tested in tolerability studies of compound HDP 30.2301 bearing stable linker. The starting dose for compound HDP 30.2301 was set to the equivalent of the tolerated dose of compound HDP 30.2284. The results of MTD study for HDP 30.2301 are presented in *Table 4.2* and in *Figure 4.11*.

Table 4.2 Doses of HDP 30.2301 used in MTD study with indicated equivalents of α-amanitin.

Compound	Dose HDP 30.2301 [mg/kg]	Dose of α-amanitin [µg/kg]
HDP 30.2301	0.020	9.38
HDP 30.2301	0.040	18.75
HDP 30.2301	0.080	37.5
HDP 30.2301	0.160	75
HDP 30.2301	0.320	150
HDP 30.2301	0.640	300
HDP 30.2301	1.280	600
HDP 30.2301	2.560	1200
HDP 30.2301	3.840	1800

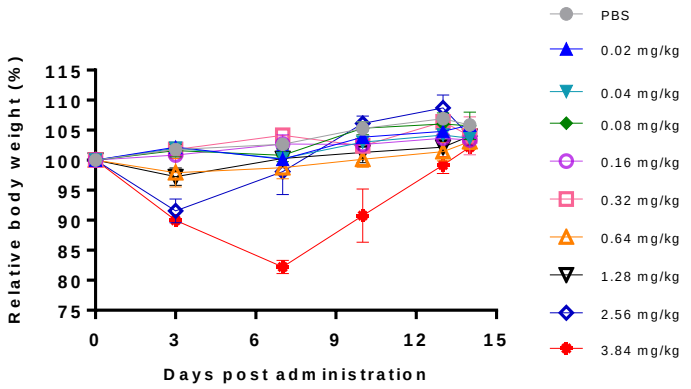

Figure 4.11 Tolerability of HDP 30.2301 measured as relative body weight change after single dose administration (Cb 17 Scid male mice, relative body weight ± SEM, n=3).

Unexpectedly, the dose ranges from 0.02 to 1.28 mg/kg did not affect the body weight of animals. At the dose level of 2.56 mg/kg the animals did not show any clinical symptoms and a body weight loss of approximately 10 % at day three following administration. As the dose 2.56 mg/kg already impacted the body weight the next dosing level was escalated as an increment of 1.5-fold. 3.84 mg/kg resulted in marginally acceptable weight loss of ca. 20 % at day 7 after administration and recovered during the follow-up period. A similar profile of toxicity was observed for the dose level of 0.046 mg/kg of HDP 30.2284 (*Figure 4.10*). Based on the previous observation of toxicity for HDP 30.2284 further dose escalation

of conjugate HDP 30.2301 was stopped and MTD set for 3.84 mg/kg. MTD of HDP 30.2301 is 12 times higher than tolerability of unconjugated α-amanitin and 96 times higher compared to the analogue bearing cleavable linker - HDP 30.2284.

4.1.5 Pharmacokinetic study of conjugates HDP 30.2284 and HDP 30.2301

In order to determine the frequency of dosing for *in vivo* efficacy studies, a pharmacokinetics of HDP 30.2284 and HDP 30.2301 after single dose administration was determined. Concentration measurement of HDP 30.2284 and HDP 30.2301 in mouse serum was performed in accordance to the procedure described in section 3.2.10. Conjugate HDP 30.2284 was injected at a dose corresponding to 4x of the MTD - 0.184 mg/kg in order to ensure a detectable concentration of conjugate in serum. This dose did not influence the wellbeing of animals as dissection was performed before full toxicity symptoms were developed, what normally happens 3-7 days after administration of a toxic dose. HDP 30.2301 was administered at a dose of 1.28 mg/kg (1/3 MTD) - the dose planned for further efficacy study. For the calculation of the half-life single-compartmental model and the linear pharmacokinetics are assumed. Concentrations were determined in a competitive anti-α-amanitin ELISA using anti-α-amanitin antiserum containing polyclonal antibody for capturing. This analytical method allows to measure the total plasma concentration of compounds presenting α-amanitin core in the structure, including possible metabolites.

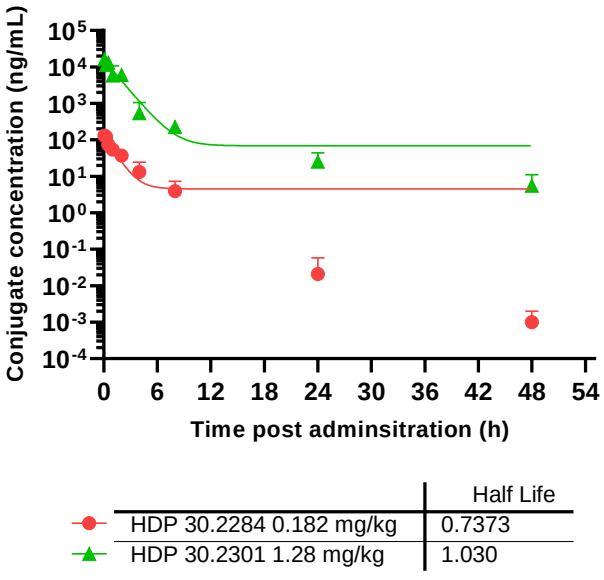

Figure 4.12 Pharmacokinetic profile and half-life of HDP 30.2284 and HDP 30.2301 in Cb 17 Scid male mice (median concentration ± SEM, n=3).

The plasma half-life of HDP 30.2284 and HDP 30.2301 was determined for ca. 44.2 min and 61.8 min, respectively. As expected, due to small molecular size the conjugates are rapidly cleared *via* renal filtration. According to the calculated half-life after the equivalent of 8 half-lifetimes: for HDP 30.2284 at 5.9 h and for HDP 30.2301 at 8.24 h following injection approximately 99 % of the conjugate is eliminated from the blood stream. The very short half-life determined for both small molecular DUPA-α-amanitin conjugates indicates that a dosing regimen should be frequent in order to provide a maximal exposure to the drug during the therapy.

4.1.6 Efficacy study of conjugates HDP 30.2284 and HDP 30.2301

For first tested conjugate HDP 30.2284 a pilot study evaluating different dosing regimens was set up in order to understand the relation between dosing frequency and tumor response. HDP 30.2284 was administered in three dosing schemes: 1) ½ MTD (0.023 mg/kg) two times per week; 2) ¼ MTD (0.0115 mg/kg) three times per week; and 3) ¼ MTD (0.0115 mg/kg) 5 times per week. The therapy was applied for a period of two weeks in mice xenografted with PSMA positive LNCaP tumors. All tested dosing regimens were well tolerated (Panel B *Figure 4.13*). The observed cachexia is generally associated with LNCaP model and is also observed in the vehicle injected group.

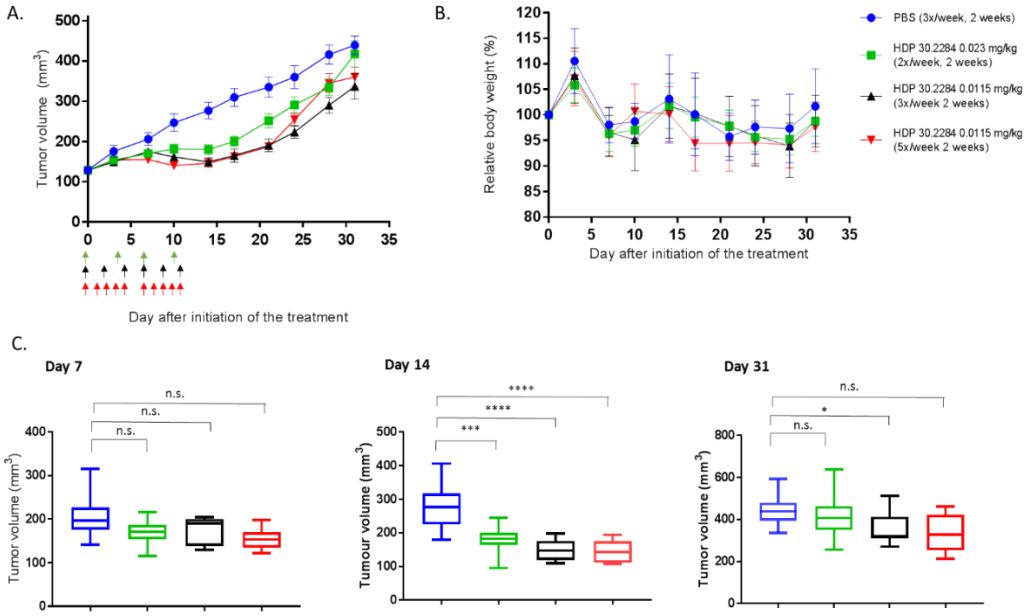

Figure 4.13 *In vivo* evaluation of antitumor activity of HDP 30.2284in Cb17 Scid mice xenografted with LNCaP tumors.

A. Efficacy (presented is average tumor volume ± SEM; n.s. – non-significant, n=10); **B.** Tolerability (presented is average body weight ± SEM, n=10); **C.** Box plots comparing tumor volumes at day 7, 14 and 31 after initiation of the treatment (boxes present distribution of tumor volume with the whiskers indicating minimum to maximum tumor volume observed, n.s. – non-significant, n=10).

Until the day 7 after initiation of the treatment no statistically significant differences in median tumor sizes between the vehicle and the conjugate treated arms of the study were observed (*Figure 4.13* Panel A and C). The differences in tumor sizes started to be more prominent at day 10 after initiation of the therapy. Upon termination of the treatment (last administration at day 11) tumor stasis was observed only until the day 14 (*Figure 4.13* Panel C). At day 14 the tumors started to re-grow with kinetics similar to the vehicle injected group. Interestingly a slightly better performance of the conjugate at a lower dose of 0.0115 mg/kg (1/4 MTD) but using more frequent administration scheme was observed compared to the dose of 0.023 mg/kg (1/2 MTD) administered twice per week. The 0.0115 mg/kg dose either being administered three or five times per week showed a similar performance. Starting at day 24 onward the tumor sizes between groups started to converge and appeared almost identical in the end of the follow up period (*Figure 4.13* Panel C Day 31). In general,

the tumor growth inhibition was limited to the period of administration and was not sustained after treatment cessation.

Since tolerability of HDP 30.2301 was much higher the efficacy of this compound was tested in order to verify whether the administration of higher dose would improve the efficacy. Since highest antitumor efficacy for HDP 30.2284 was observed at the administration frequency three times per week the same dosing regimen was applied for the therapy with the HDP 30.2301. Due to better tolerability HDP 30.2301 was administered for a period of five weeks at the dose corresponding to 1/3 of the MTD (1.28 mg/kg) (*Figure 4.14*). This dose level was chosen based on the results of MTD study and observation that it did not lead to any significant body weight loss (*Figure 4.11*).

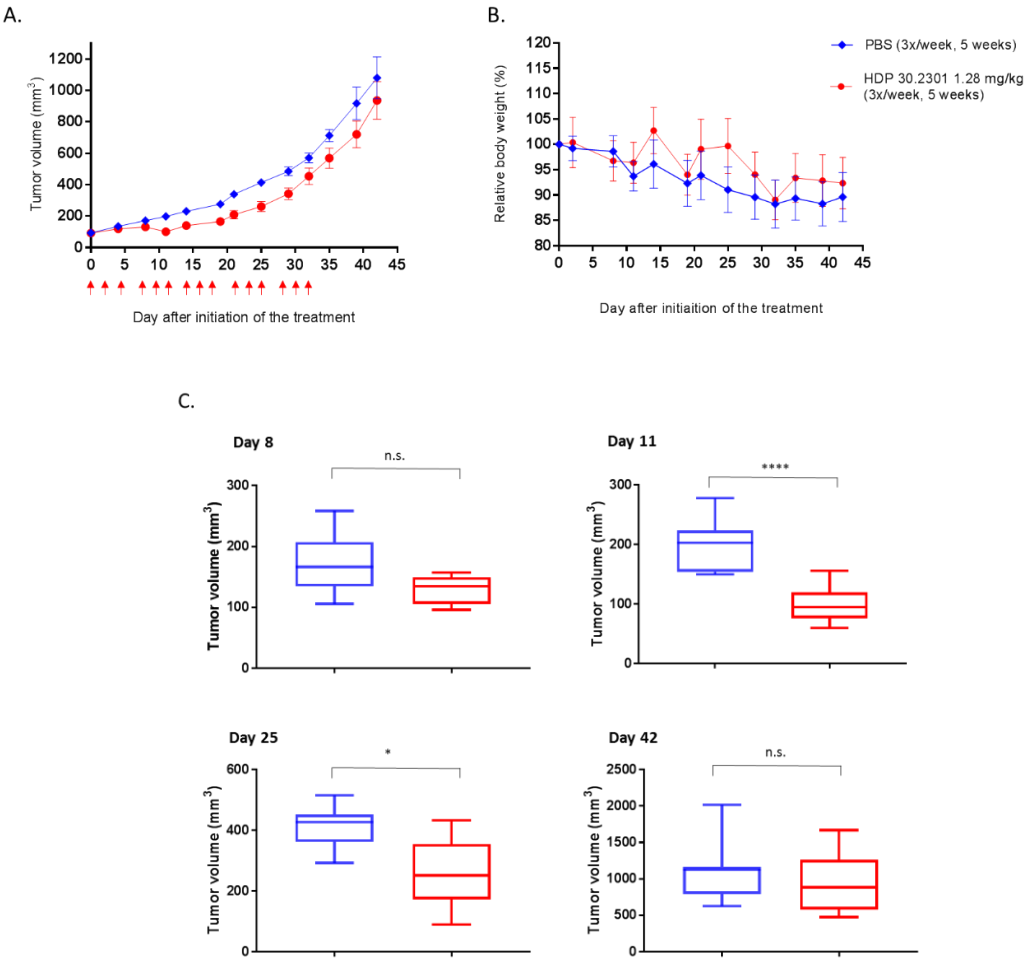

Figure 4.14 *In vivo* evaluation of antitumor activity of HDP 30.2301 in Cb 17 Scid mice xenografted with LNCaP tumors.

A. Efficacy (presented is average tumor volume ±SEM; n=10); **B.** Tolerability (presented is average body weight ±SEM, n=10); **C.** Box plots comparing tumor volumes at day 7, 14 and 31 after initiation of the treatment (boxes present distribution of tumor volume with the whiskers indicating minimum to maximum tumor volume observed, n=10).

Until day eight no statistically significant differences between the two study arms - vehicle and active substance were observed (*Figure 4.14* panel A and C). At day 11 a slight regression of the tumors in the HDP 30.2301 treated group followed by tumor re-growth was observed. Once the tumors reached a volume of ca. 200 mm^3 (around day 24) they stopped to respond to the therapy (*Figure 4.14* C). Comparison of the tumor volume results presented in *Figure 4.13* and *Figure 4.14* suggests lower antitumor activity of HDP 30.2301 compared to the conjugate HDP 30.2284. Even though the administered dose of α-amanitin equivalents for HDP 30.2301 was ca. 129 x higher compared to HDP 30.2284 and the duration of the treatment with HDP 30.2301 was longer compared to the duration of therapy with

HDP 30.2284 (5 *vs.* 3 weeks, respectively) the antitumor activity of conjugate HDP 30.2301 was lower compared to tumor responses observed in the efficacy study of HDP 30.2284.

Since only limited efficacy for both conjugates HDP 30.2284 and HDP 30.2301 at the tolerated dose levels was observed in the LNCaP xenografts the efficacy study was performed in another PSMA positive xenograft model: C4_2. Nanomolar activity of both conjugates was confirmed in *in vitro* cytotoxicity experiment on C4_2 cell (*Supplementary figure 1*). Androgen independent C4_2 cells are derived from an androgen dependent LNCaP cell line. Even though the C4_2 cell line originates from the LNCaP cells the type of tumors formed by the C4_2cell line *in vivo* is very different in the structure compared to the tumors formed by LNCaP cell line. LNCaP tumors are very stiff, well vascularized and characterized by a low growth rate while C4_2 tumors are less compacted, softer, characterized by a lower level of vascularization and a very rapid growth rate (internal Heidelberg Pharma Research GmbH observation). To exclude the possibility that limitation of the therapy is caused by tumor architectural factors the efficacy of both conjugates was tested in optimized dosing scheme in the comparative head-to-head efficacy experiment in C4_2 xenograft model (*Figure 4.15*).

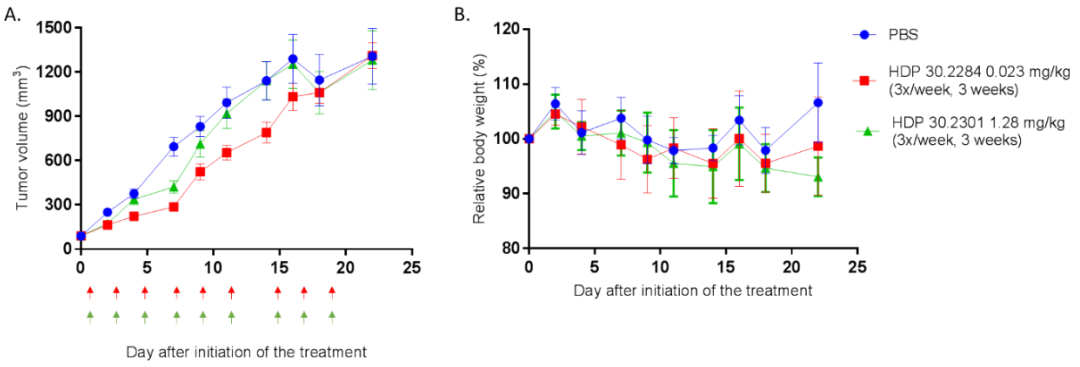

Figure 4.15 *In vivo* evaluation of antitumor activity of HDP 30.2284 and HDP 30.2301 in Cb17 Scid mice xenografted with C4_2 tumors at the optimized dosing regimen.

A. Efficacy (presented is average tumor volume ± SEM; n=10; **B.** Tolerability (presented is average body weight ± SEM; n=10).

Direct comparison confirms a slightly better efficacy for the HDP 30.2284. For both conjugates tumor growth delay was observed only until day seven after initiation of the treatment. From day seven onward the tumors started to re-grow very quickly.

Until day 15 growth rate in the study arm treated with HDP 30.2284 seems to be slightly lower compared to the group treated with HDP 30.2301. *In vivo* efficacy of both conjugates was very limited since tumor sizes in all experimental groups converged at day 18. Overall similar limited *in vivo* efficacy was observed independently to the xenograft models used in the study. Limited ability to inhibit tumor growth *in vivo* seems to be attributed to the properties of the conjugate rather than to the physical limitations of xenograft model such as tumor physical structure.

4.1.7 Biodistribution study of lead conjugates HDP 30.2284 and HDP 30.2301

The biodistribution study upon single dose administration was carried out in LNCaP tumor bearing Cb17 Scid mice. The concentration of conjugates and related α-amanitin containing metabolites was determined in serum, tumor and main organs involved in drug metabolism and elimination: liver and kidney. Similar as in presented in section 4.1.5 pharmacokinetic study the concentration of conjugates and possible metabolites presenting α-amanitin core in the structure were determined using the competitive anti-α-amanitin ELISA in organ extracts and serum of animals treated with conjugates as described in section 3.2.14. The results are presented as the concentration of conjugate detected in gram of wet tissue (*Figure 4.16*).

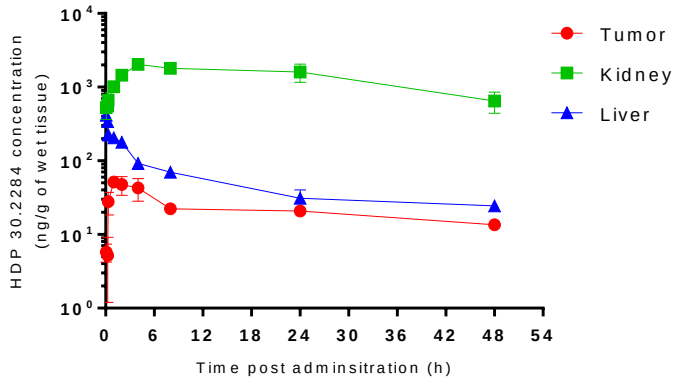

Figure 4.16 Biodistribution study of HDP 30.2284.

Concentrations of HDP 30.2284 conjugate detected in tumor, kidney and liver of Cb 17 Scid male mice xenografted with LNCaP tumors after single dose administration of HDP 30.2284 - 0.184 mg/kg (n=3).

The tumor concentration of HDP 30.2284 increased gradually to reach maximum 1 h after administration (ca. 51.3 ng/g). HDP 30.2284 was still detectable at the concentration of approximately 13.5 ng/g 48 h after administration. At the early time-point after administration higher liver levels were observed, what is most possibly related to the high serum concentrations. Once the HDP 30.2284 is eliminated from the blood stream the conjugate concentration drops but HDP 30.2284 is still detectable at the concentration of 24.4 ng/g of tissue 48 h after administration.

In contrast gradually increasing concentration of conjugate and related metabolites was determined in the kidney. A peak of kidney concentration - 2.03 µg/g was observed 4 h following single dose administration. Kidney concentration of conjugate very slowly decreased overtime, and even 24 h and 48 h after administration a high concentration of approximately 1.6 µg/g and 0.64 µg/g were measured, respectively. Thus, HDP 30.2284 is accumulated in high concentrations in the kidney, which seems to be the organ of toxicity.

For HDP 30.2301 a similar biodistribution profile was observed (*Figure 4.17*). The peak of kidney concentration of approximately 4.98 µg/g was detected 2 h after administration and this concentration remained almost unchanged up to 8 h following administration. A slight drop in the kidney level compared to preceding time-point was observed 24 h and 48 h upon administration but even at this time the kidney concentration was as high as 3.6 µg/g and 2.81 µg/g, respectively. Still high, however much lower compared to the kidney concentration of HDP 30.2301 was detected in the tumor and liver even 24 h and 48 h after administration.

HDP 30.2301 due to high administered dose level demonstrated higher than HDP 30.2284 concentration in the tumor and kidney throughout the whole duration of the experiment. High initial liver and tumor levels (time-points 5 min. - 2 h) are related to the presence of the conjugate in the blood, and clearly drop after complete elimination of HDP 30.2301 from the systemic circulation (approximately 8 h after administration see *Figure 4.12* for PK data). From the time-point 4 h onward the concentrations detected in tumor and liver were stable, ranging between 313-602 ng/g and 532-692 ng/g, respectively and as expected were higher compared to the organ levels measured after administration of 0.182 mg/kg of HDP 30.2284.

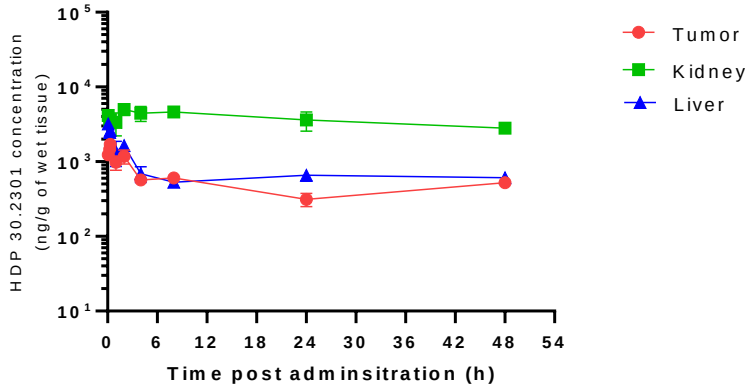

Figure 4.17 Concentrations of HDP 30.2301 in tumor, kidney and liver in Cb17 Scid male mice xenografted with LNCaP tumors.

HDP 30.2301 was administered as a single dose, 1.28 mg/kg - 1/3 MTD (n=3).

Similar as for HDP 30.2284, a high accumulation of toxin was identified in the kidney. Thus, kidney seems to be the organ of primary and/or secondary toxicity for both conjugates.

The PSMA expression is reported in proximal tubule of human and murine kidney and it was demonstrated that it contributes to the kidney accumulation of DUPA based radio-diagnostics [105, 106]. The hypothesis aiming into explanation whether PSMA mediated uptake is the major mechanism underlying the kidney accumulation of the conjugates renal uptake was tested in a simple accumulation mechanistic study.

The mechanistic study of kidney accumulation relies on the determination of conjugate concentration in the kidney after PSMA blocking. PSMA blocking was performed by pre-injection of animals with 2-PMPA, at the concentration corresponding to 100x molar excess of 2-PMPA over conjugate. 30 min. following pre-injection, a co-injection of conjugate with 50x molar excess of 2-PMPA over the conjugates was performed. 2-PMPA is a well-known PSMA inhibitor and DUPA competitor (section 4.1.1) [77, 83, 87]. It was also used in *in vitro* studies of cytotoxic activity of HDP 30.2284 and HDP 30.2301 (section 4.1.2 and *Figure 1.7*). To facilitate the comparability of the results the administered dose of two tested conjugates conjugates was set to the equivalent of 75 µg/kg of unconjugated toxin (0.184 mg/kg for HDP 30.2284 and 0.160 mg/kg for HDP 30.2301). The animals were dissected 6 h after the co-injection and kidney concentrations of the conjugate related metabolites were determined by a competitive anti α-amanitin ELISA (*Figure 4.18*).

A total kidney concentration of approximately 3.3 µg/g of tissue was detected after administration of HDP 30.2284. Lower kidney concentration of approximately 2.2 µg/g was detected after administration of HDP 30.2301 (*Figure 4.18*). Interestingly inhibition of PSMA in the kidney had only minimally affected levels of the toxin detected after injection with HDP 30.2284. In contrast pre- and co-injection of 2-PMPA with HDP 30.2301 decreased the concentration of the toxin in the kidney by approximately 50 % (*Figure 4.18*).

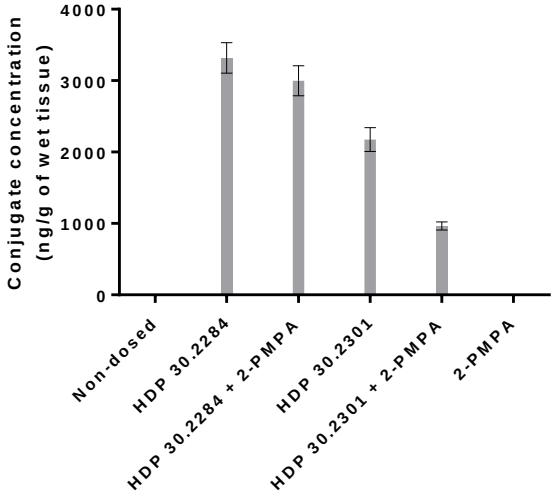

Figure 4.18 Determination of kidney concentrations of conjugates HDP 30.2284 and HDP 30.2301 after pre and co-injection with 2-PMPA.

Animals were pre-injected with 100x molar excess of 2-PMPA over conjugates and co-injected with 50 x molar excess of 2-PMPA over conjugates. 0.184 mg/kg of HDP 30.2284 and 0.160 mg/kg of HDP 30.2301 was administered. Kidneys were collected 6 h following co-injection of conjugate with 2-PMPA (Cb17 Scid male mice, presented is median kidney concentration ± SEM, n=3).

The results of the kidney accumulation study upon PSMA blocking indicate that kidney uptake of HDP 30.2284 is non-PSMA mediated or is only partially PSMA mediated for HDP 30.2301.

In the literature nephrotoxicity and accumulation of unconjugated α-amanitin had been already reported [60, 63]. The atrophy and degeneration upon unconjugated α-amanitin administration was observed mainly in the kidney structures such as proximal and distal tubules [58]. In order to verify whether the kidney uptake may be related to the α-amanitin core presented in the conjugates structure a study of kidney accumulation

of naked toxin was performed and kidneys were collected 4 h, 6 h and 24 h following toxin administration. α-amanitin was administered at the sub-toxic dose corresponding to 1/2 of the MTD - 75 µg/kg. In contrast to conjugates HDP 30.2284 and HDP 30.2301 α-amanitin was not accumulated in the kidney (measured concentrations were below the lower limit of quantification, data not shown).

The results of mechanistic study investigating the kidney accumulation using 2-PMPA co-injection suggest that in case of conjugate HDP 30.2284 other than PSMA mediated uptake plays a major in the renal accumulation. For HDP 30.2301 bearing non-cleavable linker conjugation of α-amanitin to DUPA leads to increased kidney uptake which is only partially PSMA mediated. In case of two conjugates kidney uptake seems to be not related to the α-amanitin core present in the structure of both compounds, at least at tested dose level corresponding to 75 µg/kg. Linker strategy seems to impact the mechanism of kidney uptake and possibly related toxicity. Observed toxicity seems to be related to the secondary, unidentified pharmacodynamic effects.

Although for both conjugates a significant kidney accumulation was observed, it seems that in case if conjugate related nephrotoxicity appears, it is transient and reversible. This conclusion is based on the observation of a good tolerability of all proposed doses of treatment in the presented efficacy studies (*Figure 4.13*, *Figure 4.14* and *Figure 4.15*).

Based on previous observations of dose limiting toxicity of HDP 30.2284 (Val-Ala-PAB) and limited *in vivo* efficacy for HDP 30.2301 (C_6 non-cleavable linker) the further path aiming into enhancement of *in vivo* activity was to improve the *in vivo* tolerability and enable intracellular release of the toxin. To this end, conjugates bearing a disulfide linker were developed, optimized and characterized *in vitro* and *in vivo*.

4.2 DUPA-ALPHA-AMANITIN CONJUGATES BEARING DISULFIDE LINKER - ENABLING INTRACELLULAR RELEASE OF TOXIN AND CONCOMITANT IMPROVING OF *IN VIVO* TOLERABILITY

The usage of disulfide linkers for cytotoxic payload conjugation has been shown to be particularly advantageous in the efficacy of SMDCs. The majority of small molecule toxin conjugates which reached clinical development based on e.g. folic acid or bicyclic peptides targeting the tumor stroma bear unprotected disulfide linker [100, 107]. The greater *in vivo* activity of non-hindered disulfide linkers could be founded in the self-amplifying release of the toxin not only inside of the tumor cells but also outside, in the tumor micro-environment, which is enriched with glutathione released from decaying cells. The simplified scheme of toxin release *via* glutathione is presented in *Figure 4.19*.

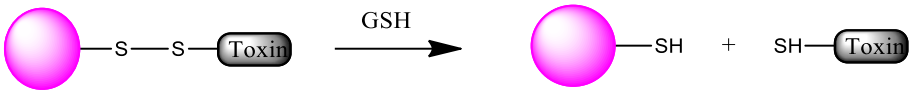

Figure 4.19 Schematic presentation of disulfide linker cleavage and toxin release by intracellular glutathione (GSH).

Based on the developed DUPA disulfide linker bearing conjugate that targets Tubulysin B to prostate cancer cells which is currently undergoing a Phase I clinical study (EC1169, Endocyte, ClinicalTrials.gov Identifier: NCT02202447), a small library of DUPA-α-amanitin conjugates with different levels of steric hindrance of the disulfide bond was synthesized. The conjugate showing the best activity *in vitro* was selected for subsequent *in vivo* characterization.

4.2.1 Optimization of *in vitro* activity of DUPA-α-amanitin conjugates bearing disulfide linker

The conjugates bearing disulfide linker were designed to feature increasing steric hindrance at the carbon atoms adjacent to either sides of disulfide bond. This strategy has been applied in the field of ADCs to optimize cytotoxic potential and plasma stability of linkage between toxin and antibody [49]. The structures of all tested disulfide conjugates are presented

in *Figure 4.20*. For details related to the synthetic strategy please refer to the PhD thesis of Francesca Gallo.

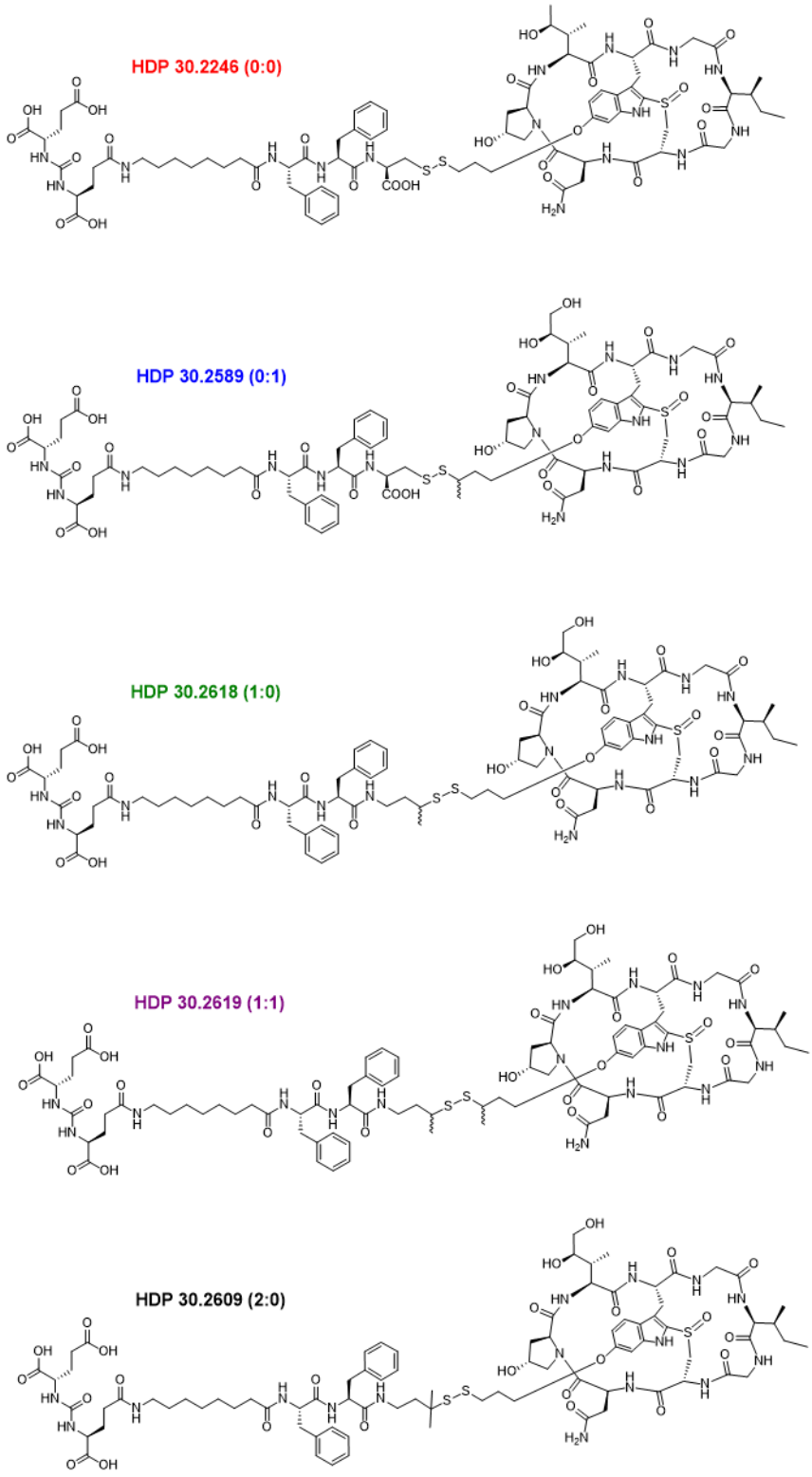

Figure 4.20 Chemical structure of DUPA-α-amanitin conjugates bearing disulfide linker featuring different levels of disulfide bond hindrance.

The hindered disulfide conjugates are denoted by the number of methyl groups on the DUPA site and the α-amanitin site, e.g. the conjugate with one monomethyl hindrance on the DUPA site and no hindrance on α-amanitin site is abbreviated as (1:0). The presented library is missing the (2:1), (1:2) and (2:2) format. The introduction of two methyl groups at the α-amanitin site to produce the (1:2) and (2:2) derivatives was not feasible due to synthetic difficulties. It can be speculated that this is due to the steric hindrance impairing the formation of disulfide bond between toxin and α-amanitin derivative. The synthetic yield of compound (2:1) was low and this compound was isolated in an amount not sufficient for further *in vitro* tests. Moreover, the development of (2:1) format was not supported by initial *in vitro* data, which demonstrated that already a conjugate with the double hindrance HDP 30.2609 (2:0) showed more than 10-fold decrease in cytotoxic potential compared to the best performing mono-hindered derivatives (1:0)/(0:1) and the double hindered (1:1) formats *(Figure 4.21* and *Table 4.3* for IC_{50} results). Thus, preparation of (2:1) format was abandoned as a further decrease in the *in vitro* potency of conjugate was expected.

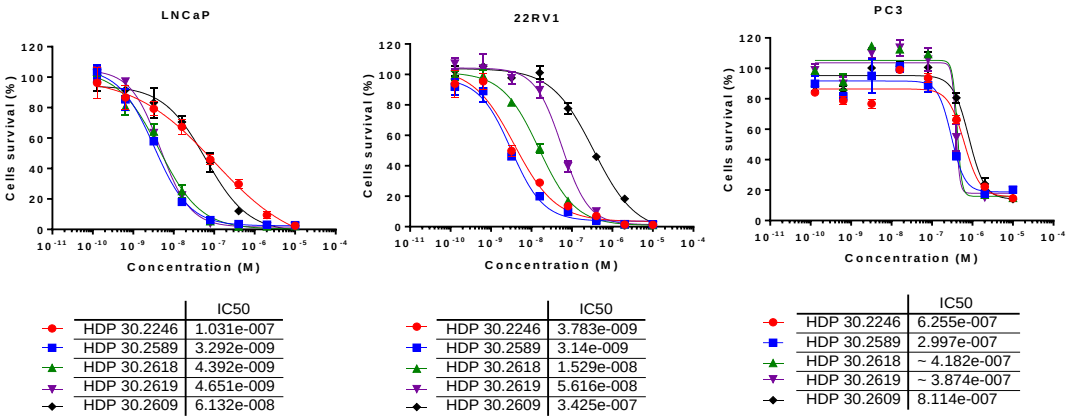

Figure 4.21 Dose-response cytotoxicity curves of conjugates bearing disulfide linker in three prostate cancer cell lines LNCaP (PSMA +++), 22RV1 (PSMA +) and PC3 (PSMA -).

Table 4.3 Tabulated summary of IC_{50} values of DUPA-α-amanitin conjugates bearing disulfide linker in three prostate cancer cell line LNCaP (PSMA +++), 22RV1 (PSMA +) and LNCaP (PSMA -).

Compound code	IC_{50}(M)		
	LNCaP	22RV1	PC3
HDP 30.2246 (0:0)	1.03×10^{-7}	3.78×10^{-9}	6.26×10^{-7}
HDP 30.2589 (0:1)	3.29×10^{-9}	3.14×10^{-9}	3.00×10^{-7}
HDP 30.2618 (1:0)	4.39×10^{-9}	1.53×10^{-8}	4.18×10^{-7}
HDP 30.2619 (1:1)	4.65×10^{-9}	5.62×10^{-8}	3.87×10^{-7}
HDP 30.2609 (2:0)	6.13×10^{-8}	3.42×10^{-7}	8.11×10^{-7}

Similar as for all presented in section 4.1 conjugates the cytotoxic potential of the small library of disulfide linker bearing conjugates was assesses in three prostate cancer cell lines expressing different levels of PSMA. In the LNCaP PSMA positive cell line HDP 30.2446 (0:0) and HDP 30.2609 (2:0) showed a lower activity than HDP 30.2589 (0:1), HDP 30.2618 (1:0) and HDP 30.2619 (1:1). The non-hindered HDP 30.2246 (0:0) showed an IC_{50} of 103 nM in LNCaP cells, similar to the cytotoxicity of unconjugated α-amanitin (IC_{50}=275 nM, data shown in section 4.1.2). The cytotoxic potential of HDP 30.2246 (0:0) was low on both: PSMA positive LNCaP and the PSMA negative PC3 cell line (IC_{50} of 103 nM *vs.* 626 nM, respectively). Activity of conjugate HDP 30.2609 (2:0) was higher on LNCaP receptor positive cell (IC_{50} 61.3 nM) line compared to HDP 30.2246 (0:0) but lower compared to conjugate featuring intermediate levels of hindrance. The double hindrance of the two methyl groups in HDP 30.2609 (2:0) should provide additional stability in cell culture medium and plasma. However, the additional bulk of neighboring groups can have a negative impact on reduction of the disulfide bond and impair the release of the toxin after internalization in consequence leading to lower cytotoxicity. In the LNCaP cell line the compounds with moderate steric hindrance HDP 30.2589 (0:1), HDP30.2618 (1:0) and HDP 30.2619 (1:1) demonstrated optimal cytotoxic potential in the range of 3.29 – 4.65 nM. As expected, the conjugates were not active in the PSMA negative PC3 cell line and shown IC_{50} in the range of concentration observed for unconjugated α-amanitin (ca. 10^{-7} M). The high cytotoxic potential with the IC_{50} of 3.78 nM and 3.14 nM for the conjugates HDP 30.2246

(0:0) and HDP 30.2589 (0:1), respectively was observed in 22RV1 cells and was confirmed in several independent experiments. Cytotoxic potential with IC_{50} determined for 15.3 nM and 56.2 nM were observed for conjugates HDP 30.2618 (1:0) and HDP 30.2619 (1:1), respectively.

Further focus in the characterization of the small library of conjugates DUPA-α-amanitin featuring different levels of disulfide linker hindrance was determining how the level of disulfide bond steric hindrance influences plasma stability of the conjugates. The stability of all tested conjugates was tested in different matrices as described in the section 3.2.4. The results are presented as dose response cytotoxicity curves of the conjugates after 0-72 h of incubation in mouse plasma (MP), human plasma (HP) or in PBS as a control. Additionally, the results are presented as tabulated summaries where IC_{50} value and relative cytotoxicity reduction factor in relation to the time-point 0 are shown.

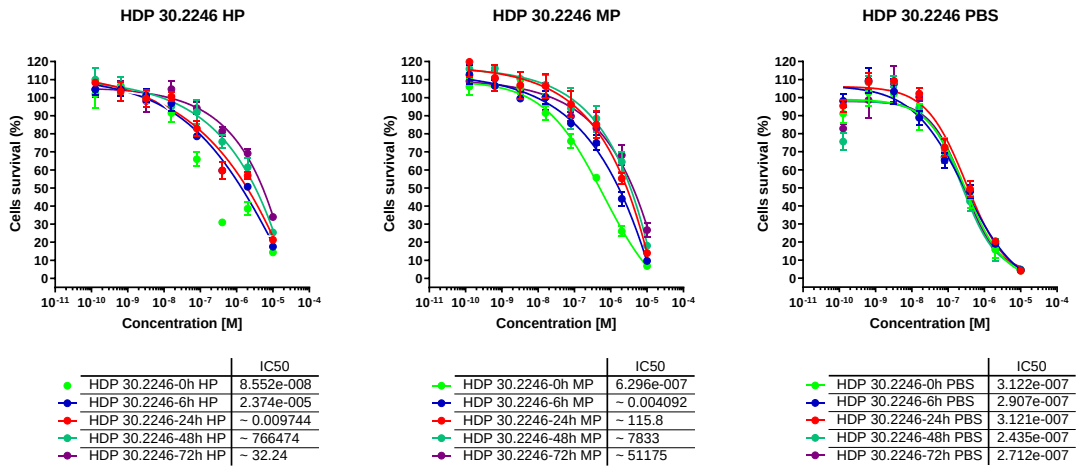

Figure 4.22 Plasma stability results of HDP 30.2246 (0:0) in LNCaP cells (PSMA +++). MP -mouse plasma, HP- human plasma.

Table 4.4 IC_{50} summary -plasma stability results of HDP 30.2246 (0:0) in LNCaP cells (PSMA +++).

Matrix	Compound	IC_{50} [M]	Fold of cytotoxicity reduction
Human Plasma	HDP 30.2246 0 h	8.552×10^{-8}	x
	HDP 30.2246 6h	ca. 2×10^{-6}	23.47
	HDP 30.2246 24 h	ca. 2×10^{-6}	23.47
	HDP 30.2246 48 h	ca. 2×10^{-6}	23.47
	HDP 30.2246 72 h	ca. 3×10^{-6}	35.08
Mouse Plasma	HDP 30.2246 0 h	6.296×10^{-7}	X
	HDP 30.2246 6 h	ca. 1×10^{-6}	1.59
	HDP 30.2246 24 h	ca. 2×10^{-6}	3.18
Mouse Plasma	HDP 30.2246 48 h	ca. 3×10^{-6}	4.76
	HDP 30.2246 72 h	ca. 3×10^{-6}	4.76
PBS	HDP 30.2246 0 h	3.122×10^{-7}	X
	HDP 30.2246 6 h	2.907×10^{-7}	0.93
	HDP 30.2246 24 h	3.121×10^{-7}	1
	HDP 30.2246 48 h	2.435×10^{-7}	0.78
	HDP 30.2246 72 h	2.712×10^{-7}	0.87

HDP 30.2246 (0:0) demonstrated a higher cytotoxic potential at the time-point 0 h in mouse plasma (85.5 nM) than in human plasma (629.6 nM). It might suggest that kinetics of conjugate reduction in human plasma progresses much quicker than in mouse plasma. Already after 6 h of incubation in both mouse and human plasma the compound lost majority of activity and demonstrated cytotoxicity with the IC_{50} in the micromolar range of concentration (time-points from 6 h onward). HDP 30.2246 (0:0) proved to be more stable in mouse than in human plasma. Compound incubated in PBS was stable and demonstrated similar activity independently to the duration of incubation.

Second tested conjugate was HDP 30.2589 (0:1). *In vitro* plasma stability results for this conjugate are presented in *Figure 4.23* and *Table 4.5*.

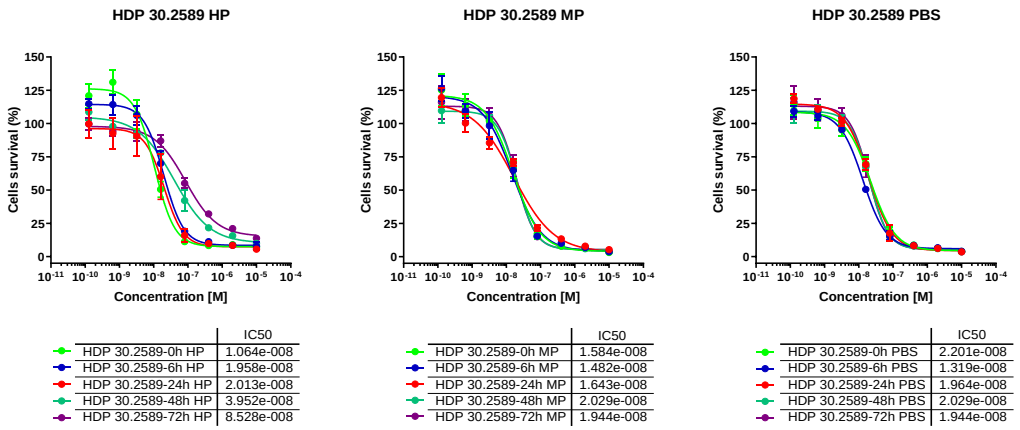

Figure 4.23 Plasma stability results of HDP 30.2589 (0:1) in LNCaP cells (PSMA +++). MP -mouse plasma, HP- human plasma.

Table 4.5 IC_{50} summary -plasma stability results of HDP 30.2589 (0:1) in LNCaP cell line (PSMA +++).

Matrix	Compound	IC_{50} [M]	Fold of cytotoxicity reduction
Human Plasma	HDP 30.2589 0 h	1.064×10^{-8}	X
	HDP 30.2589 6 h	1.958×10^{-8}	1.84
	HDP 30.2589 24 h	2.013×10^{-8}	1.89
	HDP 30.2589 48 h	3.952×10^{-8}	3.71
	HDP 30.2589 72 h	8.528×10^{-8}	8.02
Mouse Plasma	HDP 30.2589 0h	1.584×10^{-8}	X
	HDP 30.2589 6 h	1.482×10^{-8}	0.93
	HDP 30.2589 24 h	$1.643x\ 10^{-8}$	1.04
	HDP 30.2589 48 h	3.611×10^{-8}	2.28
	HDP 30.2589 72 h	4.798×10^{-8}	3.03
PBS	HDP 30.2589 0 h	2.201×10^{-8}	X
	HDP 30.2589 6 h	1.319×10^{-8}	0.60
	HDP 30.2589 24 h	1.964×10^{-8}	0.89
	HDP 30.2589 48 h	2.029×10^{-8}	0.92
	HDP 30.2589 72 h	1.944×10^{-8}	0.88

For HDP 30.2589 (0:1) a higher cytotoxic potential at the time-point 0 h was observed than for HDP 30.2246 (0:0). Initial IC_{50} was determined be 10.64 nM for conjugate prepared in human plasma, 15.84 nM for conjugate prepared in mouse plasma and 22.01 nM for conjugate prepared in PBS. Conjugate was stable in both human and mouse plasma up to

24 h as shown by similar IC_{50} as these determined at the time-point 0 h. Incubation for 48 h or longer has led to more prominent increase in IC_{50} value (*Table 4.5*). HDP 30.2589 (0:1) was more stable in mouse than in human plasma. Comparison of these results and the results obtained for HDP 30.2246 (0:0) indicates that a significant improvement in the cytotoxic activity related to increased plasma stability was provided. It appears that the steric hindrance due to methylation of the carbon neighboring with the disulfide bond on the toxin site protects the disulfide bond of conjugate outside of the cell while still enabling the efficient payload release inside of the cell once the conjugate is internalized.

The third tested conjugate HDP 30.2609 (2:0) features double hindrance at the toxin site. Results of *in vitro* toxicity upon stressing are presented in *Figure 4.24* and

*Table **4.6**.*

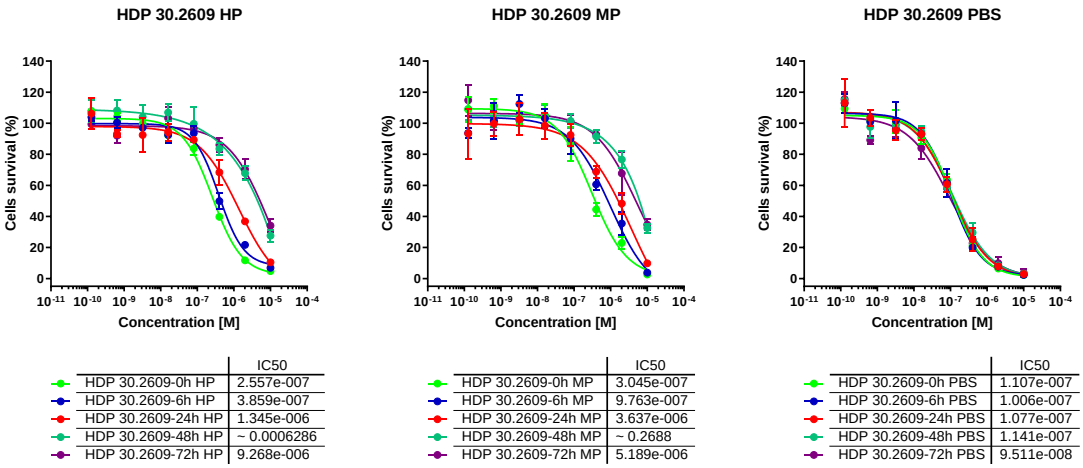

	IC50
HDP 30.2609-0h HP	2.557e-007
HDP 30.2609-6h HP	3.859e-007
HDP 30.2609-24h HP	1.345e-006
HDP 30.2609-48h HP	~ 0.0006286
HDP 30.2609-72h HP	9.268e-006

	IC50
HDP 30.2609-0h MP	3.045e-007
HDP 30.2609-6h MP	9.763e-007
HDP 30.2609-24h MP	3.637e-006
HDP 30.2609-48h MP	~ 0.2688
HDP 30.2609-72h MP	5.189e-006

	IC50
HDP 30.2609-0h PBS	1.107e-007
HDP 30.2609-6h PBS	1.006e-007
HDP 30.2609-24h PBS	1.077e-007
HDP 30.2609-48h PBS	1.141e-007
HDP 30.2609-72h PBS	9.511e-008

Figure 4.24 Plasma stability results of HDP 30.2609 (2:0) on LNCaP cells (PSMA +++). MP-mouse plasma, HP-human plasma.

Table 4.6 IC_{50} summary - plasma stability results of HDP 30.2609 (2:0) on LNCaP cells (PSMA +++).

Matrix	Compound	IC_{50} [M]	Fold of cytotoxicity reduction
Human Plasma	HDP 30.2609 0 h	2.557×10^{-7}	x
	HDP 30.2609 6 h	3.859×10^{-7}	1.51
	HDP 30.2609 24 h	1.345×10^{-6}	5.26
	HDP 30.2609 48 h	ca. 2×10^{-6}	7.82
	HDP 30.2609 72 h	ca. 2×10^{-6}	7.82
Mouse Plasma	HDP 30.2609 0 h	3.045×10^{-7}	X
	HDP 30.2609 6 h	9.763×10^{-7}	3.21
	HDP 30.2609 24 h	3.637×10^{-6}	11.94
	HDP 30.2609 48 h	ca. 3×10^{-6}	9.85
	HDP 30.2609 72 h	ca. 3×10^{-6}	9.85
PBS	HDP 30.2609 0 h	1.107×10^{-7}	X
	HDP 30.2609 6 h	1.006×10^{-7}	1
	HDP 30.2609 24 h	1.077×10^{-7}	0.97
	HDP 30.2609 48 h	1.141×10^{-7}	1.03
	HDP 30.2609 72 h	9.518×10^{-8}	0.86

For HDP 30.2609 (2:0) IC_{50} for the time point 0 h was determined to be 255.7 nM for conjugate prepared in human plasma, 304.5 nM for conjugate prepared in mouse plasma and 110.7 nM for conjugate prepared in PBS matrix. This cytotoxic potential is higher than determined for HDP 30.2246 (0:0) but lower than for HDP 30.2589 (0:1). Surprisingly, despite of double hindrance the compound losses its potency what is observed from the time-point 24 h onward however, this loss is not as severe as in case of HDP 30.2246 (0:0). HDP 30.2609 (2:0) displayed similar stability in mouse and in human plasma. The conjugate HDP 30.2609 (2:0) was completely stable in PBS.

The fourth characterized disulfide linker bearing conjugate is HDP 30.2618 (1:0) featuring hindrance presented by single methyl group at the toxin site. Results of *in vitro* toxicity upon stressing are presented in *Figure 4.25* and *Table 4.7*.

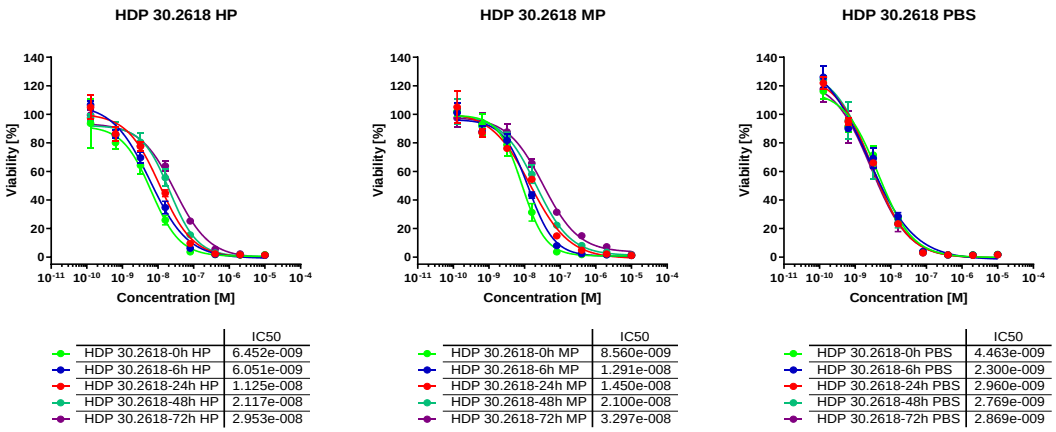

Figure 4.25 Plasma stability results of HDP 30.2618 (1:0) on LNCaP cells (PSMA +++). MP -mouse plasma, HP- human plasma.

Table 4.7 IC_{50} summary - plasma stability results of HDP 30.2618 (1:0) on LNCaP cells (PSMA +++).

Matrix	Compound	IC_{50} [M]	Fold of cytotoxicity reduction
Human Plasma	HDP 30.2618 0 h	6.452×10^{-9}	x
	HDP 30.2618 6 h	6.051×10^{-9}	0.94
	HDP 30.2618 24 h	1.125×10^{-8}	1.74
	HDP 30.2618 48 h	2.117×10^{-8}	3.28
	HDP 30.2618 72h	2.953×10^{-8}	4.58
Mouse Plasma	HDP 30.2618 0 h	8.56×10^{-9}	X
	HDP 30.2618 6 h	1.291×10^{-8}	1.51
	HDP 30.2618 24 h	1.45×10^{-8}	1.69
	HDP 30.2618 48 h	2.1×10^{-8}	2.45
	HDP 30.2618 72 h	3.297×10^{-8}	3.85
PBS	HDP 30.2618 0 h	4.463×10^{-9}	X
	HDP 30.2618 6 h	2.3×10^{-9}	0.52
	HDP 30.2618 24 h	2.96×10^{-9}	0.66
	HDP 30.2618 48 h	2.769×10^{-9}	0.62
	HDP 30.2618 72 h	2.869×10^{-9}	0.64

HDP 30.2618 (1:0) demonstrated initial cytotoxic potential with the low IC_{50} of 6.45 nM for conjugate prepared in human plasma, 8.56 nM for conjugate prepared in mouse plasma and 4.46 nM for conjugate in PBS. HDP 30.2618 (1:0) incubated in both plasmas started to slightly lose the cytotoxic activity from 24 h onward but even after 72 h of stressing IC_{50}

was determined for 29.53 nM after incubation in human plasma and 32.97 nM after incubation in mouse plasma. The conjugate showed similar stability in both mouse and human plasma. Stability of this conjugate was improved compared to three aforementioned conjugates HDP 30.2246 (0:0), HDP 30.2589 (0:1) and HDP 30.2609 (2:0).

The last tested disulfide linkage bearing conjugate was HDP 30.2619 (1:1). The results of stability for this compound are presented in *Figure 4.26* and

*Table **4.8**.*

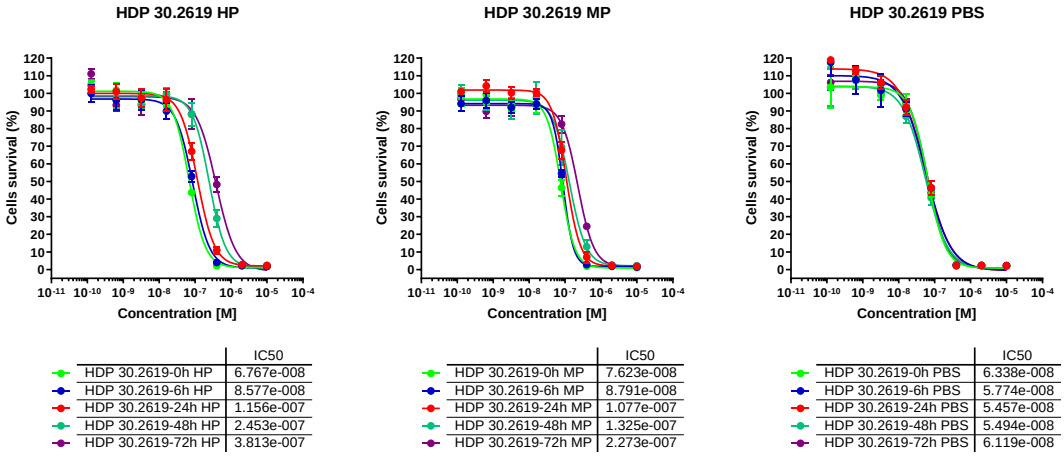

Figure 4.26 Plasma stability results of HDP 30.2619 (1:1) in LNCaP cells (PSMA +++). MP -mouse plasma, HP- human plasma.

Table 4.8 IC_{50} summary - plasma stability results of HDP 30.2619 (1:1) on LNCaP cells (PSMA +++).

Matrix	Compound	IC_{50} [M]	Fold of cytotoxicity reduction
Human Plasma	HDP 30.2619 0 h	6.767×10^{-8}	x
	HDP 30.2619 6 h	8.577×10^{-8}	1.27
	HDP 30.2619 24 h	1.156×10^{-7}	1.71
	HDP 30.2619 48 h	2.453×10^{-7}	3.62
	HDP 30.2619 72 h	3.813×10^{-7}	5.63
Mouse Plasma	HDP 30.2619 0 h	7.623×10^{-8}	X
	HDP 30.2619 6 h	8.791×10^{-8}	1.15
	HDP 30.2619 24h	1.077×10^{-7}	1.41
	HDP 30.2619 48 h	1.325×10^{-7}	1.74
	HDP 30.2619 72 h	2.273×10^{-7}	2.98
PBS	HDP 30.2619 0 h	6.338×10^{-8}	X
	HDP 30.2619 6 h	5.774×10^{-8}	0.91
	HDP 30.2619 24 h	5.457×10^{-8}	0.86
	HDP 30.2619 48 h	5.494×10^{-8}	0.87
	HDP 30.2619 72 h	6.119×10^{-8}	0.96

For HDP 30.2619 (1:1) the IC_{50} at the time-point 0 h was determined to be 67.7 nM for conjugate prepared in human plasma, 76.23 nM for conjugate prepared in mouse plasma and 63.38 nM for conjugate prepared in PBS. Cytotoxicity of HDP 30.2619 (1:1) is lower compared to the initial cytotoxicity of HDP 30.2618 (1:0). In general, the stability of HDP 30.2619 (1:1) was similar to the stability observed for conjugate HDP 30.2618 (0:1).

Amongst all five tested conjugates featuring different levels of disulfide bond hindrance HDP 30.2618 (1:0) and HDP 30.2619 (1:1) proved to be the most promising candidates based on their favorable *in vitro* characteristics such as high cytotoxic potential and plasma stability. Both compounds showed similar cytotoxic potential on PSMA positive cells, whereas HDP 30.2618 (1:0) performed slightly better in the human plasma stability assay. For ADCs it has been reported that conjugates with the (1:1) modification pattern release the toxin more slowly than the (1:0) format in *in vitro assays*. Moreover, it was reported that ADC presenting monohindered disulfide linker (1:0) generated a better tumor response that (1:1) conjugate [49]. Based on obtained results and literature reports HDP 30.2618 was chosen for further *in vivo* characterization.

4.2.2 Single dose tolerability study of lead conjugate bearing disulfide monohindered linker HDP 30.2618 (1:0)

In vivo characterization of HDP 30.2618 (1:0) was initiated with the determination of MTD. First administered dose level 0.3 mg/kg of HDP 30.2618 correspond to the equivalent of unconjugated α-amanitin MTD which is 150 µg/kg (internal Heidelberg Pharma Research GmbH data) (*Table 4.9*). For the starting dose of 0.3 mg/kg and the subsequent dose of 0.6 mg/kg a good tolerability expressed as no significant loss in the relative body weight of animals was observed (*Figure 4.27* A). The next dose level - 1.2 mg/kg caused an approximately 10 % drop in body weight at day 7 following administration which recovered in the follow-up period. For the dose of 2.4 mg/kg a gradual loss in the median body weight with ca. 15 % decrease was observed at day nine following administration (*Figure 4.27* A). At day 13 one of the animals from the group dosed with 2.4 mg/kg showed a 23 % loss in body weight and had to be sacrificed due to its general bad condition (*Figure 4.27* B). The remaining two animals re-gained the body weight in the follow up period (*Figure 4.27* B). For the conjugates HDP 30.2284 and HDP 30.2301 (described in section 4.1.3) toxicity caused a loss in the body weight until day seven and recovery of the body weight started around day nine. For the dose 2.4 mg/kg the body weight loss persisted until day nine after administration. Moreover, one animal from this arm of the study had to be sacrificed at day eight due to body weight loss exceeding 20 % of initial mass of the animal (*Figure 4.27* B). Based on the fact that the main readout for the tolerability is survival, observations related to the body weight and toxicity observations of previously characterized SMDCs, MTD of HDP 30.2618 was set at the dose level of 1.2 mg/kg.

Table 4.9 Dose of HDP 30.2618 used in MTD study with indicated equivalents of α-amanitin.

Compound	Dose HDP 30.2618 [mg/kg]	α- amanitin dose [µg/kg]
HDP 30.2618	0.300	150
HDP 30.2618	0.600	300
HDP 30.2618	1.200	600
HDP 30.2618	2.400	1200

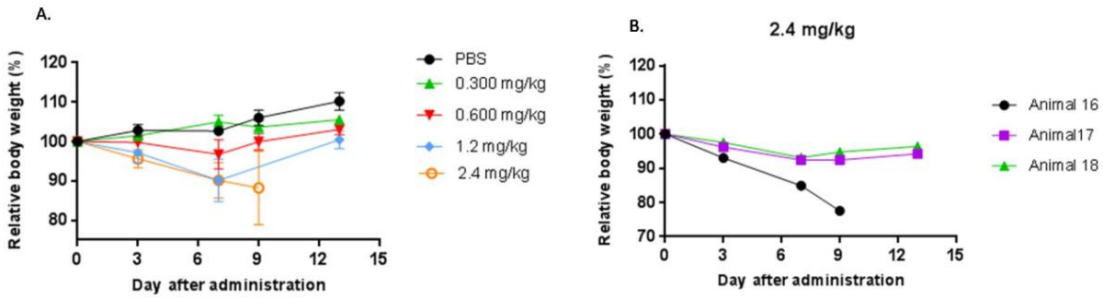

Figure 4.27 Tolerability of compound HDP 30.2618 (1:0) after single dose administration.

A. Body weight graphs after administration of different dose levels; **B.** Body weight loss of the individual animals from the group administered with 2.4 mg/kg (Cb 17 Scid male mice, n = 3).

4.2.3 Pharmacokinetic study of lead conjugate bearing monohindered disulfide linker HDP 30.2618 (1:0)

To determine the half-life of HDP 30.2618 similarly as for previously characterized *in vivo* DUPA-α-amanitin small molecular conjugates a one-compartmental model was employed. Experiment was performed in accordance to the procedure described in section 3.2.10. Half-life for this conjugate was determined to be ca. 74 min. and is in the range of the half-life observed for the conjugates HDP 30.2284 and HDP 30.2301 described in section 4.1.2.5. In the samples collected 24 h and 48 h after administration the conjugate concentration was below the lower limit of quantification. As expected, introduction of the disulfide linker in the structure of DUPA-α-amanitin SMDC had no influence on the half-lifetime of the conjugate. As for previously characterized conjugates, the administration frequency should be high to compensate for the short half-life and provide maximum systemic exposure to the conjugate.

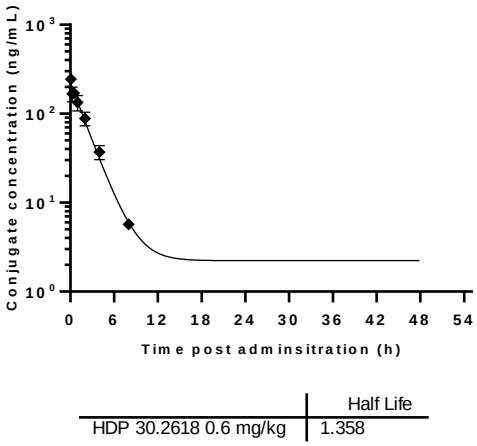

Figure 4.28 Pharmacokinetic profile and half-life of HDP 30.2618 (1:0).

4.2.4 Efficacy study of lead conjugate bearing disulfide monohindered linker HDP 30.2618 (1:0)

In the efficacy study the optimized dosing regimen was applied as for previously characterized compounds HDP 30.2284 and HDP 30.2301. HDP 30.2618 was administered three times per week over a period of three weeks. The dose of the administered conjugate was 0.6 mg/kg corresponding to 1/2 MTD (*Figure 4.29*). Dose level of 0.6 mg/kg was chosen based on the observation that it did not cause significant body weight loss upon single dose administration (*Figure 4.27*).

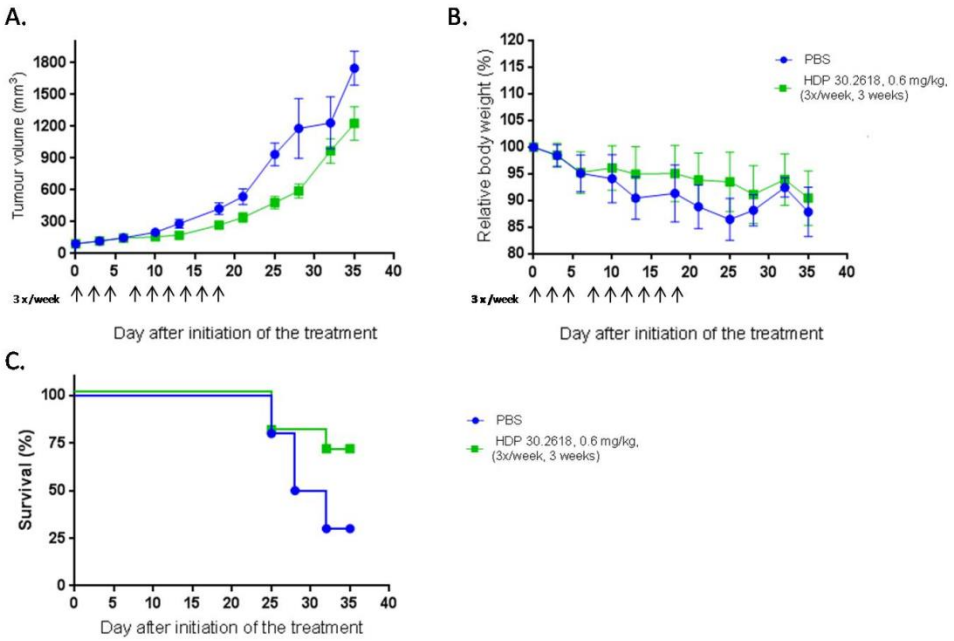

Figure 4.29 Efficacy and tolerability of the therapy with HDP 30.2618.

A. Tumor volumes (average tumor volume ± SEM); **B.** Tolerability (average relative tumor volume ± SEM); **C.** Survival of animals treated with 0.6 mg/kg of HDP 30. 2301 during the follow-up of the therapy - some of the animals had to sacrificed due to unacceptably huge tumor volume (CB17 Scid male LNCaP xenografts, for HDP 30.2618 administered group until day 21 n=10, day 25-32 n=8, day 32-35 n= 7; for vehicle injected group up to day 21 n = 10, day 25 n=8, day 27 n=5, day 32 n=4).

No statistically significant differences between the two arms of the study: vehicle (PBS) and HDP 30.2618 were observed until day 10 after administration. Despite of continued dosing once the tumors reached a volume of ca. 250 mm^3 (after day 13) they stopped responding to the therapy. Especially between day 21 and 28 the tumors of the animals injected with the vehicle grew very rapidly. During the follow up period some of the animals had to be sacrificed due to unacceptably high tumor volumes, thus the presented body weight and tumor volume data after day 25 are given only for surviving animals (*Figure 4.29* capture). Significant difference in the tumor volumes between the vehicle and HDP 30.2618 treated groups were observed only at day 25, but not before or afterwards (**$p < 0.01$, Mann-Whitney test). Overall HDP 30.2618 similarly as previously characterized conjugates HDP 30.2284 (Val-Ala-PAB linker) and HDP 30.2301 (C_6 non-cleavable linker) demonstrated only limited antitumor activity, which was non-sustained after cessation of the therapy.

The introduction of monoprotected disulfide conjugate into the structure of the DUPA-α-amanitin does not have a significant impact on the activity of conjugate.

A full biodistribution study of HDP 30.2618 was not in the scope of this work due to the time constrictions but could provide a better insight especially into the kidney toxicity profile of this particular molecule. Considering similar biodistribution profile determined for HDP 30.2284 and HDP 30.2301 which was independent to the linker strategy it is reasonable to assume that for HDP 30.2618 a similar biodistribution profile as determined for both previously characterized conjugates would be presented.

The main objective for the development of conjugates bearing disulfide linker was balancing two properties which were not optimal for conjugates HDP 30.2284 (Val-Ala-PAB linker) and HDP 30.2301 (C_6 -non-cleavable linker). For HDP 30.2284 release of the free toxin moiety upon uptake and enzymatic processing was possible and came out to be important for *in vivo* activity. Concomitantly for this conjugate a linker related dose limiting toxicity *in vivo* was observed. The second conjugate HDP 30.2301 featured high tolerability *in vivo* but lack of intracellular release of the toxin upon internalization into cells related to the stable linker resulted in the limited *in vivo* efficacy. To this end five DUPA-α-amanitin conjugates bearing different levels of disulfide linker hindrance were tested *in vitro*. Amongst all compounds from the library conjugate HDP 30.2618 (1:0) demonstrated nanomolar *in vitro* activity in PSMA positive cells and highest stability in mouse and in human plasma. MTD of HDP 30.2618 (1:0) was determined to be 1.2 mg/kg and allowed to obtain desired *in vivo* toxicity level (higher tolerability than for HDP 30.2284) and allowed for intracellular release of toxin metabolite (in contrast to HDP 30.2301). *In vivo* HDP 30.2618 (1:0) showed a short half-life of 74 min. which is in the range of half-life observed for conjugates HDP 30.2284 ($t_{1/}$ =44.2 min.) and HDP 30.2301 ($t_{1/2}$=61.8 min.) (described in section 4.1). Although the HDP 30.2618 demonstrated better tolerability than HDP 30.2284 and in contrast to HDP 30.2301 allowed for intracellular release of the toxin derivative, it still did not allow to obtain sustainable anti-tumor response. These results ultimately confirm that major factor limiting *in vivo* efficacy of DUPA-α-amanitin conjugates is sub-optimal pharmacokinetic profile most possibly related to the rapid renal clearance. Further optimization of DUPA-α-amanitin conjugates was focused on the implementation of strategies aiming into limitation of kidney accumulation and prolongation of circulatory half-life (section 4.3).

4.3 OPTIMIZATION OF THE PHARMACOKINETIC PROPERTIES OF DUPA -ALPHA-AMANITIN CONJUGATES - LIMITING KIDNEY ACCUMULATION AND PROLONGATION OF CIRCULATORY HALF-LIFE

The described so far conjugates demonstrated limited *in vivo* efficacy as a result of rapid renal clearance, a short half-life and significant kidney accumulation. In order to preserve the small molecular size of the conjugate a strategy aiming into limitation of kidney accumulation was employed. Adding a double histidine-glutamic acid motif $(His\text{-}Glu)_2$ between the supporting spacer (8-Aoc-Phe-Phe) and Val-Ala-PAB linker would lead to an overall negative charge of the molecule under physiological pH. In consequence the conjugate should be repulsed from the negatively charged membrane of the glomerular cells in the kidney [108]. Theoretically this should limit the kidney uptake and in turn lead to a slight improvement in the circulatory half-life of SMDC.

The second rescue strategy was aiming to ultimately prolong the half-life by conjugation of DUPA-α-amanitin to the Fc potion of aglycosylated human IgG1. This approach triggers the conjugate recycling *via* neonatal Fc receptor (FcRn) (*Figure 4.30*), which is responsible for long half-life of molecules such as IgG and human serum albumin [109, 110]. The benefit arising from the addition of significant molecular weight of aglycosylated Fc portion of human IgG might be of minor importance since the molecular weight of conjugate - approximately 61 kDa is on the boarder of molecular weight cut-off for molecules undergoing renal filtration (approximately 60-70 kDa)[111].

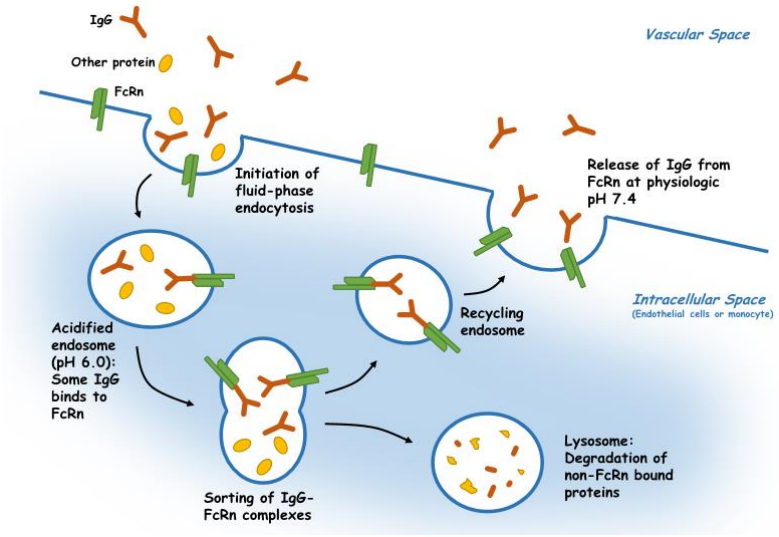

Figure 4.30 Schematic presentation of IgG uptake and recycling *via* FcRn receptor.

FcRn recycling is mediated via Fc motif of IgG. IgG molecules are internalized into endosomes by nonspecific pinocytosis. Endosomes acidic content allowing FcRn to bind IgG. Bound and unbound proteins are sorted. Unbound proteins undergo degradation in lysosomes and bound IgG is trafficked to the cell surface. Bound IgG is released back into the circulation. Figure was taken from [110].

4.3.1 Adapting strategy aiming to limit kidney accumulation - DUPA-α-amanitin conjugate bearing $(His\text{-}Glu)_2$ motif

Since amongst all tested *in vivo* small molecular DUPA-α-amanitin conjugates the lowest tolerability was observed for HDP 30.2284 (Val-Ala-PAB linker) the further optimization of this compound was based on the introduction of molecular changes aiming to limit the kidney toxicity. Based on the plasma stability assay presented in section 3.2.4 the maleimide chemistry was substituted by acetamide chemistry to yield the compound HDP 30.2594 (*Figure 4.31*). Acetamide chemistry was employed in order to avoid possible retro-Michael addition and α-amanitin exchange between conjugate and serum albumin (described in section 4.1.3). Additionally, the $(His\text{-}Glu)_2$ motif was introduced between supporting spacer (8-Aoc-Phe-Phe) and Val-Ala-PAB linker. It has been shown that introduction of a multiple histidine-glutamic acid motifs in the structure of small molecular compounds leads to deprotonation of the glutamic acid appearing under physiological pH in consequences giving an overall negative charge of the moiety. Negatively charged molecules are repulsed from the negatively charged cells of glomerular which potentially may limit renal filtration [108]. This strategy has been first employed for the optimization of the pharmacokinetic profile of a PET double targeted radio-imaging agent recognizing

PSMA and GRPr (gastrin releasing peptide receptor). It was proved that this strategy reduced the renal uptake of this particular PSMA/GRPr double targeting PET tracer by approximately 50 % [108]. Despite of limited kidney accumulation there was observed only a slight prolongation in the half-life of reported double targeted radioimaging agent [108].

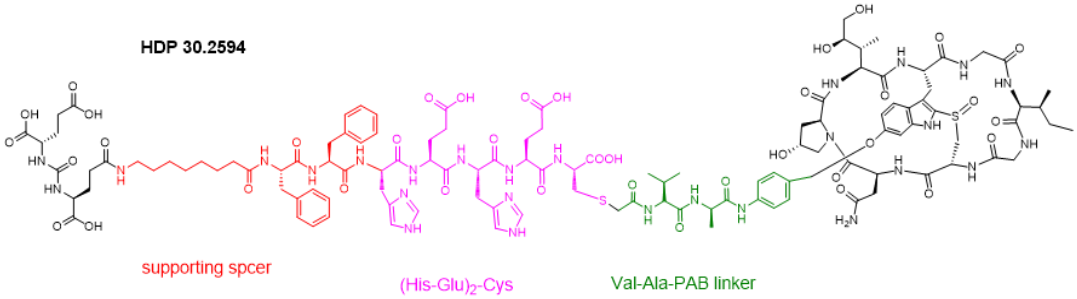

Figure 4.31 Chemical structure of compound HDP 30.2594.

4.3.1.1 *In vitro* activity of small molecular weight DUPA-α-amanitin conjugate bearing (His-Glu)$_2$ linker HDP 30.2594

First step in the characterization of HDP 30.2594 was determining whether introduction of (His-Glu)$_2$ motif has an impact on *in vitro* activity of DUPA-α-amanitin conjugate. The results of cytotoxic potential of HDP 30.2594 on three prostate cancer cell lines expressing different levels of PSMA receptor is presented in *Figure 4.32*.

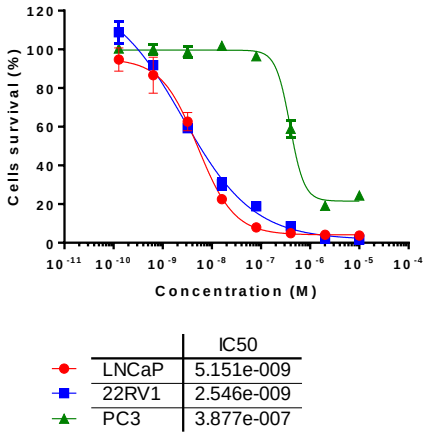

Figure 4.32 Cytotoxic potential of compound HDP 30.2594 on LNCaP (PSAM +++), 22RV1 (PSMA+) and PC3 (PSMA -) prostate cancer cell lines.

For HDP 30.2594 ((His-Glu)$_2$ linker) conjugate IC_{50} was determined to be 5.15 nM and 2.55 nM in the PSMA expressing cell lines LNCaP and 22RV1, respectively. HDP 30.2594 was approximately 75 times more active in LNCaP cells than in PC3 PSMA negative cells. This high cytotoxic potential with IC_{50} determined in one-digit nonomolar range of concentration in PSMA positive cells is in the rage of cytotoxic potential for previously characterized conjugates HDP 30.2284, HDP 30.2301 and HDP 30.2618 (0.83 nM, 6.11 nM and 4.39 nM, respectively). In order to verify whether the introduction of a (His-Glu)$_2$ linker in the structure of the DUPA-α-amanitin SMDC indeed leads to decreased kidney accumulation the next step was a head-to-head comparison of serum pharmacokinetic profiles and kidney accumulation of HDP 30.2594 to the previously characterized HDP 30.2284.

4.3.1.2 Head to head comparison of blood pharmacokinetics and kidney accumulation of HDP 30.2284 and an analogue bearing (His-Glu)$_2$ motif HDP 30.2594

For comparative pharmacokinetic and kidney accumulation study already characterized HDP 30.2284 (section 4.1.5 for serum pharmacokinetics results and section 4.1.7 for biodistribution results) and HDP 30.2594 were administered at doses corresponding to 75 µg/kg of unconjugated α-amanitin: 0.184 mg/kg for HDP 30.2284 and 0.160 mg/kg for HDP 30.2594 (*Figure 4.33*). Detection of conjugate and related metabolites presenting α-amanitin core in the structure was performed by anti-α-amanitin ELISA.

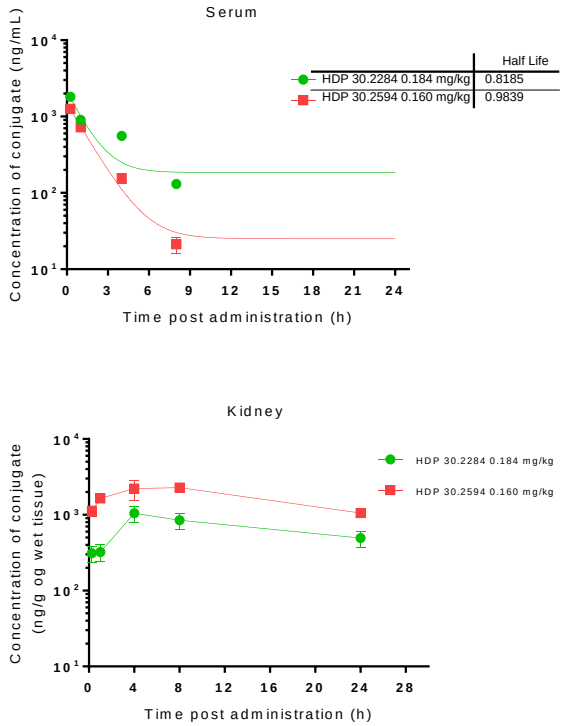

Figure 4.33 Head-to-head comparison of blood pharmacokinetics (upper panel) and kidney biodistribution (lower panel) of HDP 30.2284 (administered dose 0.184 mg/kg) and HDP 30.2594 (administered dose 0.149 mg/kg) after single dose *i.v.* injection.

Administered doses of both conjugates corresponds to 75 µg/kg equivalents of unconjugated α-amanitin. **A.** Comparative serum concentration and calculated half-life of both conjugates; **B.** Comparative kidney concentration. (Cb17 Scid male mice, median concentration ± SEM, n=3).

Despite the differences in charge, both conjugates displayed similar pharmacokinetics. Half-life of HDP 30.2284 in this particular experiment was determined to be approximately 49 min. and for approximately 59 min. for HDP 30.2594. Introduction of $(His\text{-}Glu)_2$ motif in the structure neither improved the exposure at early time-point post-administration nor significantly prolonged the half-life of conjugate (*Figure 4.33* upper panel). In contrast to initial expectations HDP 30.2594 showed significant accumulation in the murine kidney which is similar to the kidney accumulation of HDP 30.2284 (*Figure 4.33* lower panel). Due to very short half-life the efficacy similar to the observed for HDP 30.2284 is expected. The discouraging results of pharmacokinetic profiling of conjugate HDP 30.2594 and limited *in vivo* efficacy of all characterized up to the moment SMDCs did not support a further development of small molecular weight DUPA-α-amanitin conjugates. Further steps aiming

in the optimization of DUPA-α-amanitin conjugates were focused on the implementation of reliable strategy allowing to obtain prolonged half-life.

4.3.2 Viable and ultimate strategy providing prolongation of half-life - DUPA-α-amanitin conjugate presenting human IgG1 Fc portion in the structure (DUPA-Fc-α-amanitin conjugate)

In order to prolong the half-life of the small molecular DUPA-α-amanitin conjugate it was coupled to the aglycosylated Fc portion of human IgG1 (molecular weight of Fc portion is approximately 61 kDa). The DUPA-Fc-α-amanitin conjugate was developed by Francesca Gallo in collaboration with the research group of Prof. Harald Kolmar from the Technical University of Darmstadt. Technical details presenting the synthesis and characterization of DUPA-Fc-α-amanitin conjugate are presented in the PhD thesis of Francesca Gallo. Briefly, aglycosylated Fc portion of human IgG1 was produced in commercially available Expi293 Expression System in accordance to the manufacturer instructions. Fc fragment was purified by a protein A capture chromatography. Fc portion of human IgG1 used for the synthesis of conjugate bears a point mutation N297A, generated at the position which is a typical glycosylation site in human IgG. Moreover, C terminus of the Fc motif is equipped in a sequence recognized by a sortase A (LPETG) (*Figure 4.34*). Sortase A mediated reaction was used for the conjugation of DUPA motif bearing 8-Aoc-Phe-Phe supporting spacer followed by ethylene glycol $(EG_3)_2$ spacer and triazole moiety for subsequent strain-promoted azide-alkyne cycloaddition. Following the SrtA-mediated ligation, the strain-promoted azide-alkyne cycloaddition was employed for conjugation of the dibenzocyclooctyne group of toxin derivative bearing Val-Ala-PAB self-immolative linker allowing for cooper-free click conjugation of α-amanitin derivative to Fc-DUPA handle (*Figure 4.34*). Final DAR of conjugate was determined using LC-MS/MS for 1.7 molecule of toxin per one Fc fragment. The content of conjugate with DAR 2 was determined for approximately 73 % and conjugate with DAR 1 for approximately 26 %. It was proved that the limiting step in the production of DUPA-Fc-α-amanitin conjugate was the sortase A mediated reaction which yielded the mono and double loaded with DUPA motif Fc fragment. Importantly, yield of α-amanitin conjugation reaction was 100 % and there were detected no species loaded with DUPA but not conjugated to toxin, which could potentially compete for binding sites with molecules loaded with the α-amanitin. Although, a further optimization of

synthetic strategy allowing to obtain 100% of double loaded species is required, it is assumed that the quality of conjugate with DAR = 1.7 is acceptable and sufficient for the first proof of concept studies *in vitro* and *in vivo*.

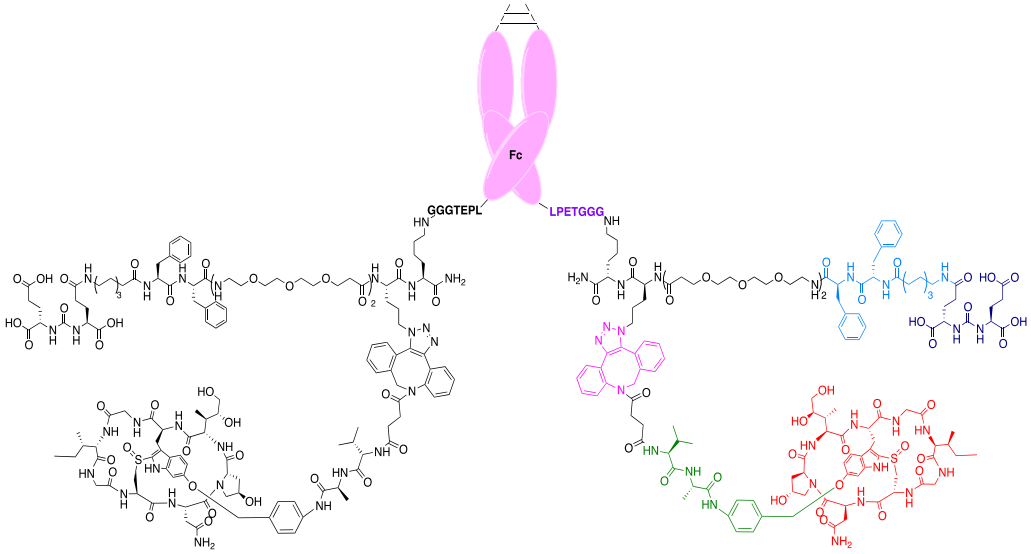

Figure 4.34 Schematic presentation of the DUPA-Fc-α-amanitin conjugate structure. The figure was kindly provided by Francesca Gallo M.Sc.

4.3.2.1 *In vitro* cytotoxicity and plasma stability of DUPA-Fc-α-amanitin conjugate

In vitro cytotoxic potential of the DUPA-Fc-α-amanitin conjugate was tested in three prostate cancer cell lines with different levels of PSMA expression (*Figure 4.35*). Results of plasma stability are presented in *Figure 4.36*.

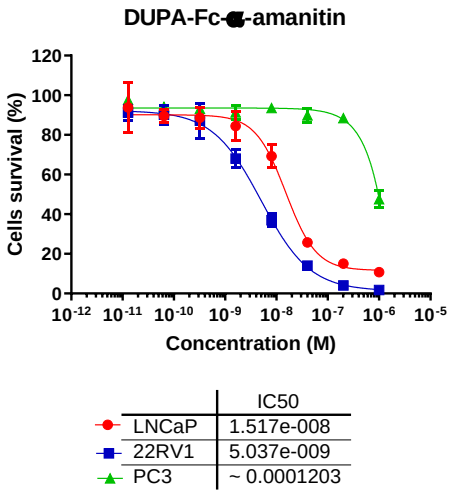

Figure 4.35 Cytotoxic potential of the DUPA-Fc-α-amanitin conjugate on three prostate cancer cell lines expressing different levels of PSMA: LNCaP (PSMA +++), 22RV1 (PSMA +) and PC3 (PSMA -).

Similar as for SMDCs the cytotoxic effect of DUPA-Fc-α-amanitin is PSMA mediated as it is observed only in PSMA expressing cell lines. In PSMA cell line demonstrating high and uniform level of PSMA expression the IC_{50} of DUPA-Fc-α-amanitin conjugate was determined to be 15.17 nM. Interestingly, the highest potential was observed in the 22RV1 cell line which heterogeneously expresses PSMA receptor. As expected, no activity of the conjugate was observed in PSMA negative PC3 cell line.

The plasma stability of the DUPA-Fc-α-amanitin conjugate was determined using Western-blot and cytotoxicity assay upon prior incubation of this molecule in mouse plasma, human plasma and PBS at 37° C. Western blot analysis (*Figure 4.36*) allows to determine whether the toxin is cleaved of from the Fc-DUPA handle. The cytotoxicity assay (*Figure 4.37* and *Table 4.10*) upon incubation at 37° C in plasma allows to determine the cytotoxic potentials of not only the conjugate but also all possible degradation products, aggregates or metabolites which may remain cytotoxic. The concentration range tested in the plasma stability assay with the read out being cytotoxicity was lower than these tested for SMDCs and was ranging between 200 nM – 2.56 pM. It was due to the fact that the final concentration of produced conjugate was approximately 52 µM. The preparation of samples for plasma stability assay requires pre-dilution of the conjugate and initial concentration of 52 µM was too low to allow for testing higher range of concentration. Due to limited availability of the material the protein concentration using centrifuge concentrators was not feasible because of significant protein loses during this procedure. Importantly tested

in plasma stability DUPA-Fc-α-amanitin range of concentration allowed to obtain sigmoidal cytotoxicity dose response curves in LNCaP cells (*Figure 4.37*).

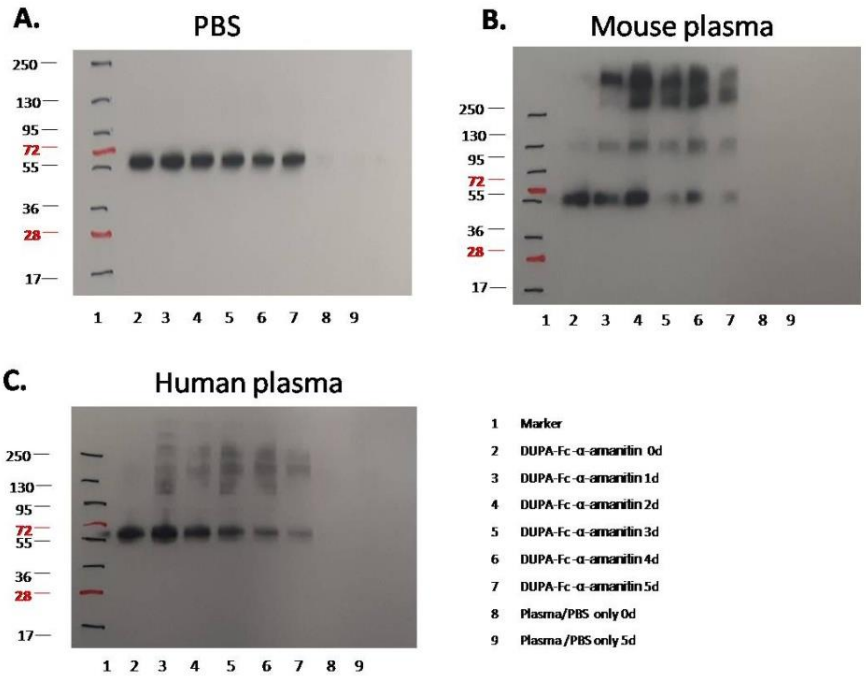

Figure 4.36 Plasma stability of DUPA-Fc-α- amanitin conjugate**.**

Anti α-amanitin western blot of conjugate stressed from time point 0 up to 5 days -reducing conditions. Conjugate was stressed in three different matrices in **A.** PBS, **B.** Mouse plasma (MP) and **C.** Human plasma (HP). Detection was done using polyclonal anti-α-amanitin serum. Exposure time - approximately 10 sec.

Stressing of conjugate in PBS had no impact on the stability of DUPA-Fc-α-amanitin (*Figure 4.36* A). In contrast for the conjugate stressed in mouse and in human plasma a high molecular weight aggregates containing α-amanitin were observed already at time-point 0 (day 0) (*Figure 4.36* B and C). For conjugate incubated in mouse plasma the products of aggregation are visible at two different molecular weights: approximately 130 kDa and huge smearing bad with the molecular weight > 250 kDa. At day zero only very faint aggregates signals are detected. The aggregation progresses with time of stressing as demonstrated by increasing intensity of band with the molecular weight ≥ 130 kDa between day zero and four. Strongest aggregates formation was observed between day two and four. The band corresponding to the conjugate (approximately 61 kDa) is visible up to day two. From the day three onward the signal corresponding to DUPA-Fc-α-

amanitin gradually fades away. For the final time point - day five the signal for both: conjugate and aggregates decreased in intensity.

Although stressing of conjugate in human plasma also led to aggregates formation it was not as prominent as for the sample incubated in mouse plasma (*Figure 4.36* B and C). The signal pattern corresponding to aggregates formed after incubation in human plasma was observed and appeared as smearing bands at the molecular weight > 90 kDa. This pattern was different than for aggregates formed in mouse plasma. Decreasing intensity in the signal corresponding to DUPA-Fc-α-amanitin conjugate was clearly observed starting at the day one throughout duration of the experiment. In general, based on the western blot analysis, in both mouse and human plasma despite of aggregates formation the conjugate can be considered as stable up to day 2.

For the determination of stability using cytotoxicity assay as readout additional prolonged incubation time-points in three different matrices were chosen in order to understand whether observed after prolonged time-points aggregates visible in western blot analysis retain cytotoxic potential and may trigger cytotoxicity on PSMA positive cell line. Results of cytotoxicity experiments are presented in *Figure 4.37* and summarized in *Table 4.10*.

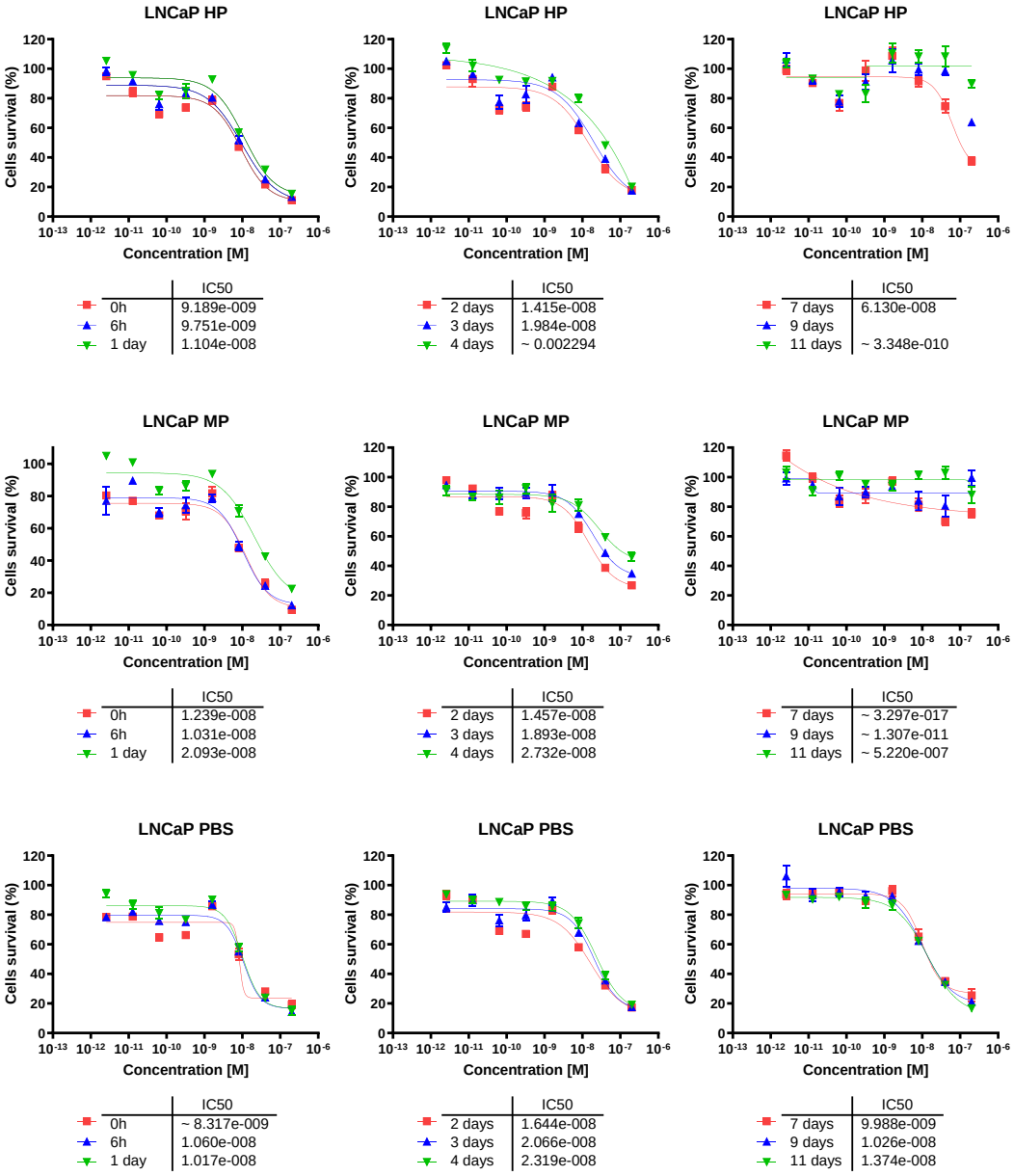

Figure 4.37 Determination of cytotoxic potential of DUPA-Fc-α-amanitin conjugate after stressing in three different matrices in LNCaP (PSMA +++) cells.

Upper panel: Human plasma; **middle panel:** Mouse plasma; and **lower panel:** PBS.

Table 4.10 Summary of the *in vitro* stability results cytotoxic potential of DUPA-Fc-α-amanitin conjugate upon stressing in human plasma mouse plasma and PBS in LNCaP cell line (PSMA +++).

Matrix	Compound	IC_{50} [M]	Fold of cytotoxicity reduction
Human Plasma	DUPA-Fc-α-amanitin 0h	9.19×10^{-9}	-
	DUPA-Fc-α-amanitin 6h	9.75×10^{-9}	1.06
	DUPA-Fc-α-amanitin day 1	1.10×10^{-8}	1.20
	DUPA-Fc-α-amanitin day 2	1.42×10^{-8}	1.55
	DUPA-Fc-α-amanitin day 3	1.98×10^{-8}	2.15
	DUPA-Fc-α-amanitin day 4	ca. 8×10^{-8}	8.7
	DUPA-Fc-α-amanitin day 7	n.d.*	X
	DUPA-Fc-α-amanitin day 9	n.d.*	X
	DUPA-Fc-α-amanitin day 11	n.d.*	X
Mouse Plasma	DUPA-Fc-α-amanitin 0h	1.23×10^{-8}	X
	DUPA-Fc-α-amanitin 6h	1.03×10^{-8}	0.83
	DUPA-Fc-α-amanitin day 1	2.09×10^{-8}	1.70
	DUPA-Fc-α-amanitin day 2	1.46×10^{-8}	1.18
	DUPA-Fc-α-amanitin day 3	1.89×10^{-8}	1.54
	DUPA-Fc-α-amanitin day 4	2.73×10^{-8}	2.30
	DUPA-Fc-α-amanitin day 7	n.d.*	X
	DUPA-Fc-α-amanitin day 9	n.d.*	X
	DUPA-Fc-α-amanitin day 11	n.d.*	X
PBS	DUPA-Fc-α-amanitin 0h	8.32×10^{-9}	X
	DUPA-Fc-α-amanitin 6h	1.06×10^{-8}	1.27
	DUPA-Fc-α-amanitin day 1	1.02×10^{-8}	1.23
	DUPA-Fc-α-amanitin day 2	1.64×10^{-8}	2.02
	DUPA-Fc-α-amanitin day 3	2.07×10^{-8}	2.49
	DUPA-Fc-α-amanitin day 4	2.32×10^{-8}	2.79
	DUPA-Fc-α-amanitin day 7	9.99×10^{-9}	1.2
	DUPA-Fc-α-amanitin day 9	1.03×10^{-8}	1.24
	DUPA-Fc-α-amanitin day 11	1.37×10^{-8}	1.65

* n.d. - could not be determined, cytotoxic potential was completely lost

For DUPA-Fc-α-amanitin stressed in human plasma the cytotoxic potential is unchanged up to day three. Conjugate stressed for four days in human plasma is clearly less effective compared day three. At day seven just two highest tested concentrations affected cells viability. The highest tested concentration (2×10^{-7} M) killed only approximately 70 % of cells. At day nine and 11 conjugate completely lost cytotoxic potential. Based on these results it can be assumed that DUPA-Fc-α-amanitin conjugate is stable up to three days in human plasma.

For conjugate stressed in mouse plasma cytotoxic potential was unchanged only after six hours of incubation. From the day one until day four the conjugate was gradually loosing potency as demonstrated by increasing offset of viable cells at highest tested concentrations. Conjugate completely lost cytotoxic potential at day seven.

Conjugate was completely stable in PBS what additionally confirms that plasma components and not thermal degradation influences conjugate activity.

In general, tested conjugate demonstrated better stability in human than in mouse plasma. DUPA-Fc-α-amanitin conjugate might be considered as stable up to day four in both human and mouse plasma. Altogether, high *in vitro* selectivity of DUPA-Fc-α-amanitin towards PSMA positive cells and acceptable conjugate stability supported further *in vivo* studies of this molecule.

4.3.2.2 Determination of maximum tolerated dose for DUPA-Fc-α-amanitin conjugate

In vivo characterization of DUPA-Fc-α-amanitin was commenced with the determination of maximum tolerated dose. The initially administered dose of 1.5 mg/kg was corresponding to the tolerated equivalents of α-amanitin administered in the form of an anti PSMA α-amanitin ADC (Heidelberg Pharma Research GmbH, internal data) (*Table 4.11*). At day seven after administration all animals demonstrated ca. 20 % loss in the relative body weight, deterioration of clinical symptoms and had to be sacrificed due to general bad condition (*Figure 4.38*). Additionally, the dissection has shown macroscopic changes in the kidneys, namely paleness. Further 50 % reduction in the administered dose - 1 mg/kg did not result in any clinical symptoms and was well tolerated. The animals showed ca. 10 % body weight loss at day 7 after administration, which was recovered in the follow-up. Thus, the dose of 1 mg/kg was set as MTD of DUPA-Fc-α-amanitin (*Figure 4.38*).

Table 4.11 Dose of DUPA-Fc-α-amanitin used in MTD study with indicated equivalents of α-amanitin

Compound	DUPA-Fc-α-amanitin dose [mg/kg]	α-amanitin dose [µg/kg]
DUPA-Fc-α-amanitin	1.5	38.6
DUPA-Fc-α-amanitin	1.0	25.7

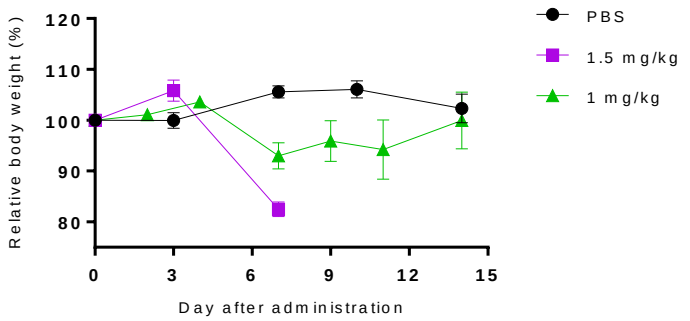

Figure 4.38 *In vivo* tolerability of DUPA-Fc-α-amanitin conjugate (Cb 17 Scid mice, n=3).

4.3.2.3 Determination of pharmacokinetic profile of DUPA-Fc-α-amanitin conjugate

To determine the dosing frequency of the DUPA-Fc-α-amanitin for an efficacy experiment the blood pharmacokinetic study was performed in accordance to the procedure described in section 3.2.16. In contrast to previously characterized small molecule drug conjugates, for DUPA-Fc-α-amanitin the biphasic elimination profile associated with two-compartmental model and FcRn recycling was observed (*Figure 4.39*). Fast elimination phase half-life was determined to be 25.2 min. and is observed at early time-points after administration (5 min. to 4 h). Slow elimination phase is clearly observed from 4 h following administration onward and half-life for this phase was determined to be 7.2 day (172.6 h) (*Figure 4.39*).

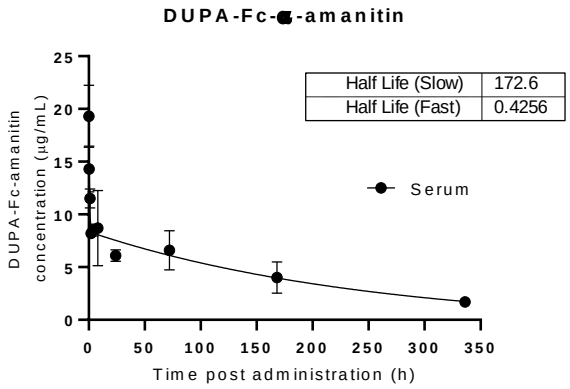

Figure 4.39 Serum concentration and half-life of DUPA-α-amanitin conjugate (shown is median concentration ± SEM, Cb17 Scid male mice, n=3).

4.3.2.4 Biodistribution study of DUPA-Fc-α-amanitin conjugate

As demonstrated in previous section, the implementation of Fc fragment in the structure of conjugate had a major impact on the pharmacokinetic properties of the molecule.

Besides of blood pharmacokinetic study an organ biodistribution of DUPA-Fc-α-amanitin conjugate was determined for tumor, liver and kidney (*Figure 4.40* A). A median concentration of approximately 2 µg/g of liver tissue was detected at the time-point 15 min. following administration. This concentration decreased slightly thereafter and reached maximum - 5.13 µg/g at 168 h (day 7) after administration. Similar profile of DUPA-Fc-α-amanitin biodistribution over time with slightly lower concentrations was determined in the kidney (*Figure 4.40* A). The detectable concentrations of DUPA- Fc-α-amanitin in the tumor were observed only at early time-points 5 min., 15 min. and 1 h following administration. For remaining time-points the concentration of conjugate in the tumor was below the lower limit of quantification (*Figure 4.40* A).

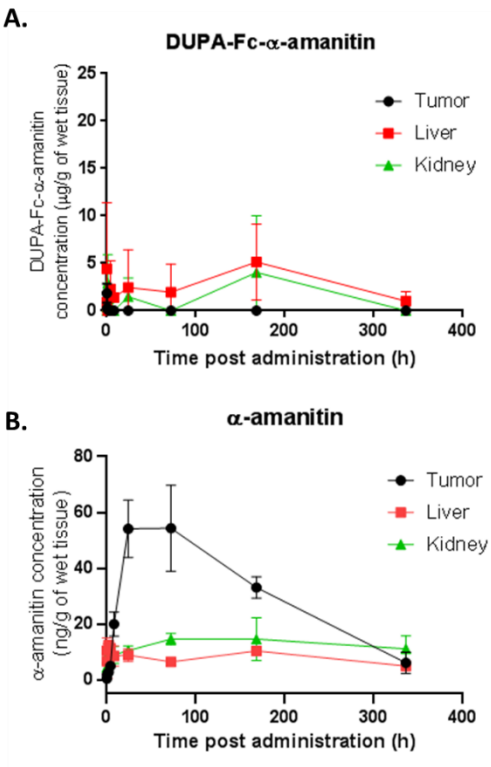

Figure 4.40 Biodistribution study of DUPA-Fc-α-amanitin and released toxin after single dose administration of 1 mg/kg in the tumor, liver and kidney extracts.

A. Biodistribution of DUPA-Fc-α-amanitin; **B.** Released from DUPA-Fc-α-amanitin toxin concentration (shown is median concentration ± SEM; Cb 17 Scid mice xenografted with LNCaP tumors, n=3). No free α-amanitin was detected in serum (data not shown).

Anti-α-amanitin ELISA was applied for the determination of free toxin concentration and related metabolites presenting α-amanitin core in the structure. Experiment was performed in accordance to the procedure described in section 3.2.12. The serum concentration of released toxin was under the lower limit of quantification throughout the whole study period (data not shown). Only minimal variation in α-amanitin levels over time was observed in liver and kidney (*Figure 4.40 B*). The maximum concentration in the kidney of 14 ng/g was detected 72 h after conjugate administration and remained on the similar level up to 14 days following administration. Free toxin concentration in the kidney was slightly higher than in the liver (*Figure 4.40* B). Conversely, much higher amount of free toxin was found in the tumor. Peak concentration of approximately 54 ng/g was detected at day one and three after administration. At day 7 following administration, α-amanitin tumor level dropped slightly to 33 ng/g but the toxin was still detectable even 14 days upon administration (*Figure 4.40* B). It was concluded that in order to obtain a toxin

accumulation in the tumor conjugate should be administered at least once per week or more frequently.

4.3.2.5 *In vivo* efficacy study of DUPA-Fc-α-amanitin conjugate

Based on the pharmacokinetic profile and tolerability of DUPA-Fc-α-amanitin conjugate six different dosing regimens were established for *in vivo* efficacy study in LNCaP xenografts. Various dose levels were tested in order to understand the relation between the administered dose, dosing frequency and tumor response (*Figure 4.41* A). The study consisted of 6 groups treated in accordance to the following scheme:

- 1 mg/kg (1 MTD), 1x / week for 3 weeks
- 0.5 mg/kg (0.5 MTD), 1x / week for 3 weeks
- 0.5 mg/kg (0.5 MTD), 2x / week for 3 weeks
- 0.25 mg/kg (0.25 MTD), 1x / week for 3 weeks
- 0.25 mg/kg (0.25 MTD), 2x / week for 3 weeks
- 0.25 mg/kg (0.25 MTD), 3x / week for 3 weeks

Results of *in vivo* efficacy study are presented in *Figure 4.41*.

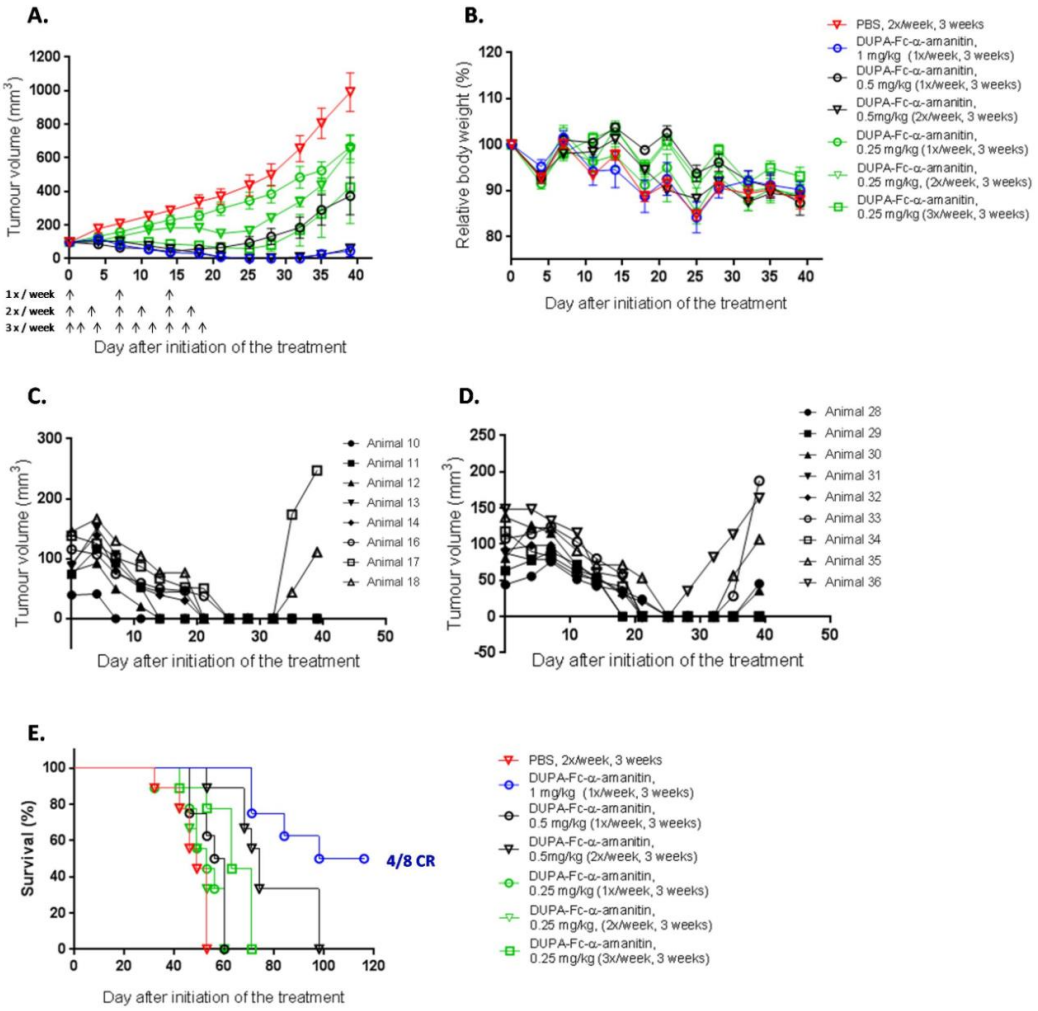

Figure 4.41 Antitumor activity of DUPA-Fc-α-amanitin conjugate in LNCaP xenografts (PSMA +++).

A. Efficacy of DUPA-Fc-α-amanitin; **B.** Mean change of the body weight presenting the tolerability of the therapy; **C.** Tumor volumes of individual animals treated with 1 mg/kg 1x/week, 3 weeks; **D.** Tumor volumes of individual animals treated with 0.5 mg/kg 2x/week, 3 weeks; **E.** Long term survival follow up of the animals treated with different dosing regimens of DUPA-Fc-α-amanitin. (Cb 17 Scid male mice, n=8-9, CR - complete response).

Anti-tumor effect of DUPA-Fc-α-amanitin conjugate is clearly administration frequency and dose dependent (*Figure 4.41* A). The tumor response in groups treated with 0.25 mg/kg of conjugate more frequently - two or three times a week is better than in the study group treated once per week. The tumor volume of the group administered with 0.5 mg/kg once per week (black circles) converges with the tumor volume of the group administered with 0.25 mg/kg three times per week (green squares) (*Figure 4.41 A*).

Moreover, a similar tumor response is observed for 1 mg/kg administered once per week (blue circles) and 0.5 mg/kg administered twice per week (black triangles), but the longer tumor response duration was observed for the animals treated with 1 mg/kg dose. Altogether, these results suggest that less frequent administration of higher dose of conjugate leads to better tumor response. Proposed dosing scheme was completely tolerated as indicated by relative body weight graphs (*Figure 4.41 B*).

The complete tumor responses were observed in the group treated with two highest doses: 0.5 mg/kg twice per week (*Figure 4.41 C*) and 1 mg/kg once per week (*Figure 4.41 D*). Unfortunately, these complete responses were followed by tumor relapse in 5/9 of the animals treated with 0.5 mg/kg up to day 39 following initiation of the therapy (*Figure 4.41 D)*. In the long-term follow-up all animals from this group experienced tumor relapse and had to be sacrificed due to unacceptably huge tumor volume (*Figure 4.41 E*). In the group administered once per week with 1 mg/kg initially complete tumor response was observed in 6/8 of animals. Between day 42-84 two out of six animals demonstrating complete response experienced tumor relapse (*Figure 4.41 C)*. The study was terminated at day 116 following initiation of the therapy (day 98 upon therapy termination). At this time-point 4/8 animals from the group treated with 1 mg/kg were alive and most importantly all were still demonstrating a complete response (*Figure 4.41 E*). A remarkably longer median survival was observed in groups treated with effective doses of DUPA-Fc-α-amanitin conjugate: 107 days for 1 mg/kg administered once per week (****$p<0.0001$) and 74 days for 0.5 mg/kg administered twice per week (***$p = 0.0001$) *vs.* 49 days for vehicle injected group (Log-rank analysis)(*Figure 4.41 E*).

This result demonstrates a great improvement in the *in vivo* efficacy of Fc containing system delivering α-amanitin to PSMA expressing tumor *via* DUPA targeting moiety. Only short-term inhibition in tumor growth observed for SMDCs: HDP 30.2284, HDP 30.2301 and HDP 30.2618 was raised to complete tumor remission sustained upon cessation of the therapy by tuning pharmacokinetic properties of the molecule.

5. DISCUSSION AND OUTLOOK

5.1 IMPACT OF LINKER AND CONJUGATION STRATEGY ON *IN VITRO* ACTIVITY AND PLASMA STABILITY OF DUPA-ALPHA-AMANITIN CONJUGATES

5.1.1 Conjugates bearing Val-Ala-PAB cleavable linker and C_6 non-cleavable linkers

Importance of supporting spacer

In 2009 Kularatne *et al.* described detailed *in silico* docking study of PSMA ligands [77]. DUPA originated from the structure of NAALDAase inhibitors which were originally developed as neuroprotective drugs helping to resolve cerebral ischemia [112]. Naked DUPA moiety was designed to fit into the active site of PSMA. The additional analysis of PSMA crystal structure revealed that active site could be reached only *via* a gradually narrowing, 20 Å deep tunnel-like structure [77, 87]. The tunnel is lined with two hydrophobic pockets and an arginine cluster (*Figure 1.8*). The structural data suggest that the design of conjugates for PSMA targeted delivery based on DUPA ligand should be complementary to the contours of the tunnel. It means that to provide the binding of DUPA in PSMA active site the targeting moiety cannot be directly followed by large and bulky structures like e.g. toxin or chelating moiety but the additional supporting spacer fitting into the tunnel in PSMA structure. The same authors screened different spacers for attachment of linker and identified that spacer -NH-$(CH_2)_6$-Phe-Phe-CO (Aoc-Phe-Phe) particularly well fitted into the contours of PSMA tunnel [77, 94]. This is due to the interaction of two hydrophobic pockets of PSMA with two aromatic rings in the phenylalanine structure.

Within presented study the comparison of two pairs of compounds lacking and featuring a supporting spacer: HDP 30.1585 *vs.* HDP 30.2301 (bearing C_6 stable linker) and HDP 30.1592 *vs.* HDP 30.2284 (bearing Val-Ala-PAB cleavable linker) demonstrated the absolute necessity of the supporting spacer for efficient toxin delivery by DUPA ligand (section 4.1.2). Implementation of supporting spacer 8-Aoc-Phe-Phe dramatically improved the activity of DUPA-α-amanitin conjugates in PSMA positive cells. *In vitro* data demonstrated that utilization of supporting motif provides selectivity and allows for efficient target binding as demonstrated by significantly lower IC_{50} compared to the molecules lacking supporting

spacer (section 4.1.1. *vs.* section 4.1.2). Since this spacer provided improved *in vitro* activity it was employed in the synthesis of all DUPA-α-amanitin conjugates developed within this project.

HDP 30.2284 bearing Val-Ala-PAB cleavable linker demonstrated slightly better *in vitro* potency than C_6 non-cleavable linker bearing analogue HDP 30.2301 (section 4.1.1. and 4.1.2). It is most probably due to α-amanitin release after cleavage by cathepsin B and self-immolation of Val-Ala-PAB linker from conjugate HDP 30.2284 in the intracellular environment. This difference in activity of conjugates bearing cleavable and non-cleavable suggests that naked α-amanitin is slightly more potent than entire HDP 30.2301 or HDP 30.2301 related metabolite. Although, the stable linker was attached to the 6-OH tryptophan in the structure of α-amanitin (*Figure 1.6* and *Figure 4.4*), which theoretically should not influence the interaction of α-amanitin with RNA Pol II a slight decrease in the *in vitro* activity of HDP 30.2301 (C_6 stable linker) was observed. This result is in line with the data reported for α-amanitin based anti-PSMA ADCs bearing Val-Ala-PAB cleavable and C_6 non-cleavable linker attached to the 6-OH tryptophan of α-amanitin where a higher *in vitro* activity of conjugates featuring cleavable linker was observed [113]. It suggests that the presence of the linker moiety in the structure of DUPA-α-amanitin conjugate has an impact on the interaction with RNA Pol II what to some extend may explain lower cytotoxic potential of conjugates with a non-cleavable linker.

Optimization of plasma stability

Both conjugates HDP 30.2284 (Val-Ala-PAB linker) and HDP 30.2301 (C_6 non-cleavable linker) were linked to DUPA-supporting spacer using maleimide coupling. It is known that maleimide conjugates can undergo retro-Michael addition and thiol-exchange upon exposure to the plasma proteins, predominantly with cysteine residues in the structure of serum albumin [114]. One of the reported strategies to avoid retro-Michael addition upon plasma exposure is the elimination of maleimide ring in the structure and employing acetamide coupling instead. Schematic presentation of both strategies and their impact on the conjugate stability is presented in *Figure 5.1*.

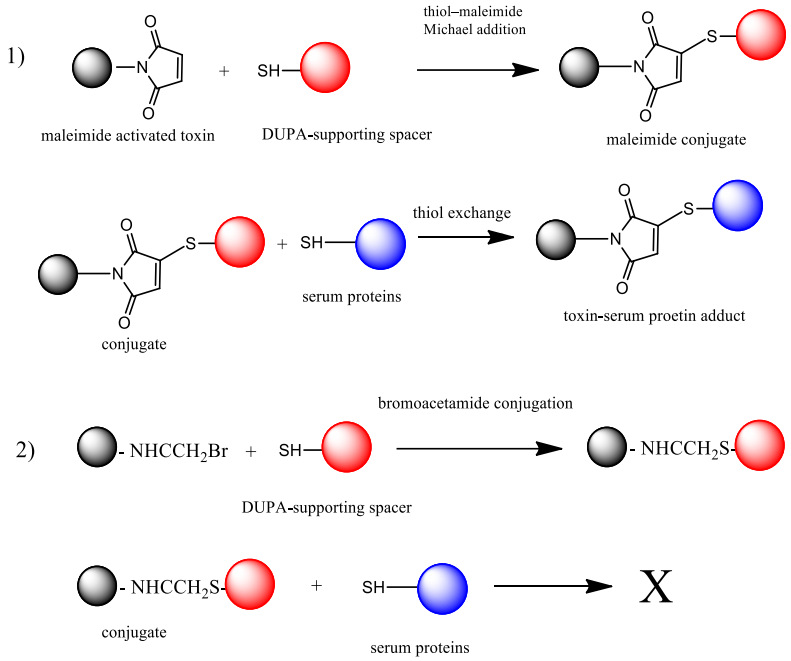

Figure 5.1 1) Maleimide chemistry and alternative **2)** acetamide chemistry as the strategy to avoid retro Michael reaction and improve plasma stability of conjugates.

The direct comparison of plasma stability of the pairs of compounds synthesized using maleimide and acetamide chemistry: HDP 30.2284 *vs.* HDP 30.2515, respectively (Val-Ala-PAB linker) and HDP 30.2301 *vs.* HDP 30.2523, respectively (C_6 stable linker) showed that for maleimide conjugates a gradual decrease in cytotoxic potential progressed with the increasing incubation time in plasma (section 4.1.3). Although, the conjugate HDP 30.2284 was approximately 10 times less potent on LNCaP (PSMA +++) cell line after plasma exposure (IC_{50} of non-exposed conjugate 0.86 nM *vs.* IC_{50} of exposed conjugate approximately 10 nM for both human and mouse plasma exposed compound, sections 4.1.2 and 4.1.3, respectively), activity of HDP 30.2301 did not change or was only approximately 2 times less potent (IC_{50} of non-exposed conjugate 6.1 nM *vs.* IC_{50} conjugate stressed in human plasma 6.3 nM and 14.6 nM for conjugate exposed to mouse plasma) and demonstrated one digit or low two-digit nanomolar IC_{50} up to 6 hours of incubation. These results suggest that possible conjugate inactivation appears quickly after exposure to plasma. This loss of cytotoxic activity after plasma exposure is especially prominent for HDP 30.2284 and progresses gradually with increasing time of incubation. It cannot be excluded that besides retro-Michael reaction which leads to payload deconjugation also other factors may contribute to the observed decrease in activity. For example, also for lower tested *in vitro* concentrations of HDP 30.2515 (Val-Ala-PAB linker, acetamide) a slight decrease

in the cytotoxic potential after prolonged exposure to plasma was observed (*Figure 4.8*, section 4.1.3).

Obtained results of plasma stability confirmed that decrease in the activity of acetamide conjugates after plasma exposure is less prominent compared to maleimide counterparts. Since the progressing decrease in the cytotoxic activity of conjugates which underwent prolonged stressing was observed for the maleimide conjugates, maleimide chemistry was avoided in the synthesis of conjugates with an expected prolonged half-life- particularly DUPA-Fc-α-amanitin conjugate.

For maleimide featuring SMDCs HDP 30.2284 and HDP 30.2301, with demonstrated very short half-lives of approximately or below 1 h extending stability beyond the pharmacokinetic half-life is not likely to have an impact on a drug exposure [104]. Thus, limited plasma stability of HDP 30.2284 and HDP 30.2301 was not considered as limiting factor and these compounds were chosen for the first proof of concept studies *in vivo*.

5.1.2 Compounds bearing disulfide linker

Although the chemically cleavable linkers such a disulfide offer a limited plasma stability the majority of SMDCs which reached clinical development stages bear disulfide linkers. The conjugates bearing disulfide linker such as EC1456 (folic acid - tubulysin B hydrazide) or EC1169 (DUPA - tubulysin B hydrazide) showed promising antitumor activity in pre-clinical *in vivo* studies [76, 115, 116]. In these compounds the targeting moieties folic acid and DUPA were conjugated *via* unprotected disulfide linkers to a hydrophobic payload able to penetrate the tumor even when released outside of the cells e.g. in the tumor microenvironment.

It was assumed that in case of such a hydrophilic toxin as α-amanitin, which does not penetrate cell membrane, a payload release in the tumor microenvironment, outside of the tumor cells would be undesirable and could lead to decreased efficacy and increased systemic toxicity. The optimization of the *in vitro* properties of this family of conjugates was focused on providing optimal balance between plasma stability and intracellular toxin release (section 4.2.1).

An expected limited *in vitro* activity of conjugate bearing unprotected disulfide linker - HDP 30.2246 (0:0) was confirmed in *in vitro* experiment. IC_{50} of HDP 30.2246 (0:0) was determined to be in a high three-digit nanomolar range of concentration similar

to cytotoxic potential of unconjugated α-amanitin in PSMA positive cells (section 4.2.1). Additionally, this already limited cytotoxic potential of HDP 30.2246 (0:0) became even lower with IC_{50} in the micromolar range of concentration after 6 h and longer exposure for either mouse or human plasma. It is due to the lack of stability of unprotected disulfide linker and thiol–disulfide exchange with proteins from fetus bovine serum (FBS), which is a component of the cell culture medium. This result confirms that the toxin release and/or thiol-disulfide exchange occurs rapidly after exposure to plasma proteins. Very low cytotoxic potential of the 30.2246 (0:0) suggest that the reduction of disulfide bond happens even before conjugate reaches the target on the cell surface.

The cytotoxic potential and plasma stability of disulfide bearing conjugates was significantly improved for the conjugates with higher level of steric hindrance, a strategy reported in the field of the ADCs [49]. For DUPA-α-amanitin conjugates the optimal cytotoxic potential was observed for the conjugates with moderate levels of disulfide bond hindrance: HDP 30.2589 (0:1), HDP 30.2618 (1:0) and HDP 30.2619 (1:1) (section 4.2.1). Amongst all tested conjugates the mono-protected disulfide-linker HDP 30.2618 (1:0) displayed an optimal balance between plasma stability and cytotoxic potential *in vitro*. Potential pre-mature release of the toxin outside of the cell was eliminated by introducing hindrance by one methyl group at the DUPA site of disulfide bond of the conjugate. Moreover, the specific toxin release once the conjugate was shuttled *via* PSMA into the glutathione rich intracellular environment was provided, as confirmed by excellent *in vitro* cytotoxic potential of HDP 30.2618 (1:0).

For compound HDP 30.2609 (2:0) with a high level of steric hindrance an additional bulk of two methyl groups at the DUPA site impaired significantly a cytotoxic potential (section 4.2.1). On the other hand, the two methyl groups at the DUPA site should provide additional stability in cell culture medium and plasma which was not observed for HDP 30.2609 (2:0) and was similar to plasma stability profile observed for HDP 30.2246 (0:0) (section 4.2.1). These results indicate that the right balance between plasma stability and accessibility of disulfide bond for reduction upon receptor mediated internalization is required to obtain desired cytotoxicity. The conjugate providing optimal balance between *in vitro* activity and plasma stability HDP 30.2618 (1:0) was chosen for further characterization *in vivo*.

Moreover, particularly for two disulfide linker bearing conjugates HDP 30.2246 (0:0) and HDP 30.2589 there was observed a high activity with IC_{50} in one digit nanomolar range

of concentration in 22RV1 cell line expressing low to moderate levels of PSMA receptor (PSMA +) (IC_{50} = 3.78 nM for HDP 30.2246 (0:0) and IC_{50} = 3.14 nM for HDP 30.2589 (0:1)) (section 4.2.1). Most of the reports regarding DUPA-toxin conjugates utilize the LNCaP cells as a model. In 2015 Roy *et al.* reported an IC_{50} of 11.4 nM for a DUPA conjugated to an indotecan analogue, a topoisomerase inhibitor, in 22RV1 cells line which is surprising since the expression of PSMA in this cell line is considered to be moderate and as demonstrated by FACS staining in not uniform (*Figure 4.1)* [94]. Recently also Lv *et al.* reported three digit nanomolar activity of DUPA-paclitaxel conjugate bearing unprotected disulfide linker [92]. To the best of our knowledge these are the only reports about cytotoxicity of a small molecular DUPA conjugates in 22RV1 cell line. The reason for this rather contradictory result considering non homogenous expression of PSMA in this cell line is still not entirely understood. The conjugates HDP 30.2284 and acetamide analogue HDP 30.2515 for which the intracellular toxin release relied on different mechanism -cathepsin B cleavage demonstrated intermediate activity IC_{50} on 22RV1 cell line, which correlated with the levels of PSMA expression. The fact that a similar result of high cytotoxic potency on 22RV1 cell line were observed for conjugates HDP 30.2594 bearing $(His\text{-}Glu)_2$ motif and DUPA-Fc-α-amanitin supports observed instability in expression of PSMA in 22RV1 cellular model (internal Heidelberg Pharma GmbH).

5.1.3 *In vitro* activity of conjugates aiming to limit the kidney accumulation - HDP 30.2594 and prolongation of pharmacokinetic profile - DUPA-Fc-α-amanitin

Both conjugates HDP 30.2594 and DUPA-Fc-α-amanitin were designed upon *in vivo* testing of HDP 30.2284, HDP 30.2301 and HDP 30.2618 in order to minimize observed abundant kidney accumulation and optimize very short half-life observed all three SMDCs. Although, the main focus in the characterization of HDP 30.2594 and DUPA-Fc-α-amanitin was the determination of *in vivo* properties, the first step undertaken in the pre-clinical evaluation of these molecules was a determination of cytotoxic *in vitro* activity. It was important to understand the impact of a significant molecular changes such as negative charge introduction (HDP 30.2594) or addition of a large and bulky Fc structure (DUPA-Fc-α-amanitin conjugate) on the PSMA recognition, binding and *in vitro* activity.

For the conjugate HDP 30.2594 an excellent activity and selectivity in PSMA positive cells was observed (section 4.3.1). IC_{50} of this conjugated was 5.15 nM which is slightly higher to the activity of most structurally related maleimide bearing analogue - HDP 30.2284

(IC_{50} 0.83 nM) in LNCaP cell line and acetamide analogue HDP 30.2515 (IC_{50} 2.57 nM). The introduction of the negatively charged spacer does not interfere with DUPA entrance *via* the tunnel like shaped structure allowing to reach and recognize the active PSMA site. Despite of commonly known fact that overall negative charge of cancer cells leads rather to the repulsion of negatively charged moieties [117, 118] the opposite is observed for urea based molecules recognizing PSMA. This high receptiveness of PSMA to the negatively charged moieties is reasoned by fact that PSMA catalyzes the cleavage of peptides containing C-terminal glutamates, which are negatively charged in the physiological pH. This particular property of PSMA allows to design negatively charged substrates without impairment of activity, which was also observed for conjugate HDP 30.2594 [119].

DUPA-Fc-α-amanitin conjugate shown the IC_{50} of 15 nM on the LNCaP PSMA positive cell line. This cytotoxic potential is slightly higher compared to previously characterized HDP 30.2284, HDP 30.2301, HDP 30.2618 and HDP 30.2594 (IC_{50} 0.86 nM, 6.11 nM, 4.39 nM and 5.15 nM, respectively). Although, the large structure of the Fc fragment could be a steric hindrance which impairs the recognition and binding of PSMA active site, the conjugate demonstrated high specificity and selectivity towards PSMA positive cells (section 4.3.2). The conjugation of human aglycosylated Fc portion of IgG1 to the DUPA targeting moiety followed by ethylene glycol $(EG_3)_2$ spacer and 8-Aoc-Phe-Phe supporting spacer motif provided sufficient distance and flexibility which allows for a free DUPA entry into the PSMA active site and avoidance of the steric hindrance possibly caused by the bulk of the Fc molecule (*Figure 4.35*).

Despite introduction of significant molecular changes such as negative charge or addition of molecular weight of human aglycosylated Fc fragment (approximately 60 kDa), the DUPA moiety retained the ability to recognize and selectively bind PSMA.

5.1.4 Summary of *in vitro* results

All tested DUPA-α-amanitin conjugates bearing a supporting spacer demonstrated excellent selectivity towards PSMA positive cells with IC_{50} in the low nanomolar range of concentration. The substitution of maleimide chemistry by acetamide conjugation allowed to increase the *in vitro* plasma stability of conjugates bearing Val-Ala-PAB and C_6 non-cleavable linker. For the disulfide linker bearing conjugates, the *in vitro* activity was optimized by introduction of a single methyl group hindering the disulfide bond. The *in vitro* cytotoxic potential of conjugates aiming into the optimization of *in vivo*

biodistribution and pharmacokinetics was maintained despite of significant molecular changes introduced, such as: negative charge for conjugate HDP 30.2594 and implementation of 61 kDa Fc fragment for DUPA-Fc-α-amanitin conjugate.

Table 5.1 Selected from the literature examples demonstrating similar or lower *in vitro* activity of SMDCs compared to unconjugated toxin.

Toxin	IC_{50} of unconjugated toxin	SMDC	IC_{50} of SMDC	Reference
Tubulysin B	0.091-2.3 nM	DUPA-Tubulysin B	3 nM	[77]
Paclitaxel (PTX)	14.24 nM	PTX-SS-DUPA	121.2 nM	[94]
MMAE	0.9 nM	AAZ*-Val-Lys-MMAE (1) and AAZ-ValArg-MMAE (2)	1.6 nM (1) and 2.1 nM (2)	[120]
α-amanitin	347 nM	cyclo[DKP-isoDGR]-PEG-4-Val-Ala-α-amanitin	165 nM	[80]
α-amanitin	Amanitin had no effect on proliferation of all investigated cell lines at internalizing and non-internalizing conditions	pHLIP-α-amanitin**	pHLIP demonstrated 4-5 times higher anti-proliferative potential in at pH 6 (internalizing conditions) compared to pH 7.4 (non-internalizing conditions)	[81]

* AAZ - acetazolamide targeting Carbonic anhydrase IX
** pHLIP - pH Low Insertion Peptide targeting acidic pH of cancer cells

For all characterized compounds DUPA motif followed by supporting 8-Aoc-Phe-Phe spacer conjugated *via* different linkers to α-amanitin, resulted in the conjugates with increased *in vitro* cytotoxicity compared to a non-conjugated α-amanitin (e.g. 320 x improved cytotoxic potential of HDP 30.2284 compared to unconjugated α-amanitin and 18 x improved cytotoxic potential of DUPA-Fc-α-amanitin conjugate compared to unconjugated α-amanitin). The property of significant increase in cytotoxic potential of naked toxin upon conjugation to the targeting molecule was not observed in the field of SMDCs. Majority of conjugates featuring hydrophobic toxins such as tubulysin B, MMAE, or paclitaxel show cytotoxic potential in the concentration range similar or even higher than observed for the corresponding naked toxins (*Table 5.1*) [77, 92, 120]. For example tubulysin B showed an IC_{50} in the range of 0.091-2.3 nM while the DUPA-tubulysin B hydrazine conjugate demonstrated an IC_{50} of 3 nM [77]. α-amanitin in contrast to the majority of currently applied in the development of ADCs and SMDCs toxic payloads is highly hydrophilic. In oppose to e.g. MMAE, DM-1 or tubulysin, α-amanitin cannot passively penetrate cell membrane to yield cytotoxic effect, but once it is conjugated to homing device providing internalization a paramount improvement in cytotoxic potential is reported (e.g. approximately 100 000 fold

increase in cytotoxic potential for antibody-α-amanitin conjugates targeting receptors abundantly expressed on the surface of solid tumors) [103, 121]. Until now, there are available only two literature reports describing α-amanitin targeting to the tumor cells using small molecular homing ligand [80, 81]. One of them is a pHLIP (pH low insertion peptide)-α-amanitin conjugate which targets acidic environment of tumor cell membranes. The cytotoxic potential of pHLIP-α-amanitin was observed to be only 4-5 times higher in the internalization conditions (pH=6) compared to non-internalizing conditions (pH = 7.4) [81]. Also, the second described α-amanitin SMDCs based on a cyclic peptide - DKP-isoDGR targeting integrins overexpressed in numerous cancers demonstrated only 2-3 times better cytotoxic potential for most active conjugates than unconjugated α-amanitin on integrin positive cell lines. Presented in chapter four of this thesis *in vitro* characterization of DUPA-α-amanitin conjugates is a first report in the field of SMDCs demonstrating that conjugation of α-amanitin to small molecular targeting moiety dramatically improves *in vitro* potency of this toxin.

5.2 IMPACT OF THE LINKER STRATEGY ON *IN VIVO* TOLERABILITY OF DUPA-ALPHA-AMANITIN CONJUGATES

One of the main focuses of SMDCs and ADCs development is the improvement of therapeutic window and enabling the usage of anti-proliferative agents which are too toxic to be applied in effective doses in the cancer therapy. This strategy allows to minimize off-target toxicities observed for standard chemotherapeutics. It was demonstrated for a panel of toxins that the conjugation to targeting moieties, particularly to antibodies improved the tolerability to the dose of toxin applied [122]. Also in the field of SMDCs it was shown that the topoisomerase 1 inhibitor - indenoisoquinoline conjugated to DUPA was tolerated at the effective dose which was non-tolerated at the equivalent dose of unconjugated toxin in mouse model [94].

For the preclinical safety evaluation and determination of dose range tested in *in vivo* efficacy study the maximum tolerated (MTD) has to be determined. The MTD is defined as the highest dose of a drug which does not exert unacceptable side effects or overt toxicity in a specific time period. The summary of MTDs findings for all tested *in vivo* DUPA-α-amanitin conjugates are presented in *Table 5. 2*.

Table 5. 2 Maximal tolerated doses of conjugates in Cb 17 Scid mice with indicated corresponding equivalents of α-amanitin dose (n = 3). * Internal Heidelberg Pharma Research GmbH data.

Compound	MTD [mg/kg]	Dose of amanitin [µg/kg]
HDP 30.2284	0.042	18.74
HDP 30.2301	3.84	1800
HDP 30.2618	0.6	600
DUPA-Fc-α-amanitin	1.0	25.7
Unconjugated α-amanitin	-	150*

The tolerability of HDP 30.2284 (Val-Ala-PAB) was approximately 16 times lower than that of the unconjugated α-amanitin (section 4.1.4). Also, DUPA-Fc-α-amanitin conjugate bearing analogous Val-Ala-PAB linker was tolerated at the lower dose level - approximately 6 times lower regarding the dose of α-amanitin compared to the unconjugated toxin (section 4.3.3). For conjugates HDP 30.2301 (C_6 non-cleavable linker) and HDP 30.2618 (disulfide 1:0 monohindered linker) higher tolerability compared to the unconjugated α-amanitin was observed (sections 4.1.4 and 4.2.2). HDP 30.2301 and HDP 30.2618 were tolerated at the dose level 12 times and 4 times higher than unconjugated α-amanitin, respectively. The tolerability of DUPA - α-amanitin conjugates and unconjugated α-amanitin can be ranked as follows: HDP 30.2301 > HDP 30.2618 > α-amanitin > DUPA-Fc-α-amanitin > HDP 30.2284. The results of MTD studies demonstrate that linker strategy dramatically influences tolerability of DUPA-α-amanitin conjugates. Apparently, the tolerability correlates with the expected linker stability.

For tested within this research work DUPA-α-amanitin conjugates higher compared to unconjugated α-amanitin *in vivo* tolerability was observed only for conjugates bearing monohindered disulfide linker HDP 30.2618 (1:0) and C_6 non-cleavable linker HDP 30.2301, but not for the conjugates featuring Val-Ala-PAB cathepsin B cleavable linker HDP 30.2284 and DUPA-Fc-α-amanitin. This uncommon phenomenon of higher toxicity of toxin upon conjugation to targeting molecule was also reported for α-amanitin based ADCs and is well founded by the physicochemical properties of α-amanitin (internal Heidelberg Pharma Research GmbH data). Hydrophilic, unconjugated α-amanitin cannot penetrated cellular membrane but upon conjugation to targeted molecule toxin uses it as a vehicle for penetration into the receptor expressing cells gaining access to its target -

RNA Pol II. This is in contrast to the toxicity of other commonly used hydrophobic cytotoxic payloads, such as MMAE or DM-1 which are able to penetrate cellular membrane and are expected to demonstrate decreased toxicity upon conjugation to a targeting molecule.

Although, the cathepsin B cleavable motifs (Val-Cit, Val-Ala) were designed to release toxin only upon receptor mediated internalization lately it was demonstrated that the ADC targeting MMAE to non-internalizing antigen - carbonic anhydrase IX (CA IX), featuring Val-Ala and Val-Cit linker demonstrated complete anti-tumor responses in xenograft models [123]. This study indisputably confirms that the extracellular cleavage of aforementioned di-peptide motifs appears in mouse models [123, 124]. Latest research identified the carboxylesterase 1C (Ces 1C) as the enzyme responsible for the extracellular hydrolysis of valine-citrulline-paraminocarbamate (Val-Cit-PABC) based linkers in rodent plasma [125]. It is reasonable to assume that this extracellular linker cleavage also applies to HDP 30.2284 and DUPA-Fc-α-amanitin bearing Val-Ala-PAB linker. Since this enzyme is reported to have increased activity in mouse plasma it is possible that some level of premature toxin release happens in the tested mouse model [125]. Despite of this possibility, even if all α-amanitin administered in HDP 30.2284 or DUPA-Fc-α-amanitin form would be released, the tolerability of conjugate should be rather similar to the tolerability of unconjugated α-amanitin, but not lower as observed for HDP 30.2284 and DUPA-Fc-α-amanitin. Thus, it is concluded that not a linker instability is the reason for low tolerability of Val-Ala-PAB bearing conjugates. Despite of observed for DUPA-Fc-α-amanitin conjugate limited kidney accumulation, a similar tolerability to HDP 30.2284 in regard to equivalents of α-amanitin was observed (25.7 µg/kg *vs.* 18.74 µg/kg, respectively) (also discussed further in section 5.3). Based on these observations it is concluded that particularly conjugation of α-amanitin *via* Val-Ala-PAB linker increases significantly the toxicity.

The most reasonable explanation justifying slightly higher tolerability of DUPA-Fc-α-amanitin compared to HDP 30.2284 is limited kidney filtration of this conjugate due to the higher molecular size and FcRn related uptake, which salvages conjugate from the renal clearance. Secondly, the chemical strategy used for the synthesis of both conjugates might have an impact on observed tolerability. DUPA-Fc-α-amanitin conjugate was produced using a click chemistry while in the synthesis of HDP 30.2284 maleimide coupling was employed. Although in the section 4.1.3 it was demonstrated that possible retro-Michael addition between maleimide coupled α-amanitin present in HDP 30.2284 and plasma proteins would

not hamper the cytotoxic potential of this molecule, it is not excluded that products of possible maleimide exchange may contribute to the observed toxicity. The hypothesis that observed toxicity might be partially related to possible adducts with plasma components - particularly plasma albumin is supported by studies which demonstrated increased kidney toxicity of α-amanitin in rat while administered as a human serum albumin conjugate [126].

Both conjugates- monohindered disulfide bearing HDP 30.2618 (0:1) and HDP 30.2301 (C_6 non-cleavable linker) showed higher tolerability compared to conjugates bearing Val-Ala cleavable linkers and better tolerability than unconjugated α-amanitin. Although, conjugates bearing stable linker are characterized by better tolerability than conjugates bearing cleavable linker, the reported differences in the field of ADCs are only in the range of approximately three folds [127]. For DUPA-α-amanitin SMDCs the difference in the tolerability of conjugate with cleavable and non-cleavable linker is approximately 190 folds. Considering that all SMDCs bear the same targeting moiety, it is concluded that for DUPA-α-amanitin conjugates the linker strategy has a dramatic impact on the tolerability. It seems to be not related to the serum stability, but rather to the activity of released toxin and/or possible metabolites. There is an additional myriad of factors in *in vivo* system which can potentially contribute to observed toxicity and it is not clear whether observed toxicity is related to the whole conjugate, possible metabolites or adducts with plasma components (also discussed further in section 5.3). Additional studies aiming into identification of possible primary and secondary pharmacodynamic effects in kidney, identification of metabolites and plasma adducts, particularly the ones accumulated/produced in the kidney should be carried out in order to clarify the mechanism underlying toxicity.

5.3 BIODISTRIBUTION OF DUPA-ALPHA-AMANITIN CONJUGATES

A full biodistribution study after single dose administration in Cb 17 Scid LNCaP xenografts was carried out for the following conjugates: HDP 30.2284 (Val-Ala-PAB linker), HDP 30.2301 (C_6 non-cleavable linker) and DUPA-Fc-α-amanitin (Val-Ala-PAB linker) (sections 4.3.3.2 and 4.7.1, respectively).

In biodistribution studies HDP 30.2284 and HDP 30.2301 were administered at different dose levels: 0.184 mg/kg (4xMTD) and 1.28 mg/kg (1xMTD), respectively due to differences in the tolerability. HDP 30.2284 was not accumulated in the liver while and HDP 30.2301 was still present in liver at the concentration of ca. 0.5 μg/g of tissue even 48 h following

administration. α-amanitin is known to be taken up *via* OATP1B3 transporter localized in the sinusoidal membrane of the hepatocytes [62]. Although the murine liver does not express the OATP1B3 it expresses the oatp1b2 which is an ortholog of the human OATP1B3. Both proteins show 80 % homology according to the UniProt database and α-amanitin was reported to be toxic to murine liver constituting a relevance of the murine model in hepatotoxicity studies [61]. Lower HDP 30.2884 and HDP 30.2301 uptake *via* OATP1B3 was confirmed in *in vitro* assay on HEK293 WT cells and HEK293 cells stably expressing OATP1B3 human transporter (section 6 Appendices and Supplementary Figures). In this experiment unconjugated α-amanitin showed nanomolar activity in HEK293 OATP 1B3 cell line and approximately 94-fold lower cytotoxic potency in HEK293 WT cell line (Section 6, *Supplementary figure 2*), constituting the suitability of this *in vitro* model to predict OATP1B3 mediated uptake of α-amanitin and α-amanitin derivatives. HDP 30.2284 and HDP 30.2301 showed 10.8-fold and 34.02-fold lower cytotoxic potential on HEK293 OATP 1B3 than unconjugated α-amanitin, respectively (Section 6, *Supplementary figure 2*), what suggests that conjugation of DUPA to α-amanitin limits OATP1B3 mediated uptake of the toxin. Despite of lower toxicity of conjugates compared to unconjugated α-amanitin in *in vivo* studies dose dependent liver accumulation was observed after single administration of HDP 30.2284 and HDP 30.2301 (section 4.1.7). Peak liver concentration of 51 ng/g was determined 1 h after administration of 0.182 mg/kg HDP 30.2284 and was decreasing as the elimination of conjugate from the systemic circulation was progressing. Peak liver concentration of 3206 ng/g was observed immediately upon administration of HDP 30.2301 (1.28 mg/kg) and similar as for HDP 30.2284 was decreasing with progressing elimination of the conjugate from systemic circulation. Considering that compounds containing α-amanitin core in the structure were detectable at the low concentration in liver for both conjugates even after elimination from the systemic circulation, and that for HDP 30.2301 administered at the higher dose higher liver concentrations were determined it is concluded that for DUPA-α-amanitin SMDCs HDP 30.2284 and HDP 30.2301 dose dependent and OATP1B3 mediated liver accumulation appears.

For both conjugates HDP 30.2284 and HDP 30.2301 accumulation in the tumor was observed. Although, for time points ≥ 8h the conjugates were completely eliminated from the systemic circulation, they were still detectable in the tumor what is the evidence of specific accumulation in the PSMA expressing tissues. Both conjugates were detectable in the tumor for up to 48 h. 48 h after administration of 1.28 mg/kg (1x MTD) HDP 30.2301

tumor concentration level was determined for approximately 523 ng/g and HDP 30.2284 was detected at the concentration level of approximately 13.55 ng/g after administration of 0.184 mg/kg (4 x MTD). For conjugate HDP 30.2301 it was expected that in the following efficacy study with an administration frequency 3 times per week the accumulation of toxin in the tumor will appear, potentially enhancing its antitumor effect (section 4.1.7). In contrast for HDP 30.2284 the dose of conjugate in the efficacy experiment was ca. 8-fold lower compared to biodistribution study. Thus, expected concentration levels in the tumors from efficacy study with HDP 30.2284 were even lower that those determined in the biodistribution study. This expected low tumor concentration could potentially limit the efficacy of the therapy with HDP 30.2284 (sections 4.1.6 and 4.1.7).

Despite of the fact that higher antitumor activity of HDP 30.2301 was expected due to higher tolerability, higher dose administered and higher concentration determined in the tumor compared to conjugate HDP 30.2284, the anti-tumor activity of HDP 30.2301 came out to be lower than anti-tumor activity of HDP 30.2284 (Section 4.1.6). Considering high cytotoxic potential of HDP 30.2301 *in vitro* (IC_{50} = 6 nM) it was unexpected (Section 4.1.6). Higher activity of HDP 30.2284 compared to HDP 30.2301 seems to be related to higher *in vivo* activity of free α-amanitin released from conjugate HDP 30.2284 compared to the activity of whole HDP 30.2301 or HDP 30.2301 related metabolite released inside of the tumor cells. This result re-emphasis the lack of predictivity of *in vitro* models and points out the relevance of *in vivo* studies in translational research.

High levels of compounds presenting α-amanitin core in the structure were detected in the kidneys of animals treated with both HDP 30.2284 and HDP 30.2301. Structures presenting α-amanitin core were present in this organ for at least 48 h upon administration. Surprisingly, the kidney accumulation only partially was dependent on the linker strategy. This was shown in the comparative kidney accumulation study where both conjugates HDP 30.2284 and HDP 30.2301 were administered at equivalent doses corresponding to the same amount of α-amanitin (section 4.1.8). For the same dose levels approximately 30 % higher kidney concentrations of toxin were measured in the organs of animals' dosed with HDP 30.2284 compared to organs of animals administered with the HDP 30.2301, what may suggest that kidney accumulation only to some limited extend may be related to the linker strategy (section 4.1.4).

Similar to observed results for DUPA-α-amanitin SMDCs the kidney accumulation of DUPA - based radio-therapeutics for prostate radiation therapy is reported in the literature [128]. The renal uptake of DUPA based radio-imaging agents and radio-therapeutics is claimed to be related mainly to the PSMA expression in the proximal tubule of murine and human kidney. The murine and human PSMA share ca. 90 % of homology (Uniprot database) and DUPA was shown to be accumulated in both human and mouse kidney [105]. It is worth to point out that level of PSMA expression in human kidney is reported to be around 2 fold lower than in the murine kidney thus, it can be assumed that the kidney accumulation and toxicity in humans would be lower than the accumulation observed in mice [105]. In the literature the pre-injection with 2-PMPA - DUPA competitive inhibitor before administration of DUPA based radio-imaging agent was reported to increase the contrast between the radio-imaging signals recorded from prostate and kidney allowing for more distinct diagnosis PCa. In these experiments the kidney accumulation was not completely eliminated [105, 129]. In the presented herein study pre- and co-injections of the DUPA competitive inhibitor - 2-PMPA with HDP 30.2284 and HDP 30.2301 was tested in order to verify, whether the kidney uptake of DUPA-α-amanitin conjugates is also PSMA mediated. For the conjugate HDP 30.2284 only a minimal, approximately 10 % decrease in the kidney uptake was observed in pre- and co-injection with 2-PMPA (section 4.1.8). This result indicates that for this particular conjugate the kidney accumulation is primarily non-PSMA mediated. In contrast approximately 50 % decrease in kidney uptake was observed for HDP 30.2301. Hence, for this conjugate the kidney uptake is partially PSMA mediated, however similar as for HDP 30.2284 it is not the only mechanism responsible for the renal uptake. Combining the results obtained in the tolerability and biodistribution study in pre and co-injection with 2-PMPA it seems that the linker strategy has limited impact on the level of renal accumulation, but it possibly influences the mechanism of kidney uptake and subsequently has a dramatic impact on the toxicity and tolerability of different conjugates and/or conjugate related metabolites. Although, the unconjugated amatoxins were shown to be primarily transported into parenchymal hepatocytes *via* OATP1B3 and cause hepatotoxicity, the kidney damage was also reported [61]. It was demonstrated that complexes of α-amanitin with anti-amanitin antibody, Fab fragment or covalent conjugate of α-amanitin and human serum albumin (HSA) show toxicity in the structures involved in the protein turnover. This includes macrophages, sinusoidal cells of the liver and protein absorbing cells in proximal tubules of the kidney [61, 126]. Assuming that the both conjugates: HDP 30.2284 and HDP 30.2301 have a slightly more hydrophobic structure when

compared with unconjugated α-amanitin, it is likely that a hydrophobic-hydrophobic interaction with serum albumin appears. Since the HSA-α-amanitin conjugate was reported to cause nephrotoxicity, it is conceivable that the pool of conjugate bound to serum albumin is taken up as a protein complex in the kidney and causes nephrotoxicity as reported for HSA-α-amanitin covalent conjugate [61, 126].

In literature the introduction of a negatively charged spacer into the linker structure of DUPA based radio-imaging agents was shown to improve the contrast of PCa imaging and lower the kidney uptake. Contrary to this hypothesis reasoning the synthesis of HDP 30.2594 bearing a $(His\text{-}Glu)_2$ spacer to limit the kidney accumulation, this compound demonstrated accumulation similar to HDP 30.2284 (section 4.3.1) [108, 119]. Although for HDP 30.2284 lacking $(His\text{-}Glu)_2$ the kidney accumulation was demonstrated to be mainly non-PSMA related, it cannot be excluded that in case of HDP 30.2594 PSMA receptor mediated uptake in proximal tubules of the kidney contributes to the overall accumulation to higher extend. It would be interesting to verify what is the *in vivo* tolerability of HDP 30.2594. Comparison of *in vivo* toxicity of HDP 30.2284, DUPA-Fc-α-amanitin and HDP 30.2594 with only the first conjugate being synthesized using maleimide chemistry would allow to elucidate whether maleimide coupling contributes to observed toxicity.

Taken together the kidney was identified as the organ of toxicity for small molecular DUPA-α-amanitin conjugates. The results of this study and literature reports suggest that the conjugation of natural α-amanitin to targeting molecules may lead to increased renal uptake and toxicity. It is not clearly understood whether this is related to plasma proteins binding and/or maleimide exchange and consequent kidney related protein turnover or possible direct PSMA mediated uptake. It seems that for different conjugates different mechanisms of uptake may play a role. Most probably kidney accumulation is a combination of several mechanisms contributing in case of HDP 30.2284 and HDP 30.2301 to the observed toxicity. It was demonstrated that PSMA uptake is valid for one of the conjugates bearing a non-cleavable linker, but minimally contributes to the overall uptake the conjugate featuring a cleavable linker (section 4.1.8). For complete elucidation of the mechanisms underlying the kidney accumulation and toxicity, a serum proteins binding studies and an identification of transporters responsible for kidney uptake should be performed. Moreover, the pathological examination of the murine kidneys upon conjugate administration could explain in which part of the nephron possible damage appears, what in turn could facilitate the identification of the toxicity mechanism. So far, the mechanism of DUPA-α-amanitin

SMDCs toxicity could be only partially understood and requires further investigation for each of the conjugates individually.

More detailed study, enabling the differentiation between the conjugate loaded with the toxin and free toxin was applied in the biodistribution study of DUPA-Fc-α-amanitin conjugate. Attachment of Fc conjugated DUPA targeting moiety to α-amanitin had as expected a major impact on the blood pharmacokinetic profile of the conjugate. Tremendous prolongation of the half-life compared to SMDCs was observed (approximately 1 h for SMDCs *vs.* approximately 7.2 days for β-elimination phase of DUPA-Fc-α-amanitin). In contrast to the SMDCs where higher kidney concentration of the toxin was detected compared to the liver, in the biodistribution study DUPA-Fc-α-amanitin the liver concentration was slightly higher than this observed in the kidney, but no significant liver accumulation was observed. Lower liver accumulation might be explained by fact that the aglycosylated antibodies are not accumulated in the liver since liver uptake is mediated mainly *via* mannose receptor [130].

Conjugation of DUPA and α-amanitin to Fc fragment allowed to avoid abundant kidney accumulation. It is most probable that the conjugation of DUPA to Fc moiety at least to some extend decreased the kidney filtration and in consequence has led to limited PSMA mediated re-absorption or conjugate from the pre-urine. Considering that molecular weight of DUPA-Fc-α-amanitin conjugate (63 kDa) is on the boarder of renal filtration cut-off (50-70 kDa) the kidney clearance probably still appears but the distribution of conjugate into the second compartment *via* FcRn salvages the conjugate from renal filtration. Remarkably lower accumulation of α-amanitin related structures in the kidney was observed for Fc fusion compared to small molecular counterpart HDP 30.2284. Despite of this limited kidney accumulation of DUPA-Fc-α-amanitin conjugate a similar tolerability to HDP 30.2284 regarding the equivalents of α-amanitin was observed (25.7 µg/kg *vs.* 18.74 µg/kg, respectively). This result suggests that toxicity of DUPA-α-amanitin conjugates is rather related to the Val-Ala-PAB linker strategy.

Importantly for DUPA-Fc-α-amanitin conjugate a tumor concentration of the free toxin was gradually increasing to achieve the maximum 3 days upon administration with the peak concentration of approximately 55 ng/g. This result constitutes the pharmacokinetic profile of α-amanitin based ADCs, where in the solid tumors there was detected no intact conjugate but only a free toxin what confirms the efficient release of the toxic payload specifically

in the tumor tissue (internal Heidelberg Pharma Research data). Lack or relatively low levels of free toxin in blood, just above the lower limit of quantification confirms the stability of this molecule *in vivo*.

5.4 IMPACT OF LINKER STRATEGY AND PHARMACOKINETIC PROFILE ON *IN VIVO* EFFICACY

As already discussed in the previous section the linker strategy had a major impact on the tolerability of tested within this project SMDCs. Despite of different linker strategies used in the production of DUPA-α-amanitin SMDCs the plasma half-lives of all three small molecule-α-amanitin conjugates HDP 30.2284 (Val-Ala-PAB), HDP 30.2301 (C_6 non-cleavable linker) and HDP 30.2618 (1:0 disulfide linker), ranged between 36-72 min. (section 4.1.5 and 4.2.3). As expected, all three SMDCs undergo very rapid renal clearance and no detectable levels of conjugates and related metabolites were present 8 - 48 h in the serum after administration in the mice. Also, conjugate HDP 30.2594 $(His\text{-}Glu)_2$ bearing negative charge demonstrated short (< 1h, section 4.3.1.2) half-life what re-emphases that neither linker strategy nor a charge of the molecule has an impact on the blood pharmacokinetic profile of SMDCs. It cannot be excluded that observed slightly longer half-life of HDP 30.2301 and HDP 30.2618 compared to HDP 30.2284 is an effect of the dose dependent pharmacokinetics of DUPA-α-amanitin conjugates [131]. At low plasma concentrations the clearance will be maximal and for some small molecular drugs it may be as high as the effective renal flow of plasma [132]. Elimination of exceptionally high doses is limited by renal filtration and longer elimination observed for conjugates administered in higher doses which might be seen as dose dependent pharmacokinetics. To completely elucidate whether observed slightly longer half-live of conjugates HDP 30.2301 and HDP 30.2618 is related to dose-dependent pharmacokinetics a blood pharmacokinetic study after single dose administration of different dose levels of these conjugates and comparison of obtained exposures and half-lives should be performed.

Another possibility of shorter half-live determined for HDP 30.2284 is a limitation of the lower limit of quantification of the method used in pharmacokinetic studies which for presented herein anti-α-amanitin ELISA was approximately 1-2 nM. Normally in the more advanced nonclinical programs the sensitivity of method would be higher to enable the detection of the drug at the picomolar range of concentration. Despite of certain limitations related to the method used for the determination of half-life or probability

of dose-dependent pharmacokinetics the half-live of all DUPA-α-amanitin SMDCs is similar to other small molecular chemotherapeutics used in the therapy of PCa such as e.g. paclitaxel demonstrating the half-life of 69 min. [133] or cabazitaxel with the α-phase half-life of 4 min. and the β-phase half-life of approximately 2 h [134].

Despite of the very low dose of HDP 30.2284 administered in the efficacy study, the anti-tumor activity of this compound was better than this observed for HDP 30.2618 or HDP 30.2301 (sections 4.1.6 and 4.2.4.). This result was surprising considering the great differences in the equivalents of toxin administered. A better efficacy was observed for the therapy with HDP 30.2284 compared to HDP 30.2301 even though the administered dose of HDP 30.2301 was 120-fold higher compared to HDP 30.2284 and the duration of the treatment with HDP 30.2301 was longer (5 *vs.* 3 weeks) (section 4.1.6). This result is in line with the higher *in vivo* activity of conjugates bearing a cleavable linker which was reported for anti PSMA α-amanitin based ADCs [113].

A small difference observed in anti-tumor activity favoring HDP 30.2284 compared to HDP 30.2301 and a large difference in the administered dose of toxin equivalents, indicates that the linker strategy has a major impact on the anti-tumor activity of DUPA-α-amanitin conjugates. Unfortunately, both conjugates showed only a limited anti-tumor activity at the tolerated dose levels. Considering the results obtained for HDP 30.2284 and HDP 30.2301, the increase of the administered dose did not compensate for the short half-life and did not improve *in vivo* efficacy. Moreover, it can be concluded that the main factor limiting efficacy for HDP 30.2284 besides of its short half-life, is the dose limiting toxicity (DLT) and consequently insufficient toxin delivery to the tumor at the tolerated dose-level to yield durable antitumor effect.

The results in the second PSMA positive xenograft model (C4_2) corroborate the hypothesis that the linker strategy influences the activity of the conjugates (section 4.1.6). The efficacy of HDP 30.2284 was slightly better than that of HDP 30.2301 in C4_2 xenografts. Moreover, comparison of the results obtained in two tumor models: LNCaP and C4_2 confirmed that the limited *in vivo* efficacy can be attributed to the functional properties of the compounds and is not caused by architectural tumor model properties such as stiffness of the tumor tissue or vascularization [135]. The results of very low anti-tumor activity of HDP 30.2301 were to some extend expected since it is commonly observed that compounds with exaggeratedly high tolerability often do not demonstrate anti-tumor activity.

Initially obtained efficacy results for conjugates HDP 30.2284 and HDP 30.2301 prompted the development of conjugate bearing disulfide linker. Successful disulfide linker optimization was supported by *in vitro* results which demonstrated that the conjugate: 1) provides high, one-digit nanomlar activity in PSMA positive cells and 2) ensures plasma stability (discussed in section 5.1.2).

Independent *in vivo* efficacy study was performed with the optimized mono-protected disulfide linker bearing conjugate HDP 30.2618 (1:0). The major reasoning for the development of this compound was the optimization of *in vivo* properties which were sub-optimal for previously characterized molecules: dose limiting toxicity (observed for HDP 30.2284) and low *in vivo* activity due to lack of toxin release (observed for HDP 30.2301).

HDP 30.2618 allowed to achieve intermediate tolerability, which was higher than for HDP 30.2284 but lower than for HDP 30.2301. Despite of significant improvements of *in vitro* activity this conjugate also demonstrated limited efficacy in LNCaP xenografts. The ability of HDP 30.2618 to release the payload in the intracellular environment and possibility of higher dose administration related to higher tolerability compared to HDP 30.2284 did not allow to obtain improved *in vivo* efficacy and similar antitumor activity was observed as for the conjugate HDP 30.2284 (section 4.2.4).

In general, all small molecular drug conjugates HDP 30.2284, HDP 30.2301 and HDP 30.2618 showed limited anti-tumor activity *in vivo*. Linker strategy has a major impact on the tolerability of small molecular DUPA-α-amanitin conjugates and it seems to have an impact on the anti-tumor activity. Although, HDP 30.2284 demonstrated a dose limiting toxicity and required a low doses in the efficacy study, it demonstrated slightly better efficacy than two remaining SMDCs HDP 30.2618 and HDP 30.2301. It is reasonable to conclude that administration of higher doses of HDP 30.2284 - equivalent to HDP 30.2301 or HDP 30.2618 would lead to better anti-tumor response. Presented results suggests that another factor limiting *in vivo* activity besides of the short half-life for conjugates HDP 30.2301 and HDP 30.2618 is lower activity of α-amanitin derivatives released from these conjugates inside of the tumor cells. Although HDP 30.2284 upon intracellular cleavage leads to release of native α-amanitin, the efficacy of this compound is limited by DLT. Due to short half-life and low plasma concentration the majority of compound is eliminated *via* kidney filtration very quickly, before it is able to make a contact with the tumor what results

in a very low exposure. Released from HDP 30.2284 toxin is delivered to the tumor in the amount not sufficient to yield the durable anti-tumor activity.

For the conjugate HDP 30.2301 despite of higher tumor delivery only a very limited anti-tumor effect was observed. Although no detailed biodistribution study was carried out for the conjugate HDP 30.2618, based on the studies of tumor accumulation of compounds: HDP 30.2284 and HDP 30.2301 it is proved that the tumor toxin concentration depends on the administered dose of the conjugate and is not related to the linker strategy. Thus, it is reasonable to speculate that higher concentration of HDP 30.2618 or related α-amanitin metabolites would be detected in the tumors of the animals injected with 1/2 of MTD HDP 30.2618 (0.6 mg/kg) than with 1/2 MTD of HDP 30.2284 (0.023 mg/kg)(doses used in the efficacy experiment). Despite of higher expected HDP 30.2618 tumor accumulation it still yields similar anti-tumor response as HDP 30.2284, what favors the theory that the highest *in vivo* anti-tumor activity is observed for native form of α-amanitin released from self immolative cathepsin B cleaved Val-Ala-PAB linker.

As the next step a DUPA-Fc-α-amanitin conjugate was developed in order to improve the pharmacokinetic profile of the conjugate and confirm whether the prolongation of the half-life may be one of the major factors limiting *in vivo* efficacy. For the development of DUPA-Fc-α-amanitin conjugate Val-Ala-PAB self-immolative linker was employed since for SMDCs release of free α-amanitin led to the best anti-tumor responses in *vivo*. Conjugation of the DUPA targeting moiety and toxin to the engineered aglycosylated Fc portion of human IgG1 provides FcRn recycling responsible for prolonged half-life of the IgG1 class of immunoglobulins. The reason behind the use of aglycosylated portion of human IgG1 was to facilitated mass spectrometry characterization of the final DUPA-Fc-α-amanitin conjugate and lower liver accumulation of aglycosylated IgGs [130]. Importantly the aglycosylation of IgG was demonstrated to have no impact on the FcRn binding and subsequent half-life of the molecule [136].

The FcRn receptor is localized mainly intracellularly and binds immunoglobulins in acidic pH ≤ 6.5 but not at neutral pH 7.4 [137]. FcRn is expressed by a variety of species in a wide panel of parenchymal cell such as: intestinal enterocytes, vascular endothelium, hepatocytes, proximal tubular cells [138]. Fc-FcRn interaction appears in intracellular compartments with acidic pH upon non-specific uptake route - pinocytosis of IgG. An FcRn bound Fc complex is directed to recycling endosome, which subsequently is directed to the cellular membrane

(*Figure 4.30*). The Fc portion containing molecule is released into the extracellular environment due to the increase in pH, which loosens the pH depended interaction between FcRn and Fc. This mechanism is responsible for rescue of IgG molecules from digestion in the lysosome and prolongation of the circulatory half-life. Importantly, the murine FcRn has been shown to recognize human Fc portion of IgG with similar or even higher affinity that human FcRn constituting the relevance of murine model in initial pharmacokinetic studies [139].

The results of the pharmacokinetic study of DUPA-Fc-α-amanitin conjugates demonstrated prolonged half-life with a biphasic elimination profile typical for the molecules presenting Fc portion in the structure (section 4.3.3.1)[140]. Although the half-life was significantly longer compared to the small-molecular DUPA-α-amanitin conjugates (7.2 days *vs.* approximately 1 h, respectively), it was shorter compared to the full format IgG1 molecule (approximately 3 weeks)[140]. This might be explained by the fact that the molecular weight of DUPA-Fc-α-amanitin (ca. 63 kDa) is on the border of molecular weight cut-off for renal clearance of proteins (50-70 kDa) and the conjugate probably still partially undergoes the renal filtration [111].

The anti-tumor effect of DUPA-Fc-α-amanitin conjugate observed in efficacy study was clearly dose and administration frequency depended (section 4.3.3.3). The DUPA-Fc-α-amanitin showed 100 % tumor response in the study groups treated with 1 mg/kg once per week and 0.5 mg/kg twice per week for the subsequent three weeks. The complete tumor response in these two groups was sustained until day 14 after termination of the treatment. In general despite of the relatively low dose of the toxin administered in the DUPA-Fc-α-amanitin form (1 mg/kg of conjugate correspond to 25.7 µg/kg of α-amanitin) the prolonged exposure and gradual delivery of the toxin to the tumor came out to be optimal and yielded complete tumor response. Although 2 weeks after last administration of DUPA-Fc-α-amanitin conjugate the tumors started to re-grow the efficacy of the Fc conjugate was dramatically improved compared to small molecular counterparts (section 4.3.3.3).

The main objective of developing Fc motif bearing molecules is improving their pharmacokinetic properties by enabling interaction between Fc part and FcRn receptor which leads to prolongation of the half-lifetime [141]. Up to the moment there are described molecules obtained by means of genetic engineering being fusions of human IgGs or Fc potions to interleukines or receptor of human cytokines [142-144]. There are also described semi-enzymatic or chemical routes of conjugation of the small targeted molecules to the Fc

portions of IgGs [145]. However, up to the moment the concept of grafting both toxin and small molecular targeting moiety onto the same Fc scaffold was not described. This is the first report proposing the chemical grafting of a small targeting molecule onto Fc portion of human IgG and subsequent conjugation to the cytotoxic payload. This innovative platform gives a future possibility to bring together the other combinations of SMDCs demonstrating sub-optimal pharmacokinetic properties *in vivo*.

5.5 CONCLUSIONS AND FURTHER STRATEGIES FOR DUPA-ALPHA-AMANITIN CONJUGATES OPTIMIZATION

Comparison of the results obtained for the small molecular DUPA-α-amanitin conjugate and DUPA-Fc-α-amanitin clearly shows that for a hydrophilic payload such as α-amanitin the prolonged half-life time is essential for obtaining sustainable tumor growth inhibition. Presented study proved that a gradual delivery of α-amanitin to the tumor over time is essential for yielding sustainable anti-tumor activity *in vivo*. Moreover, grafting toxin onto Fc portion of human IgG allowed to limit kidney accumulation and optimize a therapeutic window of DUPA-α-amanitin conjugates, which was sub-optimal for small molecular counterparts.

Despite of numerous reports about beneficial usage of non-protected disulfide linker commonly applied in the development of small molecule-toxin conjugates with highly hydrophobic payloads, this kind of linker came out to be not suitable for DUPA-α-amanitin conjugates. Commonly used in the development of SMDCs and ADCs toxins can passively penetrate cellular membrane, what suggests an additional *in vivo* benefit from the lack of linker stability and its cleavage outside of the cells e.g. in the glutathione rich tumor stroma. This theory is strengthened by the fact that for more hydrophilic auristatin derivative conjugate, like MMAF based ADC, an anti-tumor effect for non-internalizing target was not observed, while it was observed for conjugates with more hydrophobic MMAE [146]. Moreover for the MMAE based conjugates, significant anti-tumor effect was observed not only for targeted-MMAE ADCs, but also for non-targeted control ADCs which is clearly related to extracellular toxin release [147]. Altogether, these results suggest that beneficial antitumor effect for ADCs and especially SMDCs based on hydrophobic toxins might be partially related to the unspecific toxin release in the blood stream or tumor microenvironment and passive free toxin penetration into the tumor cells. On the other hand, these properties create the risk of increased off target toxicities. Strategies based

on the development of linkers unstable in mouse or human plasma are not suitable for targeted tumor delivery of such a hydrophilic payload as α-amanitin, which uses targeted receptor as a unique way to be shuttled into the tumor cell. Ultimately the pharmacokinetic profile presented by antibodies providing constant delivery of toxin to tumor over time seems to be optimal for the development of α-amanitin based therapeutics targeting toxin to solid tumors.

Reports published by Benešová *et al.* demonstrated that linker structure fitting into the PSMA tunnel like shaped structure has a versatile impact on properties such as receptor targeting, internalization and even level of PSMA targeting small molecules accumulation in the kidney [90]. For the purpose of this study only one supporting spacer 8-Aoc-Phe-Phe reported by Kularatne *et al.* was tested [77]. One of the ideas for possible explanation of DUPA-α-amanitin SMDCs kidney accumulation, would be the synthesis and comparative head-to head testing *in vitro* and *in vivo* of Val-Ala-PAB bearing conjugates with different supporting spacers. It would be interesting to verify whether employing a different supporting spacers, particularly with naphthyl-alanine and cyclohexane arrangement - analogous to structure presented in radioimaging compound - DKFZ-PSMA-617 would allow to limit the α-amanitin accumulation in the kidney (section 1.4.2) [90]. This could also further contribute to the overall understanding of the kidney uptake and toxicity mechanism.

Probably the most important step in further development and optimization of Fc based conjugates would be the determination of *in vivo* toxicity and efficacy of DUPA-Fc-α-amanitin conjugates bearing linkers analogous to tested SMDCs: mono-protected disulfide and C_6 - non-cleavable linker. The results of this comparative study of Fc fusions bearing different linkers would 1) allow to better understand whether the main factor influencing tolerability is indeed the linker strategy and 2) verify whether linker strategy impacts the efficacy even when conjugate presents prolonged half-life.

In order to further understand the mechanism underlying the toxicity a panel of receptors expressed in the kidney should be screened in order to better understand observed for SMDCs possible secondary pharmacodynamics. Lately it was reported that important receptors responsible for the majority of protein and peptide-like structures re-absorption in the proximal tubule of the kidney is a megalin and cubilin which rescue a great number of filtered ligands, including biomarkers, albumin, essential vitamins, and hormones [148, 149]. Taking into consideration that the kidney uptake

of DUPA-α-amanitin SMDCs is not clearly understood and it seems to be related to more than one mechanism it would be interesting to test tolerability and kidney accumulation of DUPA-α-amanitin SMDCs in megalin/cubilin knock-out animals. In case if SMDCs uptake would be megalin and/or cubilin mediated the blocking of this receptors by specific peptides as a pre-injection could be considered as a kidney protection strategy and possibly lead to increased tolerability of DUPA-α-amanitin SMDCs [150, 151].

Additionally, since the limited tolerability of conjugates bearing Val-Ala-PAB linker might be not only related to kidney toxicity it would be interesting to perform patophysiological analysis of different organs, especially liver.

Within the scope of this work the *in vitro* and *in vivo* properties of different DUPA-α-amanitin conjugates were evaluated. Tuning pharmacokinetic properties of DUPA-α-amanitin conjugates allowed to change the *in vivo* activity from limited efficacy observed only during time of treatment to complete tumor remission sustained after termination of the therapy. Ultimately it would be important to validate proposed platform for different small molecular tumor homing ligands such as: octreotide [152], folic acid targeting folate receptor [153] or acetazolamide based small molecules targeting carbonic anhydrase IX overexpressed in renal cell carcinoma [154, 155] combined with validated for development of ADCs and SMDCs toxins e.g. tubulysin B, MMAE, MMAF, DM-1 or PBDs.

The proof of concept *in vitro* and *in vivo* studies validated DUPA-Fc-α-amanitin platform utility in the therapy of PSMA positive prostate cancer. Within a size approximately 60 % smaller of that of a conventional ADC, proposed platform expands the landscape of currently available tumor targeting small formats alternative to full IgG. Further studies of described herein Fc platform for optimization of pharmacokinetic properties of α-amanitin based SMDCs are warranted.

6. SUMMARY

In the recent years small molecule drug conjugates (SMDCs) and antibody drug conjugates (ADC) have emerged as potent anticancer therapeutics. Targeting of toxins to the tumor cells using small molecule tumor homing motifs presents a potential alternative to huge molecular weight ADCs. Benefits of SMDCs over ADCs are e.g. decreased toxicity due to lower accumulation and shorter half-lifetime of SMDCs compared to ADCs.

A-amanitin presents completely novel mode of action in the field of targeted therapeutics, namely inhibition of eukaryotic RNA Pol II. This novel mode of action in distinct from majority of ADCs or SMDCs in the development which use microtubule inhibitors, DNA alkylators and crosslinkers as payloads. Physicochemical properties of α-amanitin, namely very good solubility in water and consequent inability to penetrate the cellular membrane make this payload interesting from the safety perspective. α-amanitin based ADC are already described in the literature and are heading towards clinical development. In contrast the information about the application of this payload in the SMDCs development are scarce. Within this work the novel α-amanitin targeted SMDCs based on well know DUPA motif having high affinity to PSMA receptor bearing different linkers were developed, characterized and optimized. Here for the first time the question whether small molecule might be applied in the targeted tumor delivery of such a hydrophilic payload as α-amanitin an whether this kind of molecule demonstrates *in vivo* activity was challenged.

In the Chapter 4.1 of presented work the structure activity relationship of DUPA-based α- amanitin conjugates bearing Val-Ala cleavable linker and C_6-stable linker was researched. First, the necessity for the implementation of supporting spacer (8-Aoc-Phe-Phe) motif between DUPA-targeting motif and bulky structure of α-amanitin was demonstrated. It was done by determination of cytotoxic potential of the pairs of conjugates bearing cleavable and stable linker *in vitro* in PSMA positive cell lines LNCaP and 22RV1 and PSMA negative PC3 cell line. Conjugates featuring supporting spacer showed IC_{50} values in the nanomolar range of concentration (HDP 30.2284 bearing Val-Ala cleavable linker IC_{50} 0.86 nM and HDP 30.2301 bearing C6-non-cleavable linker IC_{50} 6.1 nM) while conjugates lacking the supporting spacer were active only in high three-digit nanomolar range of concentration (HDP 30.1595 bearing Val-Ala cleavable linker and HDP 30.1585 bearing C_6-non-cleavable linker both IC_{50} in micromolar range of concentration). Moreover, these first *in vitro* experiment the high selectivity of DUPA-α-amanitin conjugates only

towards PSMA positive cells was observed (IC_{50} 0.89 nM on PSMA expressing cell line LNCaP cell line *vs.* on PSMA negative PC3 cell line). Two best performing *in vitro* conjugates HDP 30.2284 (Val-Ala cleavable linker) and HDP 30.2301 (C_6-stable linker) were tested in *in vivo* setting. In vivo profiling of conjugates was started with determination of Maximum tolerated dose (MTD). MTD studies revealed a tremendous difference in the tolerability of both conjugates in Cb17-Scid mice with much better tolerability of the compound bearing stable linker (MTD of HDP 30.2284 bearing Val-Ala-cleavable linker = 0.046 mg/kg what corresponds to 18.75 µg/kg of α-amanitin and MTD of HDP 30.2301 bearing C6-non-cleavable linker = 2.56 mg/kg what corresponds to 1200 µg/kg of α-amanitin). Next, the pharmacokinetic study of both conjugates conducted *in vivo* revealed very short half-life of these molecules in serum ($t_{1/2}$ HDP 30.2284 = 44 min. and $t_{1/2}$ of HDP 30.2301 = 62 min.). Adjacent to the pharmacokinetic study - biodistribution study revealed abundant accumulation of both conjugates in the kidney. Both: MTD and pharmacokinetic studies informed dose levels and dosing schedules in the following *in vivo* efficacy experiment, which was conducted in Cb17-Scid mice implanted with LNCaP tumors. Despite of the much higher dose levels of administered conjugate HDP 30.2301 which was related to better tolerability of this compound (approx. 65x better tolerability compared to HDP 30.2284) the anti-tumor activity of both HDP 30.2284 and HDP 30.2301 was very poor and limited only to the period of administration. After last administration of conjugates tumors started to re-grow very quickly with the kinetics similar to the vehicle injected group. Based on the outcome of *in vivo* efficacy it was concluded that low tolerability of HDP 30.2284 does not allow to reach the intratumoral toxin concentration allowing to yield anti-tumor activity. Poor *in vivo* performance of HDP 30.2301 as well as former observation of Heidelberg Pharma in the field of ADCs led to conclusion that non-cleavable linker and if possibly released from this compound α-amanitin derivative has very limited in vivo activity, which could not be compensated by high dose administered. It was hypothesized that: 1) improving the tolerability which was not optimal for conjugate HDP 30.2284 with 2) concomitant enabling of release of toxin from the conjugate, which was not possible for conjugate HDP 30.2301 would lead to better *in vivo* efficacy of DUPA-α-amanitin conjugates.

In Chapter 4.2 the small library of conjugates bearing disulfide linker with different level of steric hindrance of disulfide bond was tested for their cytotoxic potential and plasma stability *in vitro*. Following conjugates were tested HDP 30.2246 (0:0), HDP 30.2589 (0:1), HDP 30.2618 (1:0), (HDP 30.2619 (1:1) and HDP 30.2609). The hindered disulfide conjugates are denoted by the number of methyl group on the DUPA site and the amanitin site, e.g. the conjugate with one monomethyl group on the DUPA site and no hindrance on the α-amanitin site is abbreviated as (1:0). The

different levels of hindrance provided by methyl group(s) directly neighboring with the disulfide bond was demonstrated to provide better stability of conjugates in the serum. Considering that α-amanitin is not able to penetrate the cellular membrane it was of special importance for α-amanitin to provide the good stability of conjugate in blood and release of the toxin only after receptor mediated internalization. Amongst all tested conjugates compound HDP 30.2618 (1:0) with intermediate level of steric hindrance of disulfide bond provided optimal *in vitro* activity and plasma stability and was chosen for *in vivo* testing. In MTD study HDP 30.2618 showed intermediate level of tolerability (MTD = 1.2 mg/kg, equivalent of 600 µg/kg of unconjugated α-amanitin) compared to already characterized in vivo conjugates HDP 30.2301 (C_6-non-cleavable linker) and HDP 30.2284 (Val-Ala-PAB cleavable linker). In pharmacokinetic study blood half-life of HDP 30.2618 (1:0) was determined for 75 min. In following *in vivo* efficacy study conjugate demonstrated very limited *in vivo* efficacy only during the period of administration, similar to two previously characterized conjugates. Based on poor anti-tumor activity of all three characterized *in vivo* conjugates it was concluded that the main factor limiting anti-tumor activity of DUPA-α-amanitin SMDCs is short half-life. The conjugates were very rapidly cleared by glomerular filtration, before being able to make a contact with PSMA receptor on the tumor surface. Thus, the further strategy aiming into optimization if *in vivo* properties was focused on limitation of rapid renal filtration and conjugation strategies aiming into prolongation of the circulatory half-life.

In Chapter 4.3 there was presented the characterization of two additional DUPA-α-amanitin conjugates aiming into limitation of renal filtration and prolongation of the circulatory half-life. The first conjugate HDP 30.2594 bearing Val-Ala-PAB cleavable linker followed by additional spacer featuring two dipeptide histidine-glutamic acid $(His\text{-}Glu)_2$ motif. The reasoning behind the implementation of $(His\text{-}Glu)_2$ is that in the physiological pH the deprotonation of the glutamic acid appearing in physiological pH gives an overall negative charge to the conjugate. Negatively charged molecules would be repulsed from the negatively charged glomerular membrane of the nephron in consequence leading to both 1) limited kidney accumulation and 2) prolongation of blood half-life. First, the activity of conjugate HDP 30.2594 was tested *in vitro* in LNCaP (PSMA positive) cell line demonstrating the IC_{50} of 5.18 nM and in PC3 (PSMA negative cell line) IC_{50} of 388 nM. Next the circulatory half-life and kidney accumulation of HDP 30.2594 was determined in parallel with determination of these parameters for most structurally related, already characterized *in vivo* conjugate HDP 30.2284. In contrast to what was expected the half-life of conjugate HDP 30.2594, and its kidney accumulation was similar to a HDP 30.2284 In

response to the poor pharmacokinetic performance of HDP 30.2594 the further characterization of HDP 30.2594 was abandoned and ultimate strategy providing prolongation of circulatory half-life was applied. A completely novel "program and arm" strategy was applied for programming the DUPA-supporting spacer equipped with ethylene glycol spacer for better flexibility and (LPETG) - motif for sortase A mediated enzymatic reaction with Fc portion of human IgG1. The role of Fc portion is to provide FcRn mediated uptake and additional molecular weight of the conjugate both leading to saving the molecule from renal filtration. Additionally, the spacer was equipped with triazole moiety for "arming" - a subsequent strain-promoted azide-alkyne cycloaddition reaction with α-amanitin derivative. Resulting conjugate DUPA-Fc-α-amanitin conjugate was initially tested *in vitro* demonstrating high selectivity (IC_{50} of 15.17 nM in LNCaP PSMA positive cell line, IC_{50} could not be determined in PC3 PSMA negative cell line in the tested range of concentration). Plasma stability testing of this conjugate revealed acceptable plasma stability and supported further characterization in vivo of this molecule. Tolerability of DUPA-Fc-α-amanitin was determined to be 1.0 mg/kg what corresponds to 25.7 µg/kg of unconjugated α-amanitin. Following pharmacokinetic study has demonstrated biphasic elimination typical for molecules presenting Fc motif in the structure with β elimination half life as long as 172.6 h (ca. 7.2 days). In adjacent biodistribution study it was shown that intact DUPA-α-amanitin conjugate is minimally accumulated in the kidney and liver. Free toxin was detected in high concentration only in the tumor what is the evidence of 1) good plasma stability (no free toxin detected in serum samples) and 2) specific release of the toxin only in tumor cells. In vivo efficacy study demonstrated dose dependent and long-lasting anti-tumor response sustained in half of tested animals as long as 3 months after termination of the therapy.

In contrast to the majority of SMDCs which utilize more hydrophobic payloads able to passively penetrate tumor cells, SMDCs featuring a hydrophilic payload like α-amanitin are not a suitable format for obtaining long-lasting therapeutic effect due to the short *in vivo* half-life. Prolongation of half-life is necessary to ensure exposure of the target tissue to the hydrophilic drug in the conjugated form allowing to obtain sustainable anti-tumor activity.

7. APPENDICES AND SUPPLEMENTARY FIGURES

Appendix 1: Composition of cell culture media

1. Composition of RPMI 1640, w/o: L-Glutamine, w: 2.0 g/L NaHCO3

   Pan Biotech Cat# P04-17500

Group of components	Component	Concentration (mg/mL)
Inorganic salts	Calcium nitrate x 4 H_2O	100.00
	Potassium Chloride	400.00
	Magnesium sulfate anhydrous	48.83
	Sodium Chloride	6 000.00
	di-sodium hydrogen phosphate	800.49
Other components	D(+)-Glucose anhydrous	2 000.00
	Glutathione reduced	1.00
	Phenol red	5.00
Aminoacids	L-Arginine x HCl	241.86
	L-Aspargine x H_2O	50.00
	L-Asparticacid	20.00
	L-Cysteine x 2 Hcl	65.19
	L-Glutamine	0.00
	L-Glutamicacid	20.00
	Glycine	10.00
	L-Hystidine x HCl x H_2O	20.27
	L-Hydroxyproline	20.00
	L-Isoleucine	50.00
	L-leucine	50.00
	L-Lysine x HCl	40.00
	L-Methionine	15.00
	L-Phenylalanine	15.00
	L-Proline	20.00
	L-Serine	30.00

Aminoacids	L-Threonine	20.00
	L-Tryptophan	5.00
	L-Tyrosine x 2Na	28.83
	L-Valine	20.00
	p-Aminobenzoicacid	1.00
Vitamins	D-(+)-Biotin	0.20
	D-Calcium Pantothenate	0.25
	Cholinecloride	3.00
	Folicacid	1.00
	myo-Inositol	35.00
	Nicotinamide	1.00
	Pyridoxine x HCl	1.00
	Riboflavin	0.20
	Thiamine x HCl	1.00
	Vitamine B12	0.005
	$NaHCO_3$	2 000.00

2. Composition of DMEM medium: 4.5 g/L Glucose, w/o: L-Glutamine, w: Sodium puryvate, w: 3.7 g/L NaHCO3; Pan Biotech Cat# P04-03600

Group of components	Component	Concentration (mg/mL)
Inorganic salts	Calcium cloride anhydrous	200.00
	Iron (III)-nitrate x 9 H_2O	0.10
	Magnesium sulfate anhydrous	97.66
	Potassium Chloride	400.00
	Sodium Chloride	6 400.49
	Sodium dihydrogen phosphate anhydrous	108.69
Other components	D (+)-Glucose anhydrous	4 500.00
	Sodiumpuryvate	110.00
	Phenol red	15.00
Aminoacids	L-Arginine x HCl	84.00
	L-Cysteine x 2 HCl	62.58
	L-Glutamine	0.00
	Glycine	30.00
	L-Hystidine x HCl x H_2O	42.00
	L-Hydroxyproline	0.00
	L-Isoleucine	104.80
	L-Leucine	104.80
	L-Lysine x HCl	146.80
	L-Methionine	30.00
	L-Phenylalanine	66.00
	L-Proline	0.00
	L-Serine	42.00
	L-Threonine	95.20
	L-Tryptophan	16.00
	L-Tyrosine x Na	103.79
	L-Valine	93.60
Vitamins	p-Aminobenzoicacid	0.00
	D-(+)-Biotin	0.0

Vitamins	D-Calcium Pantothenate	4.00
	Cholinecloride	4.00
	Folicacid	4.00
	myo-Inositol	7.00
	Nicotinamide	4.00
	Pyridoxine x HCl	4.00
	Riboflavin	0.40
	Thiamine x HCl	4.00
	Vitamine B12	0.00
	$NaHCO_3$	3700.00

3. Composition of DMEM/F12, w: 4.5 g/L Glucose, w/o: L-Glutamine, w: Sodium pyruvate, w: 3.7 g/L NaHCO3

   Pan Biotech Cat# P04-41450

Group of components	Component	Concentration (mg/mL)
Inorganic salts	Calcium cloride 2 x H_2O	154.45
	Iron (III)-nitrate x 9 H_2O	0.05
	Iron (III)-sulfate x 7 H_2O	0.42
	Potassium Chloride	311.83
	Copper[23]-sulfate x 5 H_2O	0.001
	Magnesium chloride anhydrous	28.57
	Magnesium Sulfate	48.85
	Sodium Chloride	6 999.50
	Sodium dihydrogen phosphate anhydrous	54.35
	Do-Sodium hydrogen phosphate	70.98
	Zinc sulfate x 7 H_2O	0.43
Other components	D (+)-Glucose anhydrous	3 151.00
	Hypoxantine	2.04
	Linoleic acid	0.04
	DL-68 Lipolic acid	0.103
	Sodium puryvate	1100.00
	Phenol red	8.10
	Putrescin x 2HCl	0.081
	Tymidine	0.36
Aminoacids	L-Arginine x HCl	147.35
	L-Alanine	4.45
	L-Asparagine x H_2O	7.50
	L-Asparticacid	6.65
	L-Cysteine x 2 HCl	31.29
	L-Glutamine	0.00
	Glycine	18.75
	L-Hystidine x HCl x H_2O	31.46

	L-Hydroxyproline	0.00
	L-Isoleucine	54.37
	L-Leucine	58.96
	L-Lysine x HCl	91.37
	L-Methionine	17.24
	L-Phenylalanine	35.48
	L-Proline	17.27
	L-Serine	26.25
	L-Threonine	53.55
	L-Tryptophan	9.02
	L-Tyrosine x Na	55.81
	L-Valine	52.66
Vitamins	p-Aminobenzoicacid	0.00
	D-(+)-Biotin	0.004
	D-Calcium Pantothenate	2.12
	Cholinecloride	8.98
	Folicacid	2.66
	myo-Inositol	12.51
	Nicotinamide	2.02
	Pyridoxine x HCl	2.03
	Riboflavin	0.22
	Thiamine x HCl	2.17
	Vitamine B12	0.68
	$NaHCO_3$	1 200.00

Supplementary Figures

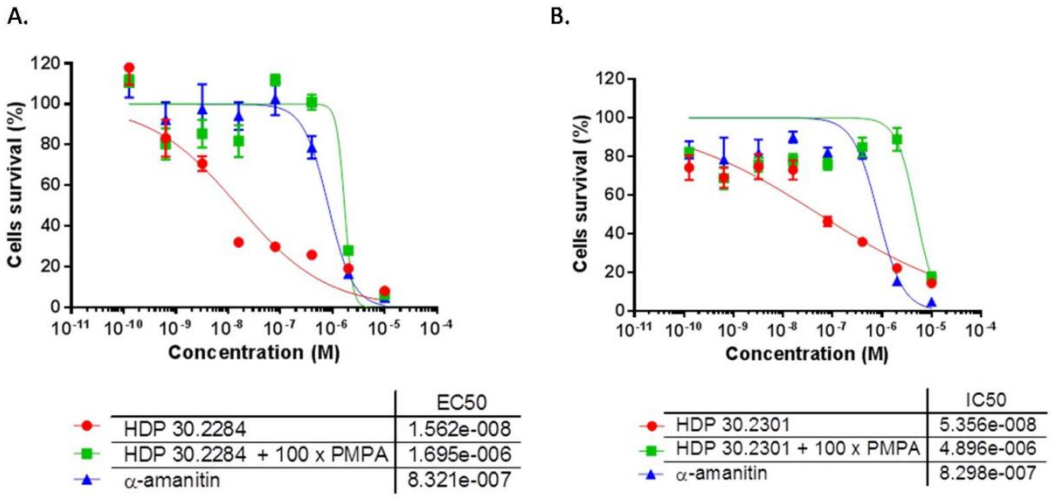

Supplementary figure 1. Cytotoxicity of (A) HDP 30.2284 and (B) HDP 30.2301 in C4_2 (PSMA +++) cell line.

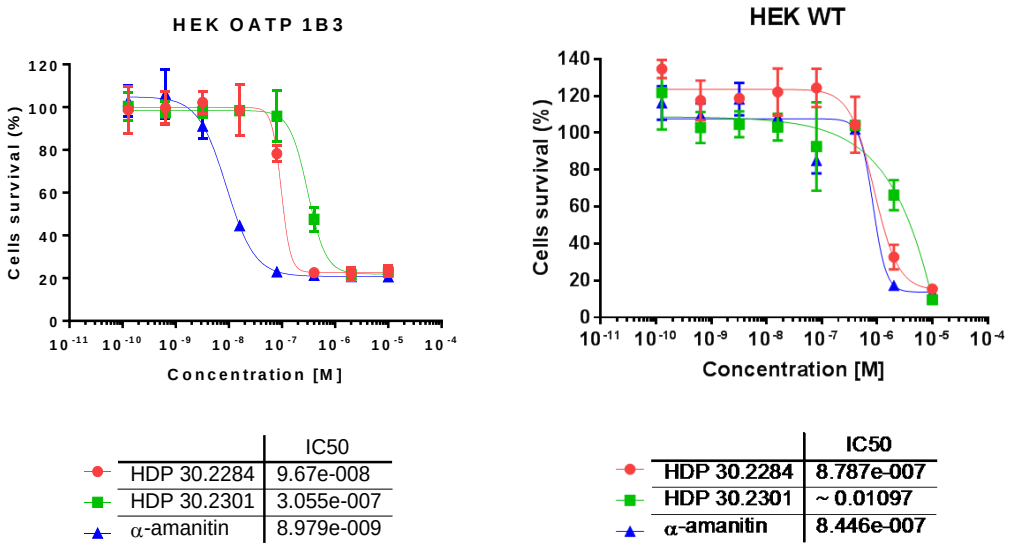

Supplementary figure 2. Cytotoxicity of unconjugated α-amanitin and HDP 30.2284 and HDP 30.2301 on HEK293 cells stably expressing OATP1B3 transporter (left panel) and HEK293 cells wild type cell line (right panel).

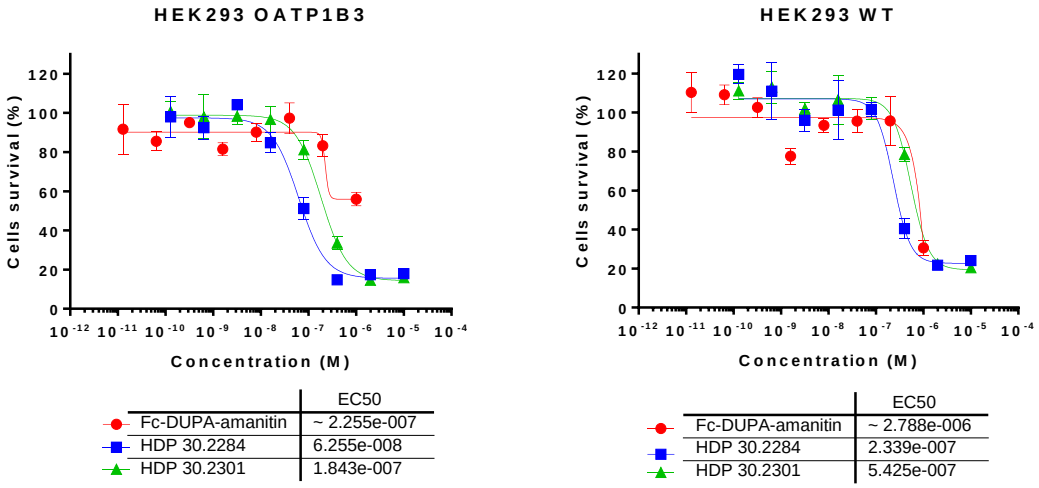

Supplementary figure 3. Cytotoxicity of DUPA-Fc-α-amanitin conjugate directly compared with HDP 30.2284 and HDP 30.2301 on (A) HEK293 cells stably overexpressing OATP1B3 transporter and (B) HEK293 wild type cell line.

8. REFERENCES

1. Coleman, W.B., *Molecular Pathology 2nd Edition; Chapter 25 Molecular Pathogenesis of Prostate Cancer.* 2018.
2. Ferlay, J., et al., *Cancer incidence and mortality worldwide: sources, methods and major patterns in GLOBOCAN 2012.* Int J Cancer, 2015. **136**(5): p. E359-86.
3. Mandair, D., et al., *Prostate cancer and the influence of dietary factors and supplements: a systematic review.* Nutr Metab (Lond), 2014. **11**: p. 30.
4. Gilligan, T., et al., *Racial differences in screening for prostate cancer in the elderly.* Arch Intern Med, 2004. **164**(17): p. 1858-64.
5. Cooperberg, M.R. and J.M. Chan, *Epidemiology of prostate cancer.* World J Urol, 2017. **35**(6): p. 849.
6. Kimura, T., *East meets West: ethnic differences in prostate cancer epidemiology between East Asians and Caucasians.* Chin J Cancer, 2012. **31**(9): p. 421-9.
7. Kheirandish, P. and F. Chinegwundoh, *Ethnic differences in prostate cancer.* Br J Cancer, 2011. **105**(4): p. 481-5.
8. Goh, C.L., et al., *Genetic variants associated with predisposition to prostate cancer and potential clinical implications.* J Intern Med, 2012. **271**(4): p. 353-65.
9. Li, D., et al., *The role of BRCA1 and BRCA2 in prostate cancer.* Front Biosci (Landmark Ed), 2013. **18**: p. 1445-59.
10. Brechka, H., et al., *HOXB13 mutations and binding partners in prostate development and cancer: Function, clinical significance, and future directions.* Genes Dis, 2017. **4**(2): p. 75-87.
11. Hughes, C., et al., *Molecular pathology of prostate cancer.* J Clin Pathol, 2005. **58**(7): p. 673-84.
12. Silberstein, J.L., M.N. Taylor, and E.S. Antonarakis, *Novel Insights into Molecular Indicators of Response and Resistance to Modern Androgen-Axis Therapies in Prostate Cancer.* Curr Urol Rep, 2016. **17**(4): p. 29.
13. De Santis, M. and F. Saad, *Practical Guidance on the Role of Corticosteroids in the Treatment of Metastatic Castration-resistant Prostate Cancer.* Urology, 2016. **96**: p. 156-164.
14. Oudard, S., et al., *Cabazitaxel Versus Docetaxel As First-Line Therapy for Patients With Metastatic Castration-Resistant Prostate Cancer: A Randomized Phase III Trial-FIRSTANA.* J Clin Oncol, 2017. **35**(28): p. 3189-3197.
15. Sweeney, C.J., et al., *Chemohormonal Therapy in Metastatic Hormone-Sensitive Prostate Cancer.* N Engl J Med, 2015. **373**(8): p. 737-46.
16. James, N.D., et al., *Addition of docetaxel, zoledronic acid, or both to first-line long-term hormone therapy in prostate cancer (STAMPEDE): survival results from an adaptive, multiarm, multistage, platform randomised controlled trial.* Lancet, 2016. **387**(10024): p. 1163-77.
17. Smith, M.R., et al., *Apalutamide Treatment and Metastasis-free Survival in Prostate Cancer.* N Engl J Med, 2018. **378**(15): p. 1408-1418.
18. Nevedomskaya, E., S.J. Baumgart, and B. Haendler, *Recent Advances in Prostate Cancer Treatment and Drug Discovery.* Int J Mol Sci, 2018. **19**(5).
19. Crumbaker, M., L. Khoja, and A.M. Joshua, *AR Signaling and the PI3K Pathway in Prostate Cancer.* Cancers (Basel), 2017. **9**(4).

20. Wise, H.M., M.A. Hermida, and N.R. Leslie, *Prostate cancer, PI3K, PTEN and prognosis.* Clin Sci (Lond), 2017. **131**(3): p. 197-210.
21. Marques, R.B., et al., *High Efficacy of Combination Therapy Using PI3K/AKT Inhibitors with Androgen Deprivation in Prostate Cancer Preclinical Models.* Eur Urol, 2015. **67**(6): p. 1177-1185.
22. Ramakrishnan Geethakumari, P., et al., *PARP Inhibitors in Prostate Cancer.* Curr Treat Options Oncol, 2017. **18**(6): p. 37.
23. Mateo, J., et al., *DNA-Repair Defects and Olaparib in Metastatic Prostate Cancer.* N Engl J Med, 2015. **373**(18): p. 1697-708.
24. Martin, G.A., A.H. Chen, and K. Parikh, *A Novel Use of Olaparib for the Treatment of Metastatic Castration-Recurrent Prostate Cancer.* Pharmacotherapy, 2017. **37**(11): p. 1406-1414.
25. Rappaport, J.A. and S.A. Waldman, *The Guanylate Cyclase C-cGMP Signaling Axis Opposes Intestinal Epithelial Injury and Neoplasia.* Front Oncol, 2018. **8**: p. 299.
26. Kantoff, P.W., et al., *Sipuleucel-T immunotherapy for castration-resistant prostate cancer.* N Engl J Med, 2010. **363**(5): p. 411-22.
27. Hargadon, K.M., C.E. Johnson, and C.J. Williams, *Immune checkpoint blockade therapy for cancer: An overview of FDA-approved immune checkpoint inhibitors.* Int Immunopharmacol, 2018. **62**: p. 29-39.
28. Schepisi, G., et al., *Immunotherapy for Prostate Cancer: Where We Are Headed.* Int J Mol Sci, 2017. **18**(12).
29. Alaia, C., et al., *Ipilimumab for the treatment of metastatic prostate cancer.* Expert Opin Biol Ther, 2018. **18**(2): p. 205-213.
30. Junghans, R.P., et al., *Phase I Trial of Anti-PSMA Designer CAR-T Cells in Prostate Cancer: Possible Role for Interacting Interleukin 2-T Cell Pharmacodynamics as a Determinant of Clinical Response.* Prostate, 2016. **76**(14): p. 1257-70.
31. Hartmann, J., et al., *Clinical development of CAR T cells-challenges and opportunities in translating innovative treatment concepts.* EMBO Mol Med, 2017. **9**(9): p. 1183-1197.
32. Troyer, J.K., M.L. Beckett, and G.L. Wright, Jr., *Detection and characterization of the prostate-specific membrane antigen (PSMA) in tissue extracts and body fluids.* Int J Cancer, 1995. **62**(5): p. 552-8.
33. Baccala, A., et al., *Expression of prostate-specific membrane antigen in tumor-associated neovasculature of renal neoplasms.* Urology, 2007. **70**(2): p. 385-90.
34. Yao, V., et al., *Moderate expression of prostate-specific membrane antigen, a tissue differentiation antigen and folate hydrolase, facilitates prostate carcinogenesis.* Cancer Res, 2008. **68**(21): p. 9070-7.
35. Bařinka, C., Rojas, C., Slusher, B., & Pomper, M. (2012). Glutamate carboxypeptidase II in diagnosis and treatment of neurologic disorders and prostate cancer. Current medicinal chemistry, 19(6), 856–870. https://doi.org/10.2174/092986712799034888, C., et al., *Glutamate carboxypeptidase II in diagnosis and treatment of neurologic disorders and prostate cancer.* Curr Med Chem, 2012. **19**(6): p. 856-70.
36. Davis, M.I., et al., *Crystal structure of prostate-specific membrane antigen, a tumor marker and peptidase.* Proc Natl Acad Sci U S A, 2005. **102**(17): p. 5981-6.
37. Kopka, K., et al., *Glu-Ureido-Based Inhibitors of Prostate-Specific Membrane Antigen: Lessons Learned During the Development of a Novel Class of Low-Molecular-Weight Theranostic Radiotracers.* J Nucl Med, 2017. **58**(Suppl 2): p. 17S-26S.
38. Yao, V. and D.J. Bacich, *Prostate specific membrane antigen (PSMA) expression gives prostate cancer cells a growth advantage in a physiologically relevant folate environment in vitro.* Prostate, 2006. **66**(8): p. 867-75.

39. Carter, R.E., A.R. Feldman, and J.T. Coyle, *Prostate-specific membrane antigen is a hydrolase with substrate and pharmacologic characteristics of a neuropeptidase.* Proc Natl Acad Sci U S A, 1996. **93**(2): p. 749-53.
40. Su, S.L., et al., *Alternatively spliced variants of prostate-specific membrane antigen RNA: ratio of expression as a potential measurement of progression.* Cancer Res, 1995. **55**(7): p. 1441-3.
41. Tagawa, S.T., et al., *Anti-prostate-specific membrane antigen-based radioimmunotherapy for prostate cancer.* Cancer, 2010. **116**(4 Suppl): p. 1075-83.
42. Goodman, O.B., Jr., et al., *Interaction of prostate specific membrane antigen with clathrin and the adaptor protein complex-2.* Int J Oncol, 2007. **31**(5): p. 1199-203.
43. Tsuchikama, K. and Z. An, *Antibody-drug conjugates: recent advances in conjugation and linker chemistries.* Protein Cell, 2018. **9**(1): p. 33-46.
44. Anilkumar, G., et al., *Association of prostate-specific membrane antigen with caveolin-1 and its caveolae-dependent internalization in microvascular endothelial cells: implications for targeting to tumor vasculature.* Microvasc Res, 2006. **72**(1-2): p. 54-61.
45. Henry, M.D., et al., *A prostate-specific membrane antigen-targeted monoclonal antibody-chemotherapeutic conjugate designed for the treatment of prostate cancer.* Cancer Res, 2004. **64**(21): p. 7995-8001.
46. Ma, D., et al., *Potent antitumor activity of an auristatin-conjugated, fully human monoclonal antibody to prostate-specific membrane antigen.* Clin Cancer Res, 2006. **12**(8): p. 2591-6.
47. Cho, S., et al., *Antitumor Activity of MEDI3726 (ADCT-401), a Pyrrolobenzodiazepine Antibody-drug Conjugate Targeting PSMA, in Pre-clinical Models of Prostate Cancer.* Mol Cancer Ther, 2018.
48. Huang, X., M. Bennett, and P.E. Thorpe, *Anti-tumor effects and lack of side effects in mice of an immunotoxin directed against human and mouse prostate-specific membrane antigen.* Prostate, 2004. **61**(1): p. 1-11.
49. Kellogg, B.A., et al., *Disulfide-linked antibody-maytansinoid conjugates: optimization of in vivo activity by varying the steric hindrance at carbon atoms adjacent to the disulfide linkage.* Bioconjug Chem, 2011. **22**(4): p. 717-27.
50. Milowsky, M.I., et al., *Phase 1/2 multiple ascending dose trial of the prostate-specific membrane antigen-targeted antibody drug conjugate MLN2704 in metastatic castration-resistant prostate cancer.* Urol Oncol, 2016. **34**(12): p. 530 e15-530 e21.
51. Petrylak, D.P., et al., *A phase 2 study of prostate specific membrane antigen antibody drug conjugate (PSMA ADC) in patients (pts) with progressive metastatic castration-resistant prostate cancer (mCRPC) following abiraterone and/or enzalutamide (abi/enz).* Journal of Clinical Oncology, 2015. **33**(7_suppl): p. 144-144.
52. Petrylak, D.P., et al., *Phase 1 study of PSMA ADC, an antibody-drug conjugate targeting prostate-specific membrane antigen, in chemotherapy-refractory prostate cancer.* Prostate, 2019. **79**(6): p. 604-613.
53. Petrylak, D.P., et al., *PSMA ADC monotherapy in patients with progressive metastatic castration-resistant prostate cancer following abiraterone and/or enzalutamide: Efficacy and safety in open-label single-arm phase 2 study.* Prostate, 2020. **80**(1): p. 99-108.
54. DiPippo, V.A., et al., *Efficacy studies of an antibody-drug conjugate PSMA-ADC in patient-derived prostate cancer xenografts.* Prostate, 2015. **75**(3): p. 303-13.
55. Hechler, T., Kulke, M., Müller, C., Pahl, A. and Anderl, J., *Poster presentation #664: Amanitin-based antibody-drug conjugates targeting the prostate-specific membrane antigen PSMA* AACR Annual Meeting 2014.

56. Breunig, C., Pálfi, A., Hechler, T., Müller, C., Lutz, C., Pahl, A. and Kulke, M., *Abstract 740: Preclinical evaluation of an anti-PSMA antibody-targeted amanitin conjugate (ATAC).* Proceedings: AACR Annual Meeting 2018; April 14-18, 2018; Chicago, IL, 2018.
57. Hallen, H.E., et al., *Gene family encoding the major toxins of lethal Amanita mushrooms.* Proc Natl Acad Sci U S A, 2007. **104**(48): p. 19097-101.
58. Garcia, J., et al., *Amanita phalloides poisoning: Mechanisms of toxicity and treatment.* Food Chem Toxicol, 2015. **86**: p. 41-55.
59. Poucheret, P., et al., *Amatoxin poisoning treatment decision-making: pharmaco-therapeutic clinical strategy assessment using multidimensional multivariate statistic analysis.* Toxicon, 2010. **55**(7): p. 1338-45.
60. Jaeger, A., et al., *Kinetics of amatoxins in human poisoning: therapeutic implications.* J Toxicol Clin Toxicol, 1993. **31**(1): p. 63-80.
61. Faulstich, H., K. Kirchner, and M. Derenzini, *Strongly enhanced toxicity of the mushroom toxin alpha-amanitin by an amatoxin-specific Fab or monoclonal antibody.* Toxicon, 1988. **26**(5): p. 491-9.
62. Letschert, K., et al., *Molecular characterization and inhibition of amanitin uptake into human hepatocytes.* Toxicol Sci, 2006. **91**(1): p. 140-9.
63. Garcia, J., et al., *Quantification of alpha-amanitin in biological samples by HPLC using simultaneous UV- diode array and electrochemical detection.* J Chromatogr B Analyt Technol Biomed Life Sci, 2015. **997**: p. 85-95.
64. Fiume, L., V. Marinozzi, and F. Nardi, *The effects of amanitin poisoning on mouse kidney.* Br J Exp Pathol, 1969. **50**(3): p. 270-6.
65. Ergin, M., et al., *Alpha-Amanitin Poisoning, Nephrotoxicity and Oxidative Stress: An Experimental Mouse Model.* Iran Red Crescent Med J, 2015. **17**(8): p. e28068.
66. Bushnell, D.A., P. Cramer, and R.D. Kornberg, *Structural basis of transcription: alpha-amanitin-RNA polymerase II cocrystal at 2.8 A resolution.* Proc Natl Acad Sci U S A, 2002. **99**(3): p. 1218-22.
67. Cramer, P., et al., *Architecture of RNA polymerase II and implications for the transcription mechanism.* Science, 2000. **288**(5466): p. 640-9.
68. Matinkhoo, K., et al., *Synthesis of the Death-Cap Mushroom Toxin alpha-Amanitin.* J Am Chem Soc, 2018. **140**(21): p. 6513-6517.
69. Kulke, M., Pálfi, A., Müller, C., Simon, W., Werner-Simon, S., Lutz, C., Hechler, T. and Pahl, A., *Poster presentation #735: Structure-activity relationship (SAR) of amanitin and optimization of linker-amanitin derivatives for solid tumors. .* AACR meeting 2018, 2018.
70. N., S., *Optimizing Antibodz Drug Conjugates for Targeted Delivery of therpaeutics (Pages 31-36), Published by Future Science Ltd.* 2015.
71. Rudd, M.D. and D.S. Luse, *Amanitin greatly reduces the rate of transcription by RNA polymerase II ternary complexes but fails to inhibit some transcript cleavage modes.* J Biol Chem, 1996. **271**(35): p. 21549-58.
72. Liu, Y., et al., *TP53 loss creates therapeutic vulnerability in colorectal cancer.* Nature, 2015. **520**(7549): p. 697-701.
73. Li, Y., et al., *Heterozygous deletion of chromosome 17p renders prostate cancer vulnerable to inhibition of RNA polymerase II.* Nat Commun, 2018. **9**(1): p. 4394.
74. Moldenhauer, G., et al., *Therapeutic potential of amanitin-conjugated anti-epithelial cell adhesion molecule monoclonal antibody against pancreatic carcinoma.* J Natl Cancer Inst, 2012. **104**(8): p. 622-34.
75. Pálfi, A., Kulke, M., Müller, C., Lutz, C., Pahl, A. and Hechler, T., *Poster presentation: CD19 – a potential target for Amanitin-based ADCs.* PEGS Summit Europe 2017.
76. Vlahov, I.R., et al., *Conjugates for treating diseases caused by psma expressing cells , Patent WO2014078484A1.* 2012.

77. Kularatne, S.A., et al., *Prostate-specific membrane antigen targeted imaging and therapy of prostate cancer using a PSMA inhibitor as a homing ligand.* Mol Pharm, 2009. **6**(3): p. 780-9.
78. Kim, C.H., et al., *Bispecific small molecule-antibody conjugate targeting prostate cancer.* Proc Natl Acad Sci U S A, 2013. **110**(44): p. 17796-801.
79. Deonarain MP , Y.G., Stamati I, Pomowski A ,Clarke J , Edwards BM , Diez-Posada S, Stewart AC, *Small-Format Drug Conjugates: A Viable Alternative to ADCs for Solid Tumours.* Antibodies 2018, 7, 16 2018.
80. Bodero, L., et al., *Synthesis and biological evaluation of RGD and isoDGR peptidomimetic-alpha-amanitin conjugates for tumor-targeting.* Beilstein J Org Chem, 2018. **14**: p. 407-415.
81. Moshnikova, A., et al., *Antiproliferative effect of pHLIP-amanitin.* Biochemistry, 2013. **52**(7): p. 1171-8.
82. Kozikowski, A.P., et al., *Design of remarkably simple, yet potent urea-based inhibitors of glutamate carboxypeptidase II (NAALADase).* J Med Chem, 2001. **44**(3): p. 298-301.
83. Jackson, P.F., et al., *Design, synthesis, and biological activity of a potent inhibitor of the neuropeptidase N-acetylated alpha-linked acidic dipeptidase.* J Med Chem, 1996. **39**(2): p. 619-22.
84. Thomas, A.G., et al., *N-Acetylated alpha-linked acidic dipeptidase converts N-acetylaspartylglutamate from a neuroprotectant to a neurotoxin.* J Pharmacol Exp Ther, 2000. **295**(1): p. 16-22.
85. Zhou, J., et al., *NAAG peptidase inhibitors and their potential for diagnosis and therapy.* Nat Rev Drug Discov, 2005. **4**(12): p. 1015-26.
86. Mesters, J.R., et al., *Structure of glutamate carboxypeptidase II, a drug target in neuronal damage and prostate cancer.* EMBO J, 2006. **25**(6): p. 1375-84.
87. Kularatne, S.A., et al., *Design, synthesis, and preclinical evaluation of prostate-specific membrane antigen targeted (99m)Tc-radioimaging agents.* Mol Pharm, 2009. **6**(3): p. 790-800.
88. Donin, N.M. and R.E. Reiter, *Why Targeting PSMA Is a Game Changer in the Management of Prostate Cancer.* J Nucl Med, 2018. **59**(2): p. 177-182.
89. Benesova, M., et al., *Preclinical Evaluation of a Tailor-Made DOTA-Conjugated PSMA Inhibitor with Optimized Linker Moiety for Imaging and Endoradiotherapy of Prostate Cancer.* J Nucl Med, 2015. **56**(6): p. 914-20.
90. Benesova, M., et al., *Linker Modification Strategies To Control the Prostate-Specific Membrane Antigen (PSMA)-Targeting and Pharmacokinetic Properties of DOTA-Conjugated PSMA Inhibitors.* J Med Chem, 2016. **59**(5): p. 1761-75.
91. Kularatne, S.A., et al., *Synthesis and biological analysis of prostate-specific membrane antigen-targeted anticancer prodrugs.* J Med Chem, 2010. **53**(21): p. 7767-77.
92. Lv, Q., et al., *Prostate-Specific Membrane Antigen Targeted Therapy of Prostate Cancer Using a DUPA-Paclitaxel Conjugate.* Mol Pharm, 2018. **15**(5): p. 1842-1852.
93. Peng, Z.H., et al., *Spacer length impacts the efficacy of targeted docetaxel conjugates in prostate-specific membrane antigen expressing prostate cancer.* J Drug Target, 2013. **21**(10): p. 968-80.
94. Roy, J., et al., *DUPA conjugation of a cytotoxic indenoisoquinoline topoisomerase I inhibitor for selective prostate cancer cell targeting.* J Med Chem, 2015. **58**(7): p. 3094-103.
95. Castro, F., et al., *High-throughput SNP-based authentication of human cell lines.* Int J Cancer, 2013. **132**(2): p. 308-14.
96. Schmitt, M. and M. Pawlita, *High-throughput detection and multiplex identification of cell contaminations.* Nucleic Acids Res, 2009. **37**(18): p. e119.

97. Lucas, A.T.P., L.S.L.; Schorzman, A.N.; Storrie, M.; Piscitelli, J.A.; Razo, J.; Zamboni, W.C., *Factors Affecting the Pharmacology of Antibody–Drug Conjugates.* Antibodies 2018, 7, 16, 2018. **7, 10.** .
98. Donaghy, H., *Effects of antibody, drug and linker on the preclinical and clinical toxicities of antibody-drug conjugates.* MAbs, 2016. **8**(4): p. 659-71.
99. Ko, J., Breunig, C., Figueroa, V., Lehners, N., Baumann, A., Pálfi, A., Müller, C., Lutz, C., Hechler, T., Kulke, M., Mueller-Tidow, C., Goldschmidt, H., Pahl, A. & Raab, M.S., *Poster presentation: Preclinical Evaluation of HDP-101, a Novel anti-BCMA Antibody-Drug Conjugate, in Multiple Myeloma.* The American Society of Hematology Annual Meeting, 2018.
100. Vergote, I. and C.P. Leamon, *Vintafolide: a novel targeted therapy for the treatment of folate receptor expressing tumors.* Ther Adv Med Oncol, 2015. **7**(4): p. 206-18.
101. Trudel, S., et al., *Targeting B-cell maturation antigen with GSK2857916 antibody-drug conjugate in relapsed or refractory multiple myeloma (BMA117159): a dose escalation and expansion phase 1 trial.* Lancet Oncol, 2018. **19**(12): p. 1641-1653.
102. Gorges, T.M., et al., *Heterogeneous PSMA expression on circulating tumor cells: a potential basis for stratification and monitoring of PSMA-directed therapies in prostate cancer.* Oncotarget, 2016. **7**(23): p. 34930-41.
103. Breunig C, P.A., Hechler T, Müller C, Lutz C, Pahl A, Kulke M, *Abstract 740: Preclinical evaluation of an anti-PSMA antibody-targeted amanitin conjugate (ATAC).* Proceedings: AACR Annual Meeting 2018; April 14-18, 2018; Chicago, IL, 2018.
104. Alley, S.C., et al., *Contribution of linker stability to the activities of anticancer immunoconjugates.* Bioconjug Chem, 2008. **19**(3): p. 759-65.
105. Chatalic, K.L., et al., *Towards Personalized Treatment of Prostate Cancer: PSMA I&T, a Promising Prostate-Specific Membrane Antigen-Targeted Theranostic Agent.* Theranostics, 2016. **6**(6): p. 849-61.
106. Kuo, H.T., et al., *Effects of Linker Modification on Tumor-to-Kidney Contrast of (68)Ga-Labeled PSMA-Targeted Imaging Probes.* Mol Pharm, 2018. **15**(8): p. 3502-3511.
107. Bennett G, L.R., Park P, Harrison H, Lee K, *Abstract 1167: Development of BT1718, a novel Bicycle Drug Conjugate for the treatment of lung cancer.* Proceedings: AACR Annual Meeting 2017; April 1-5, 2017; Washington, DC.
108. Liolios, C., et al., *Novel Bispecific PSMA/GRPr Targeting Radioligands with Optimized Pharmacokinetics for Improved PET Imaging of Prostate Cancer.* Bioconjug Chem, 2016. **27**(3): p. 737-51.
109. Kontermann, R.E., *Strategies for extended serum half-life of protein therapeutics.* Curr Opin Biotechnol, 2011. **22**(6): p. 868-76.
110. Ryman J.T. and Meibohm B., *Pharmacokinetics of Monoclonal Antibodies.* CPT: P Pharmacometrics Syst Pharmacol. 2017 Sep;6(9):576-588.
111. Lin, J.H., *Pharmacokinetics of biotech drugs: peptides, proteins and monoclonal antibodies.* Curr Drug Metab, 2009. **10**(7): p. 661-91.
112. Vornov, J.J., et al., *Blockade of NAALADase: a novel neuroprotective strategy based on limiting glutamate and elevating NAAG.* Ann N Y Acad Sci, 1999. **890**: p. 400-5.
113. Hechler T, K.M., Müller C, Pahl A, Anderl J, *Poster #664 Amanitin-based antibody-drug conjugates targeting the prostate-specific membrane antigen PSMA.* AACR Annual Meeting 2014.
114. Ponte, J.F., et al., *Understanding How the Stability of the Thiol-Maleimide Linkage Impacts the Pharmacokinetics of Lysine-Linked Antibody-Maytansinoid Conjugates.* Bioconjug Chem, 2016. **27**(7): p. 1588-98.

115. Reddy, J.A., et al., *Pre-clinical evaluation of EC1456, a folate-tubulysin anti-cancer therapeutic.* Sci Rep, 2018. **8**(1): p. 8943.
116. Caliceti, P. and F.M. Veronese, *Pharmacokinetic and biodistribution properties of poly(ethylene glycol)-protein conjugates.* Adv Drug Deliv Rev, 2003. **55**(10): p. 1261-77.
117. Chen, B., et al., *Targeting Negative Surface Charges of Cancer Cells by Multifunctional Nanoprobes.* Theranostics, 2016. **6**(11): p. 1887-98.
118. Utsugi, T., et al., *Elevated expression of phosphatidylserine in the outer membrane leaflet of human tumor cells and recognition by activated human blood monocytes.* Cancer Res, 1991. **51**(11): p. 3062-6.
119. Huang, S.S., et al., *Improving the biodistribution of PSMA-targeting tracers with a highly negatively charged linker.* Prostate, 2014. **74**(7): p. 702-13.
120. Cazzamalli, S., A.D. Corso, and D. Neri, *Linker stability influences the anti-tumor activity of acetazolamide-drug conjugates for the therapy of renal cell carcinoma.* J Control Release, 2017. **246**: p. 39-45.
121. Pahl, A., *Development of Amanitin-based ADCs, oral presentation.* ADC Summit 2015 San Diego, 2015.
122. Poon, K.A., et al., *Preclinical safety profile of trastuzumab emtansine (T-DM1): mechanism of action of its cytotoxic component retained with improved tolerability.* Toxicol Appl Pharmacol, 2013. **273**(2): p. 298-313.
123. Dal Corso, A., et al., *Protease-Cleavable Linkers Modulate the Anticancer Activity of Noninternalizing Antibody-Drug Conjugates.* Bioconjug Chem, 2017. **28**(7): p. 1826-1833.
124. Turk, V., et al., *Cysteine cathepsins: from structure, function and regulation to new frontiers.* Biochim Biophys Acta, 2012. **1824**(1): p. 68-88.
125. Dorywalska, M., et al., *Molecular Basis of Valine-Citrulline-PABC Linker Instability in Site-Specific ADCs and Its Mitigation by Linker Design.* Mol Cancer Ther, 2016. **15**(5): p. 958-70.
126. Bonetti, E., M. Derenzini, and L. Fiume, *Lesions in the cells of proximal convoluted tubules in rat kidney induced by amanitin-albumin conjugate.* Virchows Arch B Cell Pathol, 1974. **16**(1): p. 71-8.
127. Lu, J., et al., *Linkers Having a Crucial Role in Antibody-Drug Conjugates.* Int J Mol Sci, 2016. **17**(4): p. 561.
128. Wustemann, T., et al., *Design of Internalizing PSMA-specific Glu-ureido-based Radiotherapeuticals.* Theranostics, 2016. **6**(8): p. 1085-95.
129. Kratochwil, C., et al., *PMPA for nephroprotection in PSMA-targeted radionuclide therapy of prostate cancer.* J Nucl Med, 2015. **56**(2): p. 293-8.
130. Jones, A.J., et al., *Selective clearance of glycoforms of a complex glycoprotein pharmaceutical caused by terminal N-acetylglucosamine is similar in humans and cynomolgus monkeys.* Glycobiology, 2007. **17**(5): p. 529-40.
131. Bradshaw-Pierce, E.L., et al., *Pharmacokinetic-directed dosing of vandetanib and docetaxel in a mouse model of human squamous cell carcinoma.* Mol Cancer Ther, 2008. **7**(9): p. 3006-17.
132. van Ginneken, C.A. and F.G. Russel, *Saturable pharmacokinetics in the renal excretion of drugs.* Clin Pharmacokinet, 1989. **16**(1): p. 38-54.
133. Eiseman, J.L., et al., *Plasma pharmacokinetics and tissue distribution of paclitaxel in CD2F1 mice.* Cancer Chemother Pharmacol, 1994. **34**(6): p. 465-71.
134. Abidi, A., *Cabazitaxel: A novel taxane for metastatic castration-resistant prostate cancer-current implications and future prospects.* J Pharmacol Pharmacother, 2013. **4**(4): p. 230-7.
135. Rejniak, K.A., et al., *The role of tumor tissue architecture in treatment penetration and efficacy: an integrative study.* Front Oncol, 2013. **3**: p. 111.

136. Liu, L., *Antibody glycosylation and its impact on the pharmacokinetics and pharmacodynamics of monoclonal antibodies and Fc-fusion proteins.* J Pharm Sci, 2015. **104**(6): p. 1866-1884.
137. Jones, E.A. and T.A. Waldmann, *The mechanism of intestinal uptake and transcellular transport of IgG in the neonatal rat.* J Clin Invest, 1972. **51**(11): p. 2916-27.
138. Pyzik, M., et al., *FcRn: The Architect Behind the Immune and Nonimmune Functions of IgG and Albumin.* J Immunol, 2015. **194**(10): p. 4595-603.
139. Ober, R.J., et al., *Differences in promiscuity for antibody-FcRn interactions across species: implications for therapeutic antibodies.* Int Immunol, 2001. **13**(12): p. 1551-9.
140. Wu, B. and Y.N. Sun, *Pharmacokinetics of Peptide-Fc fusion proteins.* J Pharm Sci, 2014. **103**(1): p. 53-64.
141. Jafari, R., et al., *Fc-fusion Proteins in Therapy: An Updated View.* Curr Med Chem, 2017. **24**(12): p. 1228-1237.
142. Sarwar, S., et al., *Fusion Proteins: Aflibercept (VEGF Trap-Eye).* Dev Ophthalmol, 2016. **55**: p. 282-94.
143. Young, P.A., S.L. Morrison, and J.M. Timmerman, *Antibody-cytokine fusion proteins for treatment of cancer: engineering cytokines for improved efficacy and safety.* Semin Oncol, 2014. **41**(5): p. 623-36.
144. Yang, B.B., et al., *Development of Romiplostim for Treatment of Primary Immune Thrombocytopenia From a Pharmacokinetic and Pharmacodynamic Perspective.* Clin Pharmacokinet, 2016. **55**(9): p. 1045-58.
145. Hirasawa, S., et al., *Facile and Efficient Chemoenzymatic Semisynthesis of Fc-Fusion Compounds for Half-Life Extension of Pharmaceutical Components.* Bioconjug Chem, 2019. **30**(9): p. 2323-2331.
146. Dal Corso, A., et al., *A non-internalizing antibody-drug conjugate based on an anthracycline payload displays potent therapeutic activity in vivo.* J Control Release, 2017. **264**: p. 211-218.
147. Cazzamalli, S., et al., *Chemically Defined Antibody- and Small Molecule-Drug Conjugates for in Vivo Tumor Targeting Applications: A Comparative Analysis.* J Am Chem Soc, 2018. **140**(5): p. 1617-1621.
148. Nielsen, R., E.I. Christensen, and H. Birn, *Megalin and cubilin in proximal tubule protein reabsorption: from experimental models to human disease.* Kidney Int, 2016. **89**(1): p. 58-67.
149. Christensen, E.I. and R. Nielsen, *Role of megalin and cubilin in renal physiology and pathophysiology.* Rev Physiol Biochem Pharmacol, 2007. **158**: p. 1-22.
150. Mahadevappa, R., et al., *Megalin in acute kidney injury: foe and friend.* Am J Physiol Renal Physiol, 2014. **306**(2): p. F147-54.
151. Schmitz, C., et al., *Megalin deficiency offers protection from renal aminoglycoside accumulation.* J Biol Chem, 2002. **277**(1): p. 618-22.
152. Figueras, E., et al., *Octreotide Conjugates for Tumor Targeting and Imaging.* Pharmaceutics, 2019. **11**(5).
153. Leamon, C.P., et al., *Enhancing the therapeutic range of a targeted small-molecule tubulysin conjugate for folate receptor-based cancer therapy.* Cancer Chemother Pharmacol, 2017. **79**(6): p. 1151-1160.
154. Krall, N., et al., *A small-molecule drug conjugate for the treatment of carbonic anhydrase IX expressing tumors.* Angew Chem Int Ed Engl, 2014. **53**(16): p. 4231-5.
155. Cazzamalli, S., A. Dal Corso, and D. Neri, *Acetazolamide Serves as Selective Delivery Vehicle for Dipeptide-Linked Drugs to Renal Cell Carcinoma.* Mol Cancer Ther, 2016. **15**(12): p. 2926-2935.